INFLUENCE OF PARTICLE SIZE DISTRIBUTION ON FLUIDIZED BED HYDRODYNAMICS

By

Trevor Tsz-Leung Ip

B. E. Sc. (Chemical Engineering) University of Western Ontario

A THESIS SUBMITTED IN PARTIAL FULFILLMENT OF

THE REQUIREMENTS FOR THE DEGREE OF

MASTER OF APPLIED SCIENCE (CHEMICAL ENGINEERING)

in

THE FACULTY OF GRADUATE STUDIES

CHEMICAL ENGINEERING

We accept this thesis as conforming

to the required standard

THE UNIVERSITY OF BRITISH COLUMBIA

November 1988

In presenting this thesis in partial fulfilment of the requirements for an advanced degree at the University of British Columbia, I agree that the Library shall make it freely available for reference and study. I further agree that permission for extensive copying of this thesis for scholarly purposes may be granted by the head of my department or by his or her representatives. It is understood that copying or publication of this thesis for financial gain shall not be allowed without my written permission.

Department of Chemical Engineering

The University of British Columbia
Vancouver, Canada

Date Nov 18, 1988

Abstract

Past literature has shown that the production efficiency of a fluidized bed can be affected by changing the particle size distribution. The hydrodynamics of fine particle fluidization were studied with FCC and glass bead powders which have different surface-volume mean particle diameter (40-110 μm) and particle size distributions (narrow cut, wide cut and bimodal) under ambient conditions. Increasing the mean particle size increases the minimum fluidization velocity, minimum bubbling velocity and dense phase velocity (U_d) while decreasing the voidages at minimum fluidization and minimum bubbling and the dense phase voidage (ϵ_d) as well as the fractional bubble free bed expansion. Increasing the particle size spread increases U_d and decreases ϵ_d for FCC, but no clear conclusion can be made for glass bead powders. Increasing the static bed height decreases U_d and ϵ_d of FCC powders though it has no effect on minimum fluidization and bubbling properties. The magnitude of pressure fluctuations increases with increasing superficial gas velocity and as the size spread of the FCC powder becomes more narrow. However, the frequency of fluctuations is independent of each of these factors. Therefore, the quality and production efficiency of the fluidization process should improve with the use of a wide and continuous size distribution powder.

Table of Contents

List of Tables

List of Figures

Acknowledgement

Professor J. R. Grace, Dr. G. K. Khoe and the staff in the Department of Chemical Engineering are greatly appreciated for their technical advice and assistance in the completion of this project.

Special thanks are given to my wife, Julie S. H. Ip, who provides me with tremendous support and encouragement throughout the course of my studies.

I also wish to thank the Natural Science and Engineering Research Council for providing the financial support for this project.

Ultimate gratitude for our Heavenly Lord who makes research ever so meaningful to the existence of human kinds.

Brethren...forgetting what lies behind

and

reaching forward to what lies ahead,

I press on towards the goal

for the prize

of the upward call

of God in Jesus Christ.

(Paul in Philippians 3:13-14, NASB)

Chapter 1

Background

Fluidization has been a widely employed process in the chemical and other process industries. Essentially, fluidization occurs when the weight of a bed of powder is supported by the pressure drop across the bed. When this happens, the particles circulate inside the bed. The most common mode of fluidization is gas-solid fluidization. In this case, gas is passed through a bed of reacting powdered solids. When chemical reactions are carried out in fluidized beds, the rate of reaction is strongly influenced by the amount of contacting area between the gas and solids. A fluidized bed presents more reacting surface than a packed bed. The amount of contacting surface for a fixed amount of solid can be further increased by using finer particles. This is why the diameter of most industrial fluid bed catalysts is small, typically less than 100 μm. However, if the powder is too fine, the interparticle forces may affect the fluidization process in a negative manner. Hence, it is very important to understand the hydrodynamics of fine particle fluidization.

1.1 Classification of Powders

Not all powders have the same fluidization characteristics. Some work has been done to classify powders according to the way they fluidize. The most commonly used classification is the one proposed by Geldart (1973) for air fluidization under ambient conditions (Figure 1.1):

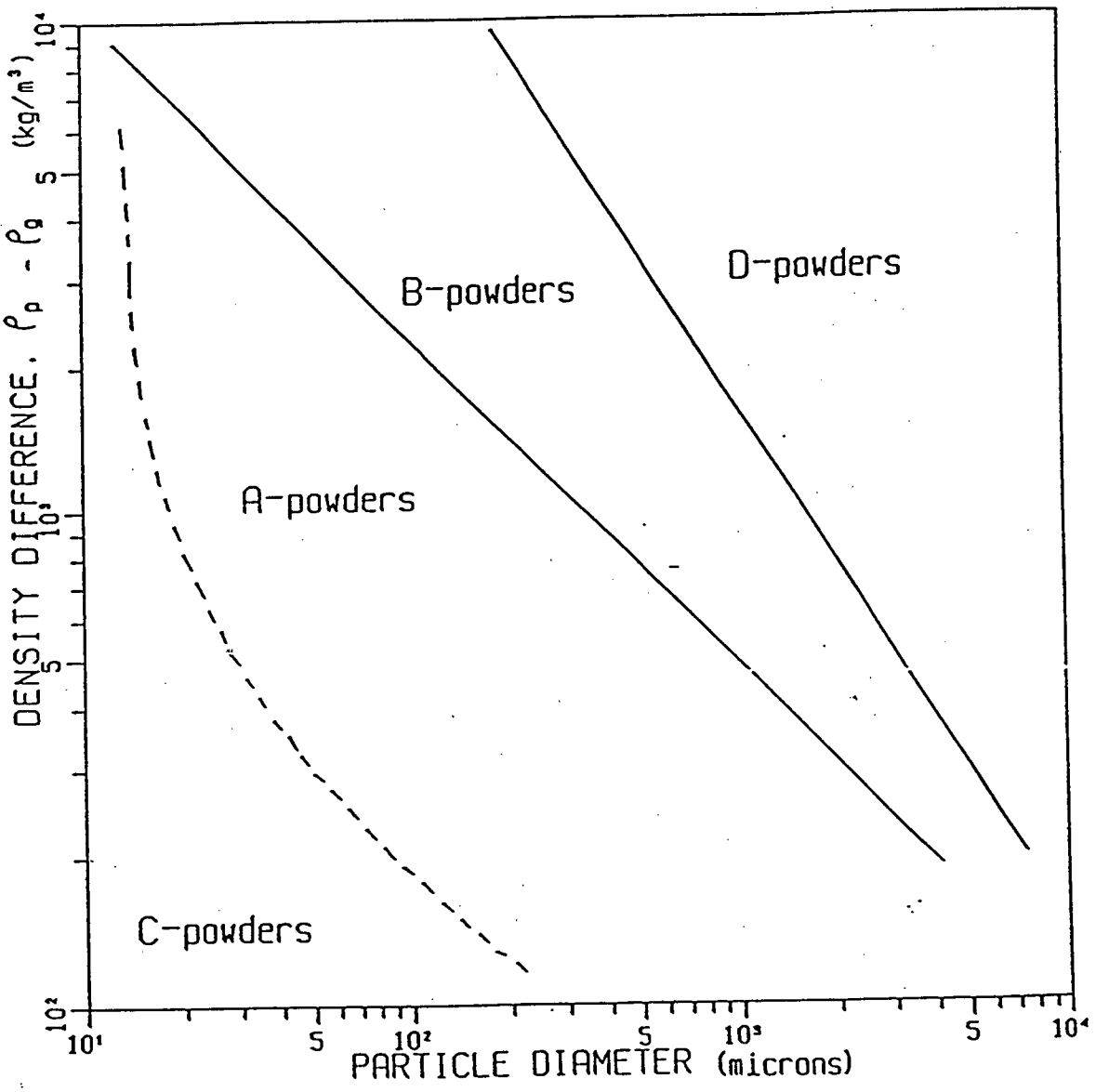

Figure 1.1: Geldart's Classification of Powder, Ambient Conditions (modified after Geldart, 1973).

1.1.1 Group A Powders

The minimum fluidization velocity, U_{mf}, is defined as the gas velocity at which the bed just starts to fluidize. The minimum bubbling velocity, U_{mb}, is the gas velocity at which gas bubbles first appear. The most striking characteristics of group A powders is that the bed expands homogenously when the superficial velocity is increased from U_{mf} to U_{mb}. Within this range of gas velocity, though the bed is fluidized and particle circulation takes place inside the bed, no bubbles appear. No phase separation occurs in the bed. This is due to some cohesivity of the powder. Because of the cohesive forces that hold the particles together, the excess gas flow passes through the interstitial space among the particles and no bubbles are formed. When U_{mb} is reached, the attraction force is insufficient to keep bubbles from forming.

1.1.2 Group B Powders

The interparticle forces for powders of this group are negligible. There is no bubble-free expansion stage. Instead, bubbles appear as soon as the bed is fluidized, i.e. U_{mb} is the same as U_{mf}. No circulation of particles takes place below the minimum bubbling point.

1.1.3 Group D Powders

This group of powders comprises larger and denser particles, typically 1 mm in size or larger. These particles can be spouted readily. Solid mixing is relatively poor compared to Group A and Group B particles.

1.1.4 Group C Powders

For very fine powders, the cohesive forces between the particles are very strong. When the minimum fluidization point is reached or sometimes even before that, channels and

cracks in the bed of solids usually appear rather than the homogenous expansion which occurs in the case of Group A powder. Gas flows through these channels. Fluidization is very difficult unless the channels are broken up by some external means such as stirring or shaking.

1.2 Regimes of Fluidization

Different regimes of fluidization are described here. Each regime has its particular properties and appearance as shown in Figure 1.2. Empirical correlations have been developed for these properties and they will be mentioned in this section.

1.2.1 Minimum Fluidization

Suppose that gas is passed vertically through a bed of particles. At low gas velocity, the particles are stationary and the bed is called a packed bed. When the gas flow is increased to the point where the pressure drop across the bed equals the weight of the powder per unit area, then the bed is said to be fluidized provided that the gas flow is uniformly distributed. A typical bed pressure drop versus superficial velocity curve is given in Figure 1.3. The minimum fluidization point is measured as the intersection of the two linear portions.

The most widely used correlation for the U_{mf} is derived from Ergun's equation which was developed from experiments on packed bed (1952) and may be written as:

$$\frac{\rho_g d_{sv}^3(\rho_p - \rho_g)}{\mu^2} = \frac{150(1-\epsilon_{mf})\rho_g d_{sv} U_{mf}}{\epsilon_{mf}^3 \mu} + \frac{1.75\rho_g^2 d_{sv}^2 U_{mf}^2}{\epsilon_{mf}^3 \mu^2} \tag{1.1}$$

ϵ_{mf} is the ratio of the volume occupied by the gas in the dense phase and bubble phase (excluding intraparticle voids) to the total volume at minimum fluidization. Grace (1982) eliminated ϵ_{mf} using empirical findings. The simplified correlations for small and large

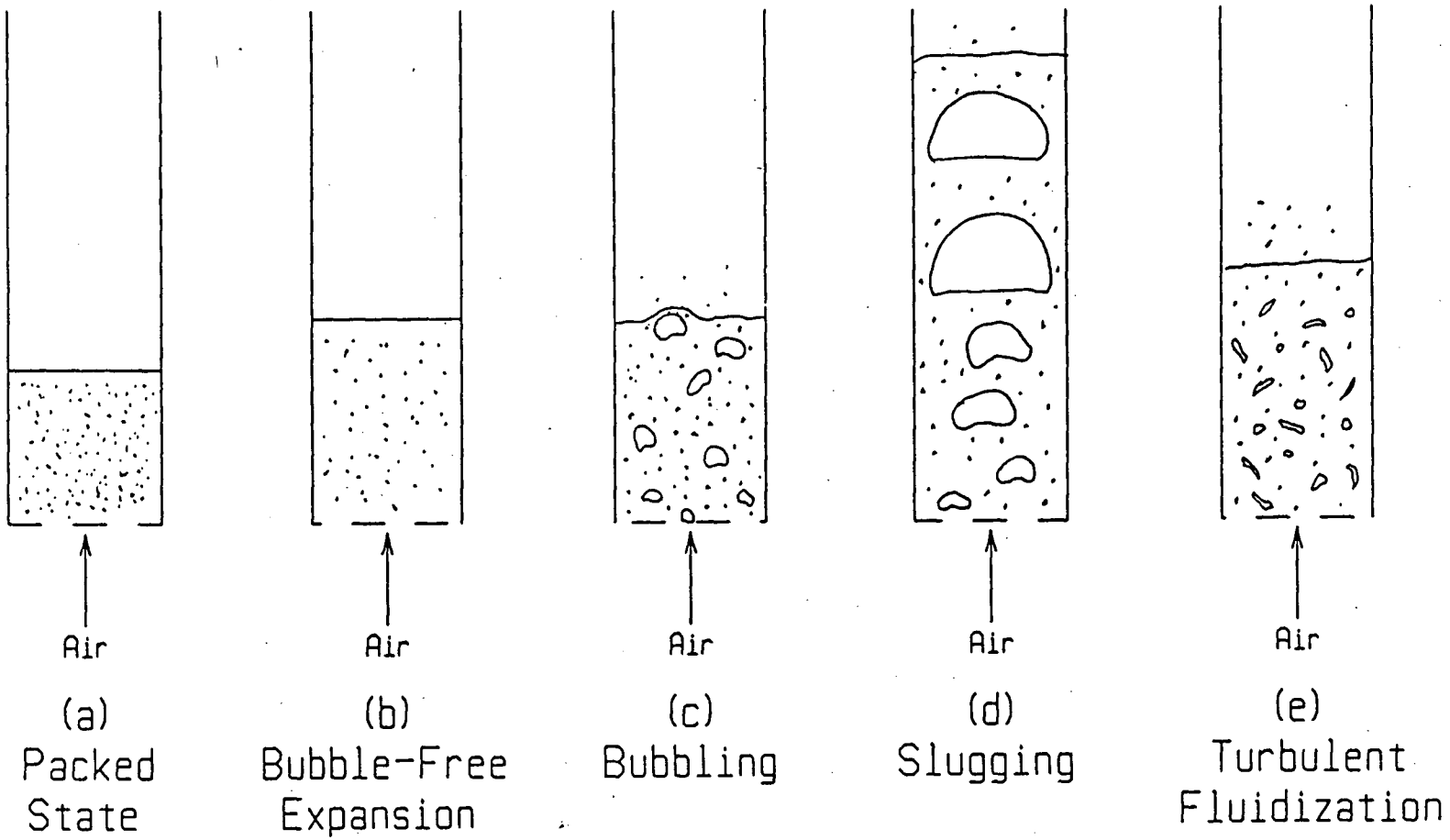

Figure 1.2: Regimes of Fluidization

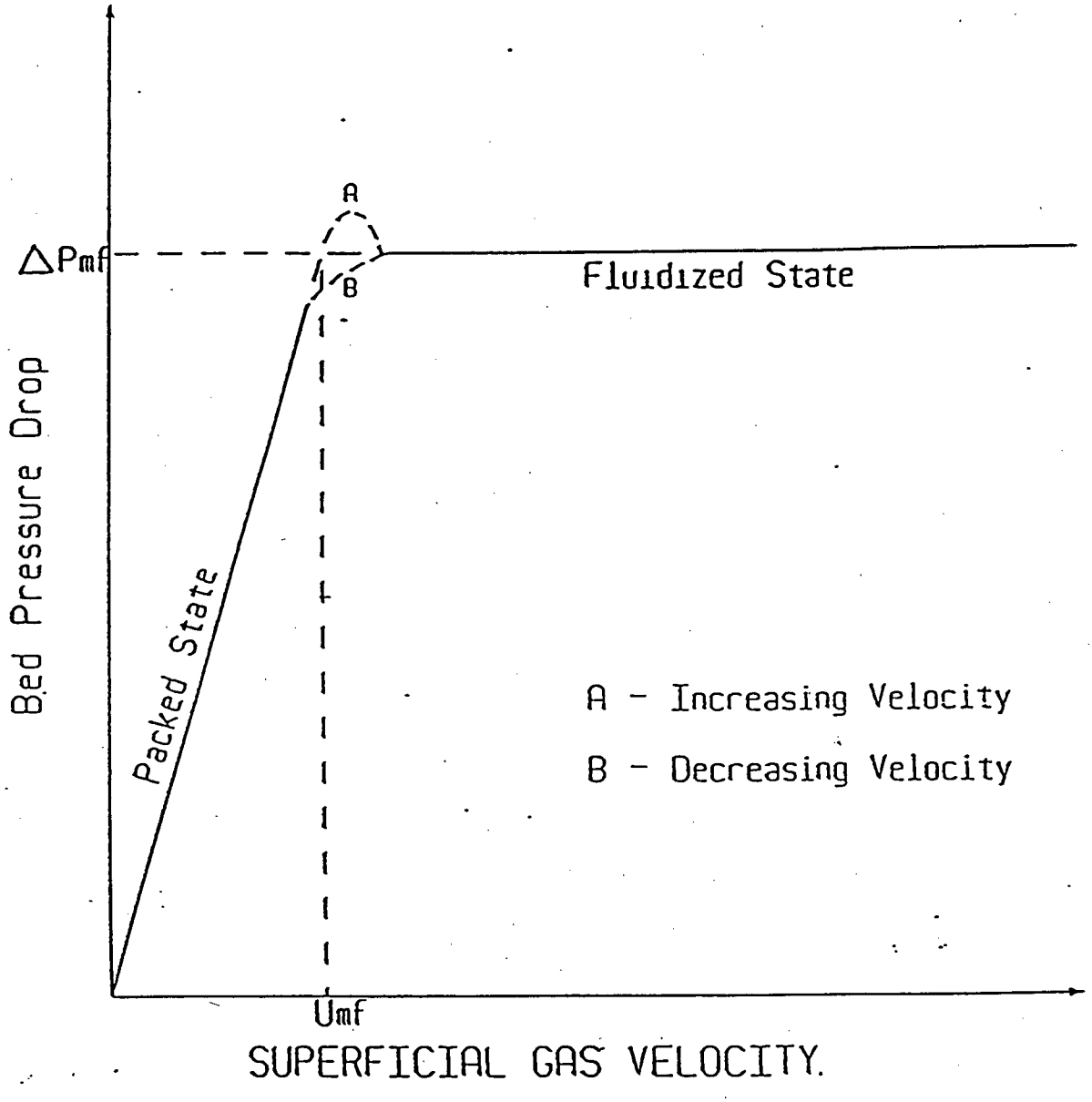

Figure 1.3: Plot of Bed Pressure Drop versus Gas Velocity (modified after Grace, 1982).

particles are as follows:

$$U_{mf} = 0.00075 * \frac{(\rho_p - \rho_g) g d_{sv}^2}{\mu} \quad for \quad Ar < 10^3 \tag{1.2}$$

$$U_{mf} = 0.202 * (\frac{(\rho_p - \rho_g) g d_{sv}^2}{\rho_g})^{0.5} \quad for \quad Ar > 10^7 \tag{1.3}$$

In essence, U_{mf} is a function of the gas density and viscosity, the particle density and the bed voidage at minimum fluidization. Other correlations for U_{mf} have been developed, but the independent variables for the best of these correlations are the same as those from the Ergun's equation with only the coefficients changed. A few of these are given here. Wen and Yu (1966a, 1966b) suggested the following correlation for laminar flow:

$$U_{mf} = \frac{(\rho_p - \rho_g) g d_v^2}{1650 \mu} \tag{1.4}$$

Baeyens and Geldart (1973) proposed the following relationship:

$$U_{mf} = \frac{0.0009 (\rho_p - \rho_g)^{0.934} g^{0.934} d_p^{1.8}}{\mu^{0.87} \rho_g^{0.066}} \tag{1.5}$$

Davies and Richardson (1966) published the correlation:

$$U_{mf} = \frac{(\rho_p - \rho_g) g d_{sv}^2}{1250 \mu} \tag{1.6}$$

where d_v is the number-volume mean particle diameter; d_p is the mean particle size obtained from standard sieve analysis using the following relationship (Abrahamsen and Geldart, 1980a):

$$d_p = (\Sigma \frac{x_i}{d_{pi}})^{-1} \tag{1.7}$$

According to these correlations, if one uses the same kind of gas and particles, changing the particle size distribution will not affect U_{mf} as long as the bed voidage and the mean particle size remain constant. However, Kunz (1970) reported that glass beads and fluid cracking catalyst particles with higher fines content (<44 μm) tend to have a

lower minimum fluidization velocity. It also becomes more difficult to measure a distinct value for U_{mf} as the fines level goes up (Dry et al., 1983; Geldart et al, 1984). Geldart et al. (1983) also reported that the ratio of bed pressure drop to the powder weight per unit area decreased from the ideal value of unity as the fines content increased. The high fines content powder was found to behave more and more like a Group C powder.

Massimilla et al. (1972) found that with the number-surface mean particle size kept constant, a FCC powder with a broad size spectrum has higher ϵ_{mf} and lower U_{mf} compared to one with a narrow size spectrum.

1.2.2 Bubble-Free Bed Expansion

Bubble-free bed expansion occurs only for Group A powders. This regime has been explained by Massimilla and Donsi (1976) who proposed that bed expansion takes place through the nucleation of microscopic cavities whose size is about one to ten times the particle diameter. They defined cavities as bed voids surrounded by particles bonded to each other by cohesive forces. These cohesive forces are mainly attractive capillary forces developed as a consequence of the formation of liquid bridges between contacting bodies in the presence of a vapour-containing atmosphere. A less significant component is the Van der Waals force related to the electromagnetic fluctuation phenomenon in solids. A third component consists of electrostatic forces due to electric charges on the particles (Clift, 1986). This is particularly important for particles smaller than 5 μm in diameter.

Mutsers and Rietema (1977, 1984) followed up on Massimilla's explanation by suggesting that the powder structure during homogenous expansion obeys the relationship:

$$-\frac{\partial}{\partial h}\tau_{hh} = E\frac{\partial \epsilon}{\partial h} \tag{1.8}$$

where E is the elasticity coefficient of the powder structure. The elasticity coefficient depends on the porosity of the bed. When the bed is expanded by an increase of air flow,

the size of an individual cavity increases. However, the number of cavities remains the same. The elasticity of the powder structure resists expansion of the bed and break-up of cavities. For increasing bed expansion, the elasticity constant remains the same as long as the maximum bed volume for that particular value of elasticity constant is not exceeded. If the limit is exceeded, some bonds that hold the microscopic cavities together will be broken and the particles will rearrange themselves to a structure with higher porosity; the value of the elasticity constant is then reduced stepwise.

Mutsers and Rietema reported that the value of the elasticity coefficient depends on the particle size distribution and types of material. Addition of a small amount of fines increases the number of contact points among particles and the elasticity coefficient. Different types of particles have different shapes. Hence the elasticity coefficient of a polypropylene bed is different from that of the fluid cracking catalyst bed.

Abrahamsen and Geldart (1980) derived an expression for bubble-free expansion for FCC, alumina and glass ballotini particles having mean particle diameter less than $75\mu m$ and gases with different densities and viscosities:

$$\frac{\epsilon^3}{1-\epsilon}\frac{(\rho_p-\rho_g)gd_p^2}{\mu} = 210(U-U_{mf}) + \frac{\epsilon_{mf}^3 U_{mf}}{1-\epsilon_{mf}}\frac{(\rho_p-\rho_g)gd_p^2}{\mu} \tag{1.9}$$

As indicated previously, the bed porosity goes up when the superficial velocity is increased beyond U_{mf}. But bed expansion goes through a maximum near the minimum bubbling point. At the minimum bubbling point, the attractive forces are overcome by the excess gas flow. As a result, the microscopic cavities disappear and bubbles are formed. The bed then becomes heterogenous.

1.2.3 Bubbling Regime

At the minimum bubbling point, the elasticity coefficient, as proposed by Massimilla et al. (1972), is reduced to its minimum. The bed does not have any more elasticity.

Any increase of gas flow results in bubble formation rather than further bubble-free bed expansion. With the interparticle forces disrupted, the bed contains two phases: a dense phase and a dilute phase. The dense phase contains the solid particles and the interstitial spaces while the dilute phase is mainly composed of gas bubbles, with a very small amount of solids carried into the bubbles by the jet stream issuing from the distributor plate. At gas velocities just beyond U_{mf}, bed contraction tends to occur because the reduction of dense phase volume is more rapid than the increase in bubble holdup (Geldart et al., 1984). Eventually, ϵ_d reaches a limiting value which is somewhere between ϵ_{mf} and ϵ_{mb}. Any further increase in gas flow leads to an increase in total bed height (due to an increase in bubble holdup), but ϵ_d is constant or increases only slightly (Abrahamsen and Geldart, 1980b; Rowe et al., 1978; and Vries et al., 1972). In this section, only the minimum bubbling properties are discussed. Dense phase properties are treated in Section 1.3.

Different methods have been used by researchers to identify U_{mb}. Normally it should be the point at which bubbles become visible on the bed surface, but this is subjective and can be inaccurate. For example, if the gas distribution or particle size distribution is not uniform in the bed, bubbles may appear only at certain locations of the bed while it is rather quiet in other areas. Other more objective ways have been used to determine U_{mb}. As mentioned in the previous section, the fluidized bed should be close to its maximum height at the minimum bubbling point. Some workers identify the minimum bubbling point by choosing the point where the bed height reaches a maximum (Jacob and Weimer, 1987; Geldart et al., 1984). They believe that bed contraction occurs as soon as the bed starts to bubble.

On a plot of bed porosity versus superficial velocity as shown in Figure 1.4, there is a constant and linear region at gas velocities below the minimum fluidization point. Another linear region often occurs at gas velocities between the minimum fluidization and

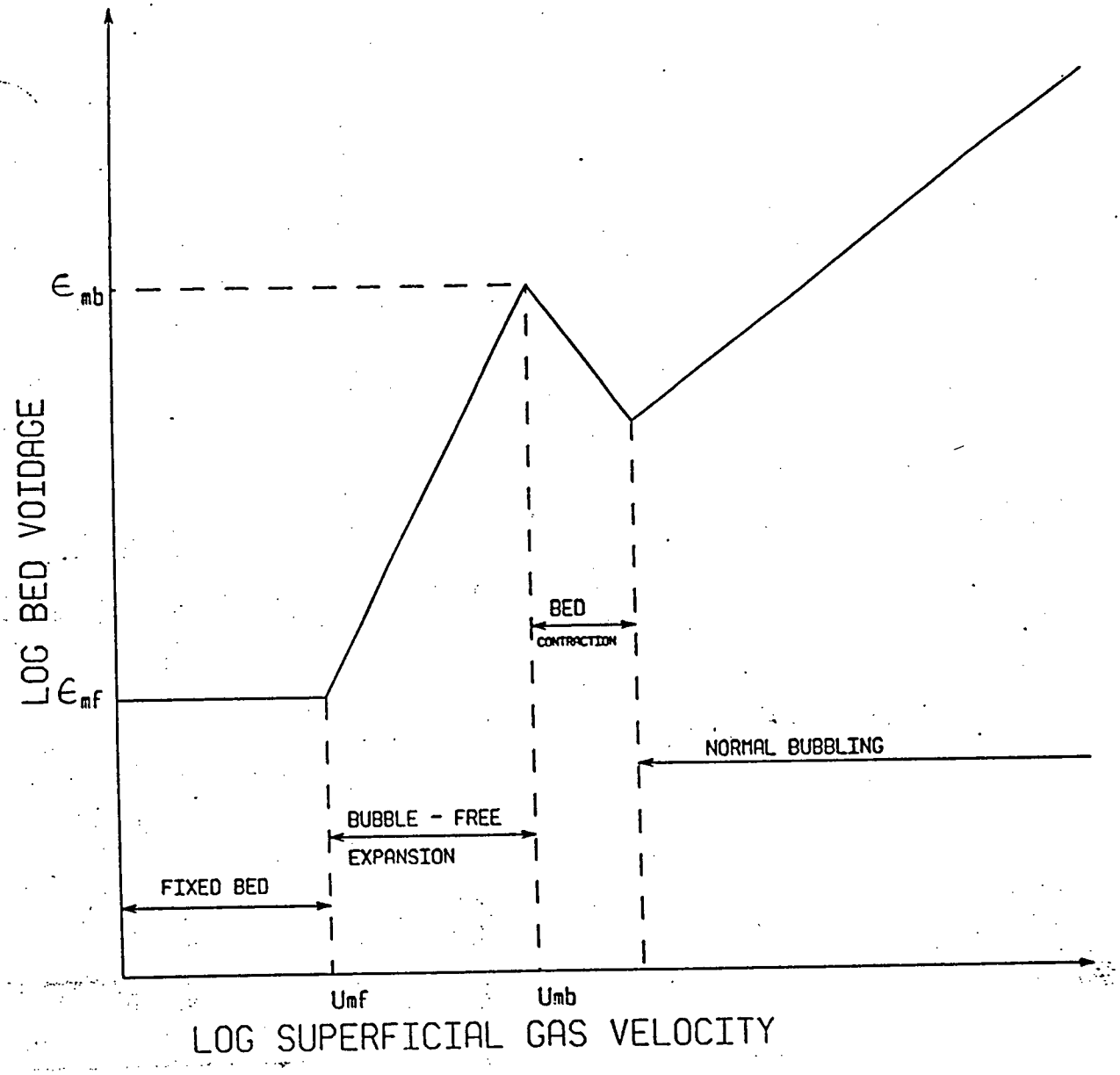

Figure 1.4: Bed Porosity versus Superficial Gas Velocity for a Typical Group A Powder (modified after Jacob and Weimer, 1980).

the minimum bubbling points. Rowe and Yacono (1976) used the intersection of these two linear regions as the minimum bubbling point. This is applicable only for group B and D powders since for group A powders the bed starts its bubble-free expansion at U_{mf}.

Correlations have been developed for the minimum bubbling point. Geldart and Abrahamsen (1978) found that for air fluidization under ambient conditions, U_{mb} can be estimated using a very simple equation:

$$U_{mb} = 100 * d_p \tag{1.10}$$

where U_{mb} and d_p are in SI units. This correlation was claimed to be satisfactory as long as the fines content (<45 μm) was less than 15% by mass. If the fines content is higher than 15%, Abrahamsen and Geldart (1980a) proposed the following relationship:

$$U_{mb} = 2.07exp(0.716F_{45})\frac{d_p\rho_g^{0.06}}{\mu^{0.347}} \tag{1.11}$$

This correlation was developed for a variety of powders, gases and operating conditions.

Foscolo and Gibilaro (1984) studied the hydrodynamic interaction between a particle and the fluid in a fluidized suspension and proposed the following criterion for the onset of bubbling:

$$[(\frac{gd_p}{U_t^2})(\frac{\rho_p - \rho_g}{\rho_p})]^{0.5} = 0.56n(1-\epsilon_{mb})^{0.5}\epsilon_{mb}^{n-1} \tag{1.12}$$

The correlation for minimum bubbling voidage provided by Abrahamsen and Geldart (1980a) considers the particle size distribution up to only the extent of weight fraction of powder smaller than a certain diameter. The effect of particle size distribution has also been studied by others. The results are contradictory. Simone and Harrison (1980) reported that the minimum bubbling velocity increases slightly going from a powder with a narrow size spectrum to one with a broad size spectrum while the surface-volume mean particle diameter is kept constant. The method used to prepare the silica-alumina

mixture was not given in their paper. De Jong et al. (1974) also reported that the minimum bubbling velocity of cracking catalyst with a broad size spectrum is slightly higher than that with a narrow size spread. The powder with a broad size spectrum was prepared by mixing the fine and the coarse fractions. It could have been a bimodal size distribution powder, depending on the size spread of the individual fractions which was not revealed.

These results are contradicted by Richardson (1971) who found a slightly lower value of minimum bubbling velocity for Diakon with a broad size spread than for a narrower distribution. Massimilla and Donsi (1976) also reported that the powder with a broad size spread has higher ϵ_{mb} and U_{mb} than one with a narrow size spectrum. However, for reasons not given in the paper, Massimilla and Donsi did not provide the mean particle diameter of the powder. They just claimed that the mean particle diameters of the two different powders were similar, although they might have been as much as 20% apart when one considers the size range of the narrow distribution.

1.2.4 Slugging and Pressure Fluctuations

As the gas flow increases, the mean bubble size also increases. Eventually, if the bed is deep enough and the maximum stable bubble size big enough, slugging will occur. Slugging is characterized by the periodic rise and fall of the entire bed surface and of the bed pressure drop (Grace, 1982). This pressure fluctuation is quite important in some fluidized beds because the vibration may damage structures such as baffles and tubes inside the fluidized bed.

In a freely bubbling bed, the bubbles are much smaller than the bed diameter. Many individual bubbles can be found on any horizontal plane of the fluidized bed. Noordergraaf et al. (1987) reported that the pressure fluctuations in this flow regime tend to have irregular frequency and amplitude. The magnitude of pressure fluctuations is somewhat

smaller than in the slugging regime.

When the bubbles become larger and have diameters comparable to that of the bed diameter, slugging occurs. In this flow regime, only a single chain of voids can be present in the bed. This results in a single dominant frequency and much more regular pressure fluctuations which also are larger in magnitude than in the bubbling regime. The period of the pressure fluctuations is usually about one to few seconds per cycle. Fan et al. (1981, 1983) have used the change in the pressure fluctuations to identify the onset of slugging and to infer the slug rise velocity.

There are two theories on the cause of pressure fluctuations. Noordergraaf et al. (1987) believed that pressure fluctuations are caused by the disintergration of a rising solid slug, followed by the 'raining' of particles. When the piston-like solid slug disintegrates at the top of the fluidized bed, many particles rain downwards and have a lower contribution to the bed pressure drop. The bed pressure is at its maximum just before the slug breaks the surface. The slugs are present only beyond a certain distance above the distributor. Below this bed level is a 'freely bubbling zone' where bubbles and jets coalesce to form slugs. In this 'freely bubbling zone', the pressure fluctuations are independent of the distance above the distributor. However, in the 'slugging zone', the average amount of particles above the pressure tap decreases. Therefore the magnitude of pressure fluctuations caused by the 'piston-rain transition' of these particles would decrease with increasing distance above the distributor.

Fan et al. (1981) has a different explanation for the pressure fluctuations. In the 'slugging zone' of the fluidized bed, the pressure fluctuations are caused by the motion of the bubbles around the pressure tap. The pressure reaches maxima and minima when the roof and the floor of the bubbles reach the pressure tap, respectively. In the 'freely bubbling zone', the pressure fluctuation is caused by a combination of the following: the jet flow and the formation of bubbles which transmit the pressure fluctuations upward

and the formation of the large bubbles which transmits the pressure fluctuations downward. The last factor accounts for the majority of the pressure fluctuations, though that contribution decreases when one gets closer to the distributor. Therefore the pressure fluctuation increases as the pressure probe moves away from the distributor and reaches a maximum at the point where slugs are formed. This is different from what Noordergraaf suggested. However, both workers concluded that the pressure fluctuation decreases in magnitude when the probe is farther away from the distributor in the 'slugging zone'.

Svoboda et al. (1984) reported that the nature of pressure fluctuations in a fluidized bed is a complex function of particle properties, bed geometry, bed pressure, and properties and flow conditions of the fluidizing fluid. This study concentrates on the effects of the particle size distribution and the mean particle diameter on the amplitude and the frequency of the pressure distribution as well as the mean pressure in the fluidized bed. Svoboda (1984) found that the mean pressure in the fluidized bed increases with increasing gas velocity and particle size. The magnitude of the pressure fluctuations increases with increasing superficial gas velocity and mean particle diameter (Satija and Fan, 1985); Fan et al., 1983; and Kang et al., 1967). This is caused by the increase of slug rise velocity and void volume. The dominant frequency of pressure fluctuations decreases with increasing mean particle diameter (Lirag and Littman, 1966; Sadasivan et al., 1980; Svoboda et al., 1984; Satija and Fan, 1985). However, the frequency is either only slightly dependent on or totally independent of the superficial velocity, as long as the gas flow is high enough that slugging occurs (Verloop and Heertjes, 1974; Sadasivan et al., 1980; and Noodergraaf et al., 1987; and Satija and Fan, 1985). Morse and Ballou (1951) found that the fluidization quality improves when a bed of solids has a broad size spectrum. This implies smaller pressure fluctuations and more predominant dense phase gas flow. The appearance of the slugs is also influenced by mean particle size. Kehoe and Davidson (1970) found that for fine particles (<70 μm), slugs are symmetrical. However, wall

slugs were observed for coarse particles. The bed height and particle density also affect the pressure fluctuations in a fluidized bed. However, they will not be investigated in this work.

1.2.5 High Velocity Fluidization Regimes

Turbulent fluidization occurs when the gas velocity is increased beyond a certain transition velocity. During turbulent fluidization, the bed surface is quite distinct and stable. Small voids darts to and fro. Pressure fluctuations are smaller in amplitude and higher in frequency than during slugging.

When the gas velocity is increased further to the transport velocity and higher, the particles are simply blown out of the top of the reactor. There is no longer any upper surface of the bed. Solids must be added to the reactor to prevent it from being emptied.

1.3 Dense Phase Properties

The dense phase of a fluidized bed is very important. This is where the gas and the solid establish intimate contact. Hence chemical reaction takes place primarily here. It is therefore vital to study the superficial dense phase gas velocities and dense phase voidages. These dense phase properties can be measured using the collapse test technique developed originally by Rietema (1967). The collapse test is of particular importance for Group A powders because of their slow de-aeration rate. In this section, the collapse test is explained. Empirical correlations for the dense phase properties are also discussed.

1.3.1 Collapse Test

Tung et al. (1989) proposed that in a collapsing gas-solid fluidized bed after the gas flow has been suddenly cut off, the gas flow can be divided into three components: 1)via

bubble translation and throughflow; 2)through the interstices of suspended particles; 3)driven out by the consolidating particles.

During the collapse of the bed of particles, all three types of gas flow take place simultaneously. After the gas supply to a bubbling bed is shut off, bubbles ascend through the bed and leave through the surface of the bed. This is the bubble escape stage. The bed level drops quickly during this period. At the end of the bubble escape stage, the gas flow through the interstices of suspended particles becomes predominant. This is the hindered sedimentation stage. The bed collapse rate is constant and slower than for the bubble escape stage. The bed is divided into two layers. Particles are piling up at the bottom of the bed. As a result, the bottom layer is denser than the top layer. The boundary between the two layers continues to rise until it reaches the top. That marks the end of the hindered sedimentation stage and the beginning of the solid consolidation stage. During the solid consolidation stage, the bed has uniform density. The gas in the interstitial space is expelled by the accumulation of particles. The rate of bed collapse is relatively slow.

The collapse test provides data for a plot of height versus time. An example is shown on Figure 1.5. Abrahamsen and Geldart (1980b) indicated that the middle, linear part of the curve corresponds to the hindered sedimentation stage. The slope of that part is the superficial dense phase gas velocity of the fluidized bed. If this linear part is extrapolated to time zero, where the intercept on the ordinate axis is the dense phase bed height. The dense phase voidage can then be calculated.

Abrahamsen and Geldart (1980b) also reported that the rate of bed collapse depends on undesirable factors such as the plenum chamber geometry and the pressure drop across the distributor. Adjustments may have to be made to either the experimental design or experimental data in order to obtain the true values for the dense phase properties.

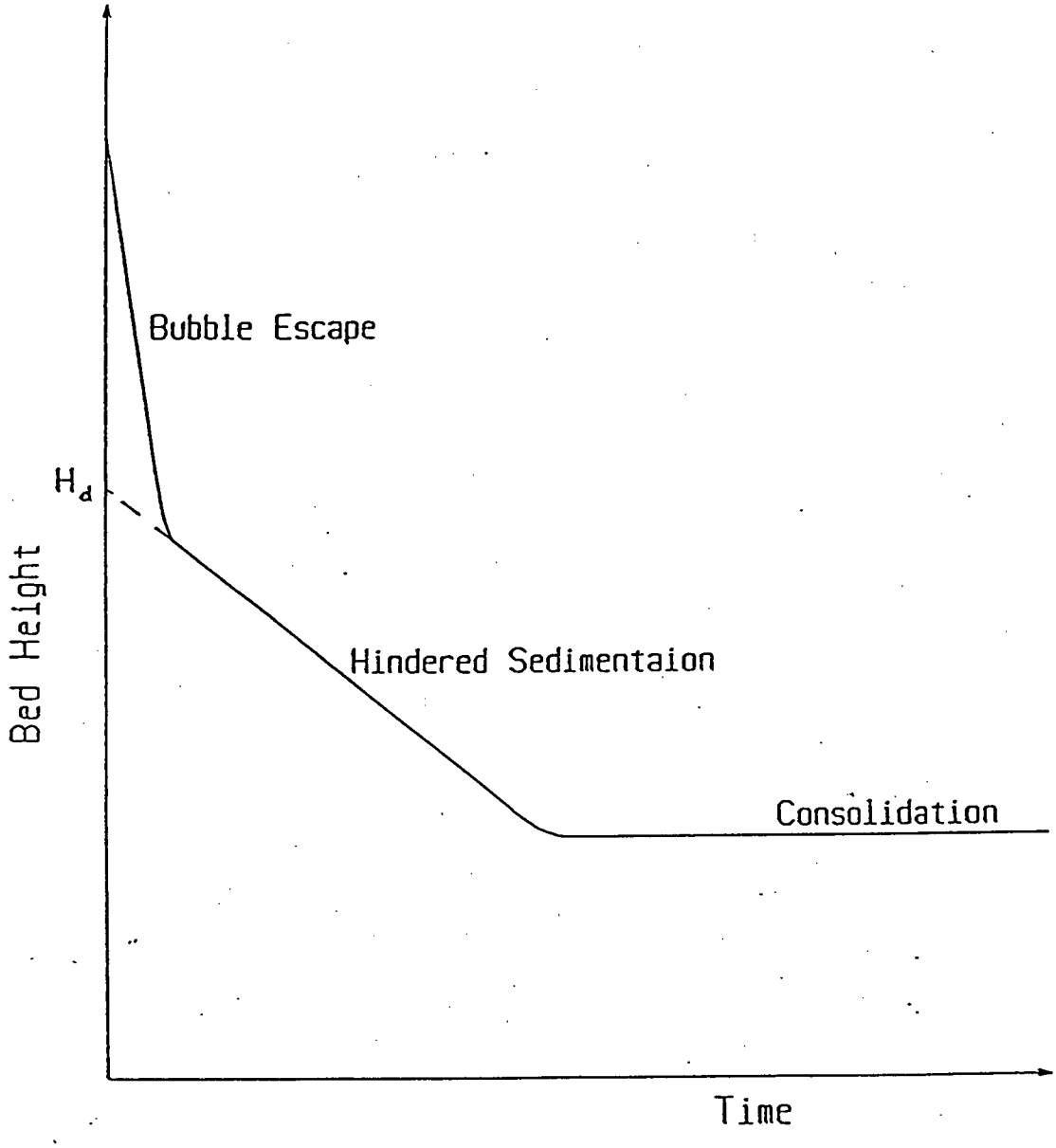

Figure 1.5: Typical Bed Height - Time Plot for a Collapse Test (modified after Abrahamsen and Geldart, 1980b).

1.3.2 Correlations for Dense Phase Properties

The dense phase properties of a bubbling bed have been of great interest to researchers. Different correlations have been developed to predict U_d and ϵ_d. Some are simpler than others, and some also take into consideration the fines content. One of the oldest theories of fluidization is the 'two-phase theory of fluidization', proposed by Toomey and Johnston (1952), and Davidson and Harrison (1963), which assumes that U_d and ϵ_d in a bubbling bed are the same as their respective values at minimum fluidization. However, Geldart (1986) indicated that numerous results have shown that the experimental values of U_d and ϵ_d exceeds those predicted using the two-phase theory.

An old correlation for the dense phase properties was derived from liquid-solid fluidization data collected by Richardson and Zaki (1954). The experiments were conducted under ambient conditions using spherical glass ballotini particles and various organic solutions. The correlation is as follows:

$$\frac{U_d}{U_t} = \epsilon_d^n \tag{1.13}$$

where

$$\begin{aligned}
n &= 4.65 \quad for \quad Re_t < 0.2 \\
n &= (4.35 + 17.5\frac{d_{sv}}{D})Re_t^{-0.03} \qquad 0.2 < Re_t < 1 \\
n &= (4.45 + 18\frac{d_{sv}}{D})Re_t^{-0.1} \qquad 1 < Re_t < 200 \\
n &= 4.45Re_t^{-0.1} \qquad 200 < Re_t < 500 \\
n &= 2.39 \qquad Re_t > 500
\end{aligned}$$

Though this correlation was developed from solid-liquid fluidization, it has been applied for gas-solid fluidization for superficial velocities between U_{mf} and U_{mb} with reasonable accuracy (Davies and Richardson, 1966; Abrahamsen and Geldart, 1980a).

Kmiec (1982) also did some solid-liquid fluidization experiments using ion-exchange particles, agalit, glass beads and water. He found that ϵ_d was well represented by:

$$\epsilon_d = \frac{(18Re_p + 2.7Re_p^{1.687})^{0.209}}{Ar^{0.209}} \tag{1.14}$$

where

$$Re_p = \frac{U_d d_p \rho_g}{\mu}$$

$$Ar = \frac{\rho_g(\rho_p - \rho_g)g d_{sv}^3}{\mu^2}$$

Kmiec claimed that his correlations produced results similar to those from Richardson and Zaki's equation.

Foscolo and Gibilaro (1983) examined the hydrodynamics from the packed bed state to the fully expanded state and obtained the correlation:

$$\frac{U_d}{U_t} = \frac{[0.0777Re_t(1 + 0.0194Re_t)\epsilon_d^{4.8} + 1]^{0.5} - 1}{0.0388Re_t} \tag{1.15}$$

Abrahamsen and Geldart (1980b) considered the dense phase properties for gas-solid fluidization of group A powders. The particles were ballotini, alumina and cracking catalyst. Different types of gas (argon, air, carbon dioxide, freon and helium) were used in order to study the effect of gas density and viscosity on dense phase properties. Fines fraction, F_{45}, defined as the weight fraction of particles with diameter (from sieve analysis) less than 45 μm, was also considered. The correlation is as follows:

$$\frac{1 - \epsilon_{mf}}{1 - \epsilon_d} = \frac{2.54\rho_g^{0.016}\mu^{0.066}exp(0.090F_{45})}{d_p^{0.1}g^{0.118}(\rho_p - \rho_g)^{0.118}H_{mf}^{0.043}} \tag{1.16}$$

$$(\frac{U_d}{U_{mf}})^{0.7} = (\frac{\epsilon_d}{\epsilon_{mf}})^3(\frac{1 - \epsilon_{mf}}{1 - \epsilon_d}) \tag{1.17}$$

From these correlations, one can see that if the mean particle size is constant, increasing the fines fraction can make the dense phase voidage go up by a factor of $\exp(0.09F_{45})$.

These correlations were claimed to be able to predict the dense phase properties within 20% of their experimental values. The correlations were also shown to fit well with data from the literature by other authors.

Dry et al. (1983) performed similar experiments with iron oxide, carbon powder, cracking catalyst and air. Their fines were defined as those particles with volume mean diameter less than 22 μm. The correlations are as follows:

$$U_d = \frac{d_v^2 g(\rho_p - \rho_g) exp(6.42 F_{22})}{2260\mu} \tag{1.18}$$

$$1 - \epsilon_d = 0.212 exp(1.13 exp(-2.07 F_{22})) \tag{1.19}$$

These correlations did not agree very well with earlier data from the literature. Dry et al. had problems determining the particle density of the porous cracking catalyst, and this may have affected the reliability of their correlations.

1.3.3 Effect of Particle Size Distribution on Dense phase Properties

Abrahamsen and Geldart (1980b) found that the dense phase behavior depends strongly on the weight fraction of fines defined as particles smaller than 45 μm in diameter. Their correlation suggests that the overall particle size distribution is not important in determining the dense phase properties, provided the fines fraction and the mean particle size (measured with standard sieve analysis) are constant. Their correlations also suggested that ϵ_d increases when the fines fraction F_{45} increases for a constant mean particle diameter.

Simone and Harriott (1980) also found that the particle size distribution does not affect the dense phase expansion in a vigorously bubbling bed when the surface-volume mean diameter of the powder is kept constant. They also found that the fractional dense phase expansion in a vigorously bubbling bed, U_d/U_{mf}, is always about 40-50% of the fractional bed expansion at minimum bubbling, U_{mb}/U_{mf}.

Geldart and Wong (1985) used powders with certain degrees of cohesiveness to study the dense phase properties. Their alumina powder had a mean particle diameter of about 30 μm (obtained with sieve analysis), so the powder is still in Group A according to Geldart's classification. Geldart and Wong made corrections for the volume of air trapped in the plenum chamber when the collapse test is started. It was found that increasing the fines fraction (F_{45}) by 10% would increase the superficial dense phase velocity by about 50%. The difference in the mean particles diameter between the two batches of powder used was only 2 μm which is too small to account for the big difference in the dense phase velocity.

The studies reviewed above appears to be the only ones in which the effect of particle size distribution on dense phase properties has been investigated with constant mean particle size. The other work appear to involve uncontrolled studies in which both the fines fraction and the mean particle size were varied at the same time. Some of this work is discussed briefly here.

As mentioned before, Dry et al. (1983) claims that the fines fraction (F_{22}) is directly responsible in the determination of the dense phase voidage of fluidized bed filled with iron oxide/carbon mixture or fluid cracking catalyst. However, in both of their experiments, the mean particle size was not kept constant.

Barreto et al. (1983) claimed that when the fines fraction (F_{45}) increases by 46%, the dense phase voidage of the zeolite bed goes up by about 10%. However, they made the same mistake of neglecting the decrease in mean particle diameter.

It is shown in Figure 1.4 that at gas velocities beyond U_{mb}, the overall bed voidage decreases initially but eventually increases again with increasing superficial velocity. However, the dense phase voidage continues to decrease and levels off to a certain value even though the overall bed voidage keeps going up (Abrahamsen and Geldart, 1980b). Rowe and Yacono (1976) found that while this means a small drop in U_d in the early stage of

the bubbling flow regime, the general trend is that the permeability of the dense phase continues to increase despite the nearly constant dense phase voidage. This is indicated by the upward trend of the superficial dense phase gas velocity with increasing gas flow, even when the superficial gas velocity is ten to fifteen times U_{mf}. This trend is more apparent when the fines fraction (F_{45}) is higher than 20% with a mean particle diameter of about 45 μm. However, other workers such as Abrahamsen and Geldart (1980b) and Dry et al. (1983) suggested that the increase or decrease of U_d should follow the variation of ϵ_d, even with powders having high fines fractions. Hence, U_d approaches a constant value with increasing gas flow in a vigorously bubbling bed.

1.3.4 Effect of Static Bed Height on Dense Phase Properties

There is some controversy regarding whether or not dense phase properties are functions of the static bed height. Some workers have found that the dependence of superficial dense phase velocity and dense phase voidage on the static bed height is negligible (Vries et al., 1972; Bohle and Swaay, 1978; and May, 1959).

Abrahamsen and Geldart (1980b) indicated that the dense phase voidage changes along the height of the bed. The region closest to the distributor plate had the highest voidage while the top region had a dense phase voidage approaching its value at minimum fluidization. Since the superficial dense phase gas velocity is related to the dense phase voidage, the latter is also a function of bed height. The results were collected with the bed height ranging from 0.3 to 0.9 m, yielding:

$$U_d \quad \alpha \quad H_o^{-0.244} \tag{1.20}$$

Dry et al. (1983) showed a weak dependence of dense phase voidage on bed height. Their results were based on a bed depth in excess of 2 m and led to:

$$\epsilon_d \quad \alpha \quad H_o^{-0.039} \tag{1.21}$$

1.4 Objectives of this Project

The correlations described above indicate that the mean particle diameter, usually the surface-volume mean, plays a very important role in the determination of minimum fluidization, bed expansion, minimum bubbling and dense phase properties. However, the influence of particle size distribution has usually been neglected.

Some workers have investigated the effect of particle size distribution on different aspects of fluidization. However, they were usually uncontrolled studies with the mean particle diameter not kept constant but changing when fines or coarse particles were added to the powder. These results cannot be used reliably to draw any valid conclusions. For example, when Geldart (1972) replotted Matheson's (1949) results with the changes in particle diameter taken into consideration, it was concluded that the Stormer viscosity of the fluidized bed does not depend on the particle size distribution, exactly opposite to the original conclusion. This shows that it is vital to consider changes in mean particle diameter when studying the effect of particle size distribution.

The powders used in the present work belong to Group A, the type of powder most frequently used for catalytic reactions in the chemical industry. The objective of this work was to study the effects of surface-volume mean particle diameter and the complete particle size distribution on different aspects of fluidization. The areas covered include minimum fluidization, bubble-free fluidization, minimum bubbling, dense phase properties and pressure fluctuations. The surface-volume mean particle diameter was kept constant while the effects of the particle size distribution were studied.

Chapter 2

Apparatus

The experimental equipment was composed of gas flow regulators, a plenum chamber (windbox), a distributor plate, pressure measuring devices, a main glass column, an expansion section, a freeboard and an air filter. A layout of the whole apparatus and a detailed drawing for the components of the fluidization column are shown in Figures 2.1 and 2.2, respectively.

2.1 Flow Regulators

The main flow regulators used in this project are a PVC diaphragm valve and a needle valve attached to a rotameter. These are high precision valves which enable the operator to control the flow very accurately. Two rotameters are used to indicate the fluid flowrate. Rotameter R1, made by Brooks Instruments, has a tube number of R-6-25-1-A. It contains a glass float and a steel float for maximum flowrates of $2.1*10^{-4}$ and $3.8*10^{-4}$ m^3/s, respectively, under conditions of 20°C and 1 atm. Rotameter R2, manufactured by Porter Instrument, has tube number B-175-60 and contains a sapphire float for maximum gas flowrate of $8.5*10^{-5}$ m^3/s under the same conditions. A pressure regulator 'PR' was used to lower the air pressure from that of the building air to a pressure that the apparatus can stand. The air coming through 'R1' can go into the stream that contains 'R2' or be vented. This is controlled by the three way valve 'V3'. Gate valve 'V4' provides a path by which the air can bypass the rest of the equipment. This is to avoid a pressure buildup during the collapse test. Needle valve 'V5' is used to control the air efflux from

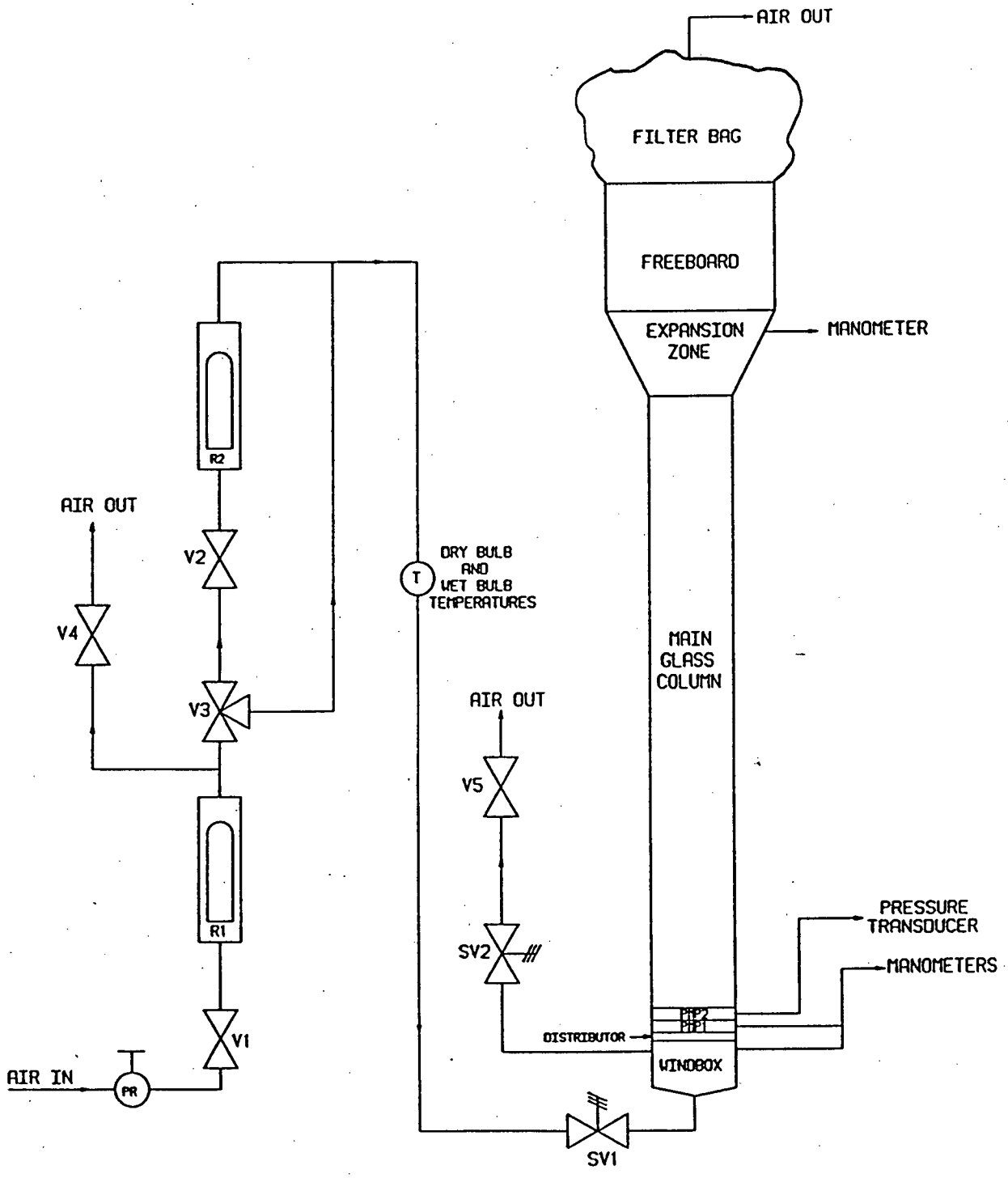

Figure 2.1: Schematic Layout of the Apparatus.

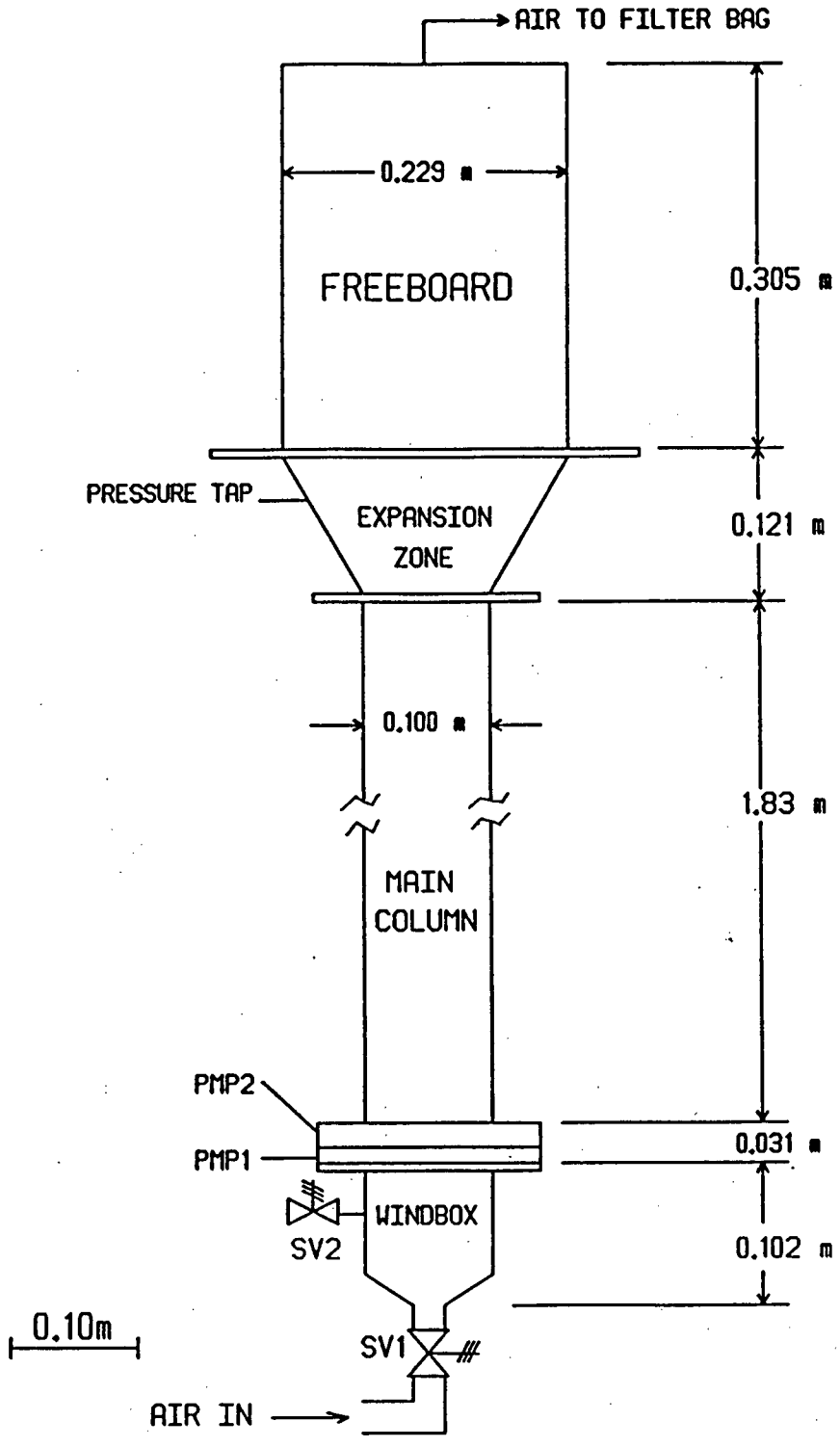

Figure 2.2: Detailed Drawing of the Fluidization Column.

the plenum chamber when solenoid valve 'SV2' is opened.

2.2 Solenoid Valves

Solenoid valves are electrically triggered valves which are either fully open or fully closed. Solenoid valve 'SV1' is normally closed (closed when no electrical current flows through the valve) while 'SV2' is normally open. The advantage of a solenoid valve over the hand-operated valve is that it takes only milliseconds to fully open or close a valve. Both valves are triggered simultaneously with a single switch. When the valves are turned on, air may flow from the main air supply to the plenum chamber and up through the distributor, but air cannot escape through 'SV2'. When the valves are off, the air supply to the plenum chamber is stopped. Air can escape from the plenum chamber through 'SV2' to leave the apparatus provided that there is a pressure differential between the two ends.

2.3 Plenum Chamber (Windbox)

The purpose of the steel plenum chamber is to develop a uniform pressure below the distributor plate so that gas flow is uniform through the distributor. Air enters through a 25 mm inlet pipe and leaves through the 100 mm diameter distributor into the glass column above. Two ports are found on the sides of the bottom cylindrical section. One of them serves as a pressure tap while the other is for letting air out through solenoid valve 'SV2'.

2.4 Distributor Plate

Some of the particles used in this project have diameters as small as 5 μm. A stainless steel perforated plate with one millimeter openings was originally used as distributor, but

it was unsuccessful because the powder could not be prevented from dropping into the plenum chamber while the column was being cleaned with the air supply shut off. Two pieces of chromatography cardboard were then used. This provided a larger pressure drop across the distributor than the perforated plate. The pressure drop across the distributor plate was at least 25% of the bed pressure drop for the range of gas flowrates used in the experiment. Gas distribution with the cardboard distributor was found to be very uniform.

2.5 Pressure Measurement Plate

A steel pressure measurement plate 'PMP1' is located right above the distributor plate. This plate provides two ports for pressure measurement. One port is for measuring the pressure drop across the bed of powder, while the other is for measuring the pressure drop across the distributor. All pressure taps are connected by plastic tubing to water or mercury manometers depending on the magnitude of the pressure gradient.

Another pressure measurement plate 'PMP2' was used to measure the pressure fluctuation in the fluidized bed in the bubbling and slugging flow regimes. This was placed at either 27 mm or 180 mm above the distributor plate. It provides an opening for a 6.3 mm steel tube. A brass sintered filter of pore size 7 μm is attached to the inner end of the steel tube so that no particles block the opening. The outer end of the steel tube is connected to a DISA capacitance type pressure transducer.

2.6 Main Glass Column

A glass column made by Pyrex Glassware contained the fluidized bed. Glass is superior to other materials such as plexiglass and steel for two reasons. Firstly, glass is transparent making it much easier to detect visually what is taking place inside the column. One

can also use a video-camera to record the experiment. Secondly, the particles have less tendency to adhere to the inside of the glass column than to a plexiglass column. The particles used for the experiments are very fine, most being smaller than 100 μm. Static electricity can be a major problem if a plexiglass column is used. The main glass column has an inner diameter of 100 mm, a wall thickness of 13 mm and a column height of 1.83 m. The inner diameter is uniform thoughout the length of the column. A metric tape was attached to the outside of the column to indicate bed levels.

2.7 Expansion Zone

A steel conical section connected the 100 mm glass column to the freeboard which is 230 mm in diameter. The slanting part has a slope of 60 degrees to the horizontal. Any particles with an angle of repose of less than that should roll down to main glass column. A pressure tap is located in this section so that one can determine the system pressure close to where the air leaves the apparatus.

2.8 Freeboard

At high gas flowrates, particles can be blown out of the main column. The freeboard is used to return these particles back to the main column. The freeboard is a short cylindrical glass section made of QVF glassware. The inner diameter and the wall thickness are 0.23 and 0.013 m respectively. The height of the section is 0.30 m. Since the freeboard has a diameter 2.3 times larger than that of the main column, the air velocity drops by a factor of 5 going from the main column to the freeboard. Particles with terminal settling velocities higher than the air velocity in the freeboard tend to be returned to the main column.

2.9 Air Filter

A paper vacuum bag is placed on top of the freeboard to trap any particles that escape the freeboard. This ensure that virtually no particles are lost from the system.

2.10 Humidity Measurement

Two thermometers placed side by side are inserted into the inlet piping. The mercury bulb on one of these thermometers is wrapped with gauze and attached to a water reservoir to ensure a constant supply of water. The wet bulb temperature is obtained from this thermometer. The other thermometer indicates the dry bulb temperature of the air entering the fluidized bed.

2.11 Powder

Two kinds of powder were used for our experiments. They are spent fluid cracking catalyst (FCC) obtained from the ESSO refinery at Ioco, B.C. and glass beads manufactured by the Potter company in New Jersey. The properties of these powders are discussed in Chapter 3.

Chapter 3

Experimental Method

The experimental procedures include preparation of the powders, measurement of the physical properties of the powders, low-velocity fluidization, collapse tests and pressure fluctuation measurements.

3.1 Powder Preparation

The original spent fluid cracking catalyst (FCC) was separated into six different size fractions using an air classifier in the Mining and Mineral Process Engineering Department at University of British Columbia. The air classifier consisted of six steel conical chambers arranged in series, and the dimensions of these are given in Figure 3.1. The separation involved two passes. The respective air flowrates for the first and second passes were 0.0021 and 0.0022 m/s^3, respectively. The original bulk FCC powder was charged into the air classifier during the first pass. The fraction collected in cone number 3 was then passed into the classifier during the second run. Four size fractions of FCC labelled 'original', 'coarse', 'intermediate' and 'fine' were collected for our experiments. 'Original' distribution was the unseparated FCC powder. 'Coarse' and 'fine' fractions were the powder collected in cones number 2 and 4, respectively, from the first pass. 'Intermediate' fraction was collected in cone number 3 from the second pass.

No separation was necessary for the glass beads because they came in three discrete size fractions.

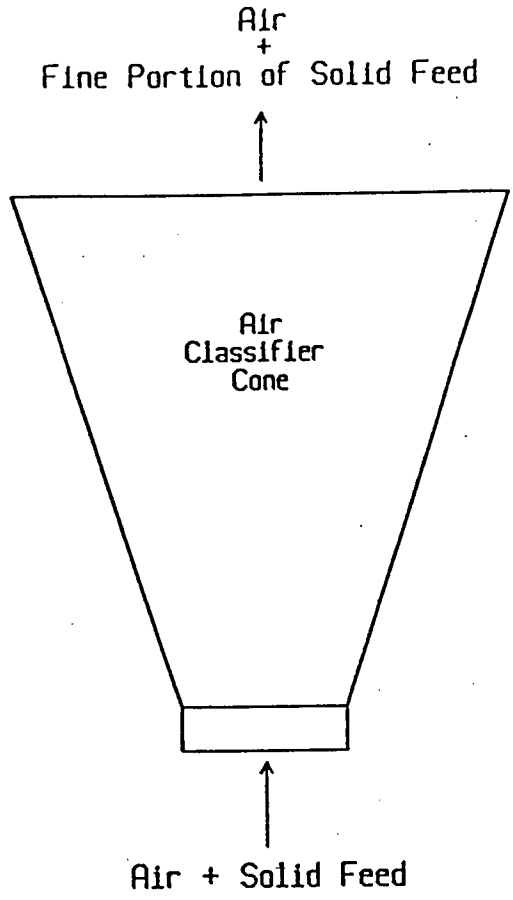

Air Classifier Cone	Top Cross-sectional Area (m^2)
1	0.00385
2	0.00709
3	0.0145
4	0.0284
5	0.0564
6	0.108

Figure 3.1: Dimensions for the Powder Collectors of the Air Classifier.

3.2 Particle Density Measurement

The skeletal density for a particle is defined as the mass of the particle per unit volume of the solid part of the particle (excluding any voids inside the particle). The particle density is defined as the mass of the particle divided by the sum of the volume of the solid and volume of the internal voids, i.e. envelope volume.

It is very difficult to get an accurate measurement of the particle density. Ergun's (1951) gas flow technique with a modification described by Abrahamsen and Geldart (1980a) was tried. This relies on making a packed bed of two different heights with the same batch of powder. However, the fluid cracking catalyst is not very compressible. The static bed height could only be changed by 2.5% which was not large enough to produce consistent results.

Skeletal density, ρ_s, was measured with the liquid displacement method using a specific gravity bottle. A known volume of liquid is added to a certain weight of solid. The volume of solid can be obtained from the volume of liquid that the solid displaces. Then the skeletal density can be calculated. The mixture of liquid and solid had to be well stirred for 15 to 30 minutes to drive out any air bubbles trapped in the liquid. Only then can measurements be taken. In the case with water, the liquid/solid mixtures were kept for a few days with periodic shaking and the results were compared to see if there was significant volume of non-visible bubbles. The results are given in Table 3.1. The skeletal density of FCC as measured with different liquids does not show any significant difference. Water is supposed to penetrate the internal pores of the particles, while carbon tetrachloride is not supposed to penetrate any. But the results show only a 3% difference in skeletal density as measured with various types of fluid. The color of the catalyst is dark grey so that it is obviously spent catalyst. The internal pores are probably coated with coke so the pores of these spent catalyst particles are likely shallower than those

Table 3.1: Skeletal Density of Fluid Cracking Catalyst as Measured by Liquid Displacement With Different Liquids. *Solid-liquid mixture degassed for few days.

Liquid	Skeletal Density (kg/m^3)
Water	2370
Ethyl Ether	2370
Methanol	2410
Carbon Tetrachloride	2310
Water*	2330

of the fresh catalyst. Carbon tetrachloride may therefore have penetrated the pores as deeply as water. Hence the two types of liquid produce similar results.

The solid-liquid mixtures showed insignificant amounts of trapped air bubbles after thirty minutes of shaking. Leaving the mixture for a few days did not make any significant difference in the measured skeletal density. The results obtained with water displacement have been chosen as the true skeletal density of the powder.

The particle density, ρ_p, is measured with the 'wet cake' method proposed by Abrahamsen and Geldart (1980a). Water is added to a sample of powder until the particles stick together like a cake, i.e. they are no longer free-flowing. If x is the volume of water needed to just cake one kilogram of powder, then the particle density can be calculated as follows:

$$\rho_p = \frac{1}{x + \rho_s^{-1}} \tag{3.1}$$

Fluid cracking catalyst particles are porous. So both the skeletal and particle densities have to be measured. Different sizes of particles may have different fractional internal voids. Hence it is best to measure the particle density for each fraction of the FCC. However, glass beads are non-porous so that the skeletal and particle densities are the same. Only the liquid displacement method was therefore necessary to derive the particle density for the glass beads.

The results on particle density of FCC and glass beads are shown in Table 3.2. The particle density of FCC increases by 12.4% going from the coarse to the fine fractions. This is perhaps due to the larger probability of bigger particle having closed or larger pores resulting in greater internal porosity for larger particles.

Table 3.2: Particle Densities for Fluid Cracking Catalyst and Glass Beads.

Powder	Size Distributions	Particle Density (kg/m^3)
FCC	Original	1444
FCC	Coarse	1384
FCC	Intermediate	1455
FCC	Fine	1556
FCC	Wide	1423
FCC	Bimodal	1440
Glass Beads	All Distributions	2450

3.3 Particle Diameter

The permeametry method was used to derive the specific surface area of the particles. The details of this procedure are given in the instruction manual for the 'Quanta-Sorb' surface area analyzer. Essentially, one needs a plot of bed pressure drop versus air velocity from a packed bed of particles whose specific surface is measured. The bed is packed to about 0.3 m in height. The Carmen-Kozeny equation is then used to calculate the specific surface which in this case refers to the 'envelope' surface of the particle. The specific volume (envelope) of the particles can easily be calculated from the particle density. Dividing the specific volume by the specific surface produces the surface-volume mean diameter of the particles (Stockham, 1978).

Three FCC powders with different particle size distributions but similar surface-volume mean diameter were used for the experiments. The first fraction is the 'intermediate size distribution' composed solely of the intermediate fraction mentioned previously. The mean particle diameter for this intermediate fraction is then matched in two other made-up mixtures. A 'bimodal size distribution' was prepared by mixing the fine fraction and the coarse fraction. A third 'wide size distribution' was made up of the original catalyst plus some of either the coarse or the fine fraction so that the final surface-volume mean diameter matches that of the intermediate fraction. In the case of glass beads, the wide size distribution is a mixture of the coarse, intermediate and fine fractions.

The particle diameter for different distributions of FCC and glass beads are given in Tables 3.3 and 3.4. The particle size distributions are shown in Figures 3.2-3.5. According to Geldart's powder classification, all the size distributions of FCC belong to Group A. For the glass beads, all the size distributions also belong to Group A except for the coarse fraction which falls into Group B. The bimodal FCC distribution is made up of fractions that are both Group A while the bimodal glass beads powder consists of a Group A

Table 3.3: Composition and Surface-Volume Mean Diameter of Different Size Distributions of FCC

Size Distribution	Composition	d_{sv} (μm)
Original	-	45.0
Coarse	-	83.3
Intermediate	-	53.2
Fine	-	34.1
Wide	65.6% Original +34.4% Coarse	53.1
Bimodal	67.5% Coarse +32.5% Fine	54.0

Table 3.4: Composition and Surface-Volume Mean Diameter of Different Size Distributions of Glass Beads

Size Distribution	Composition	d_{sv} (μm)
Coarse	-	113.0
Intermediate	-	72.7
Fine	-	37.4
Wide	10.0% Fine +50.0% Middle +38.0% Coarse	71.9
Bimodal	76.1% Coarse +23.9% Fine	73.1

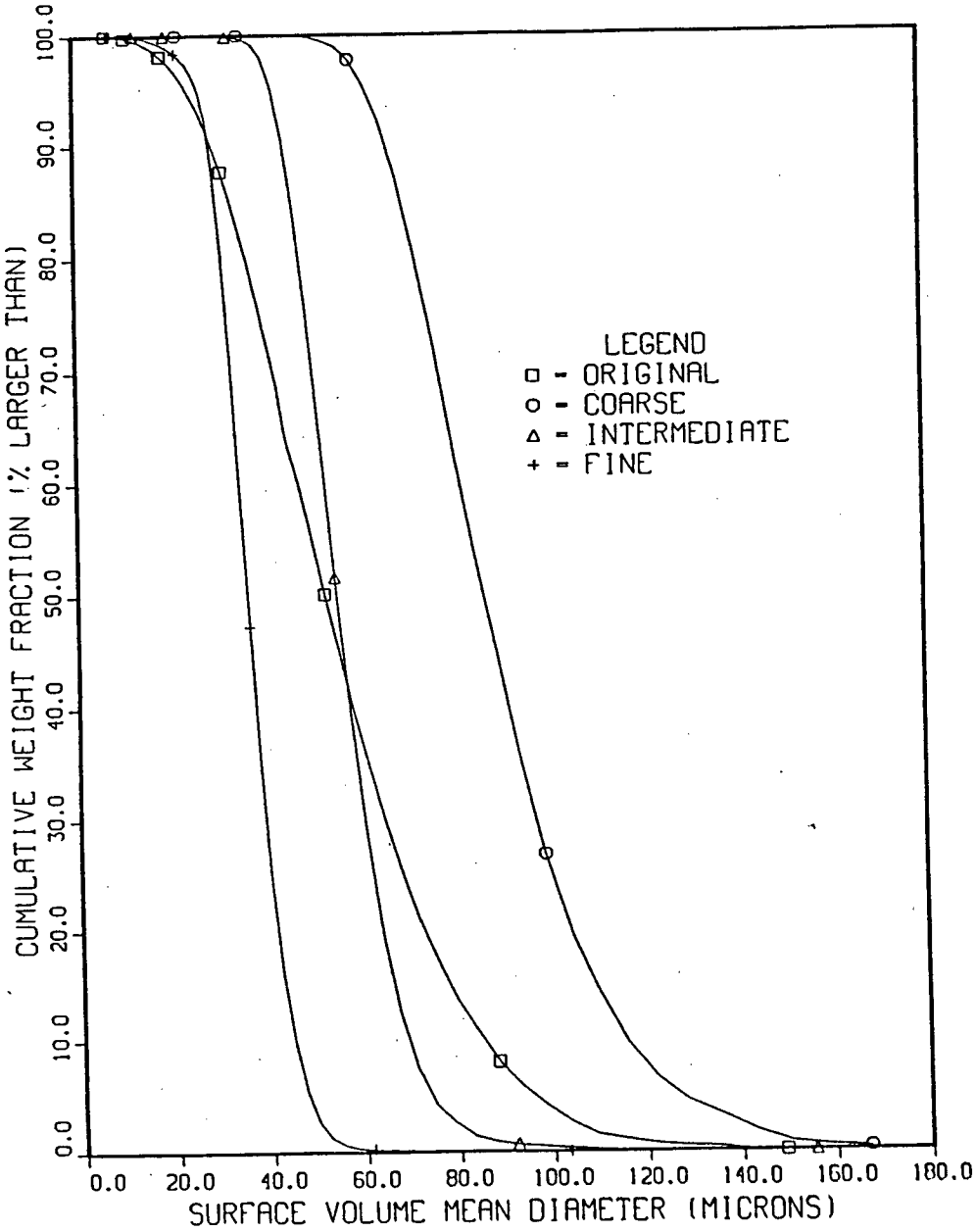

Figure 3.2: Particle Size Distributions for FCC Powders with Narrow Size Distributions.

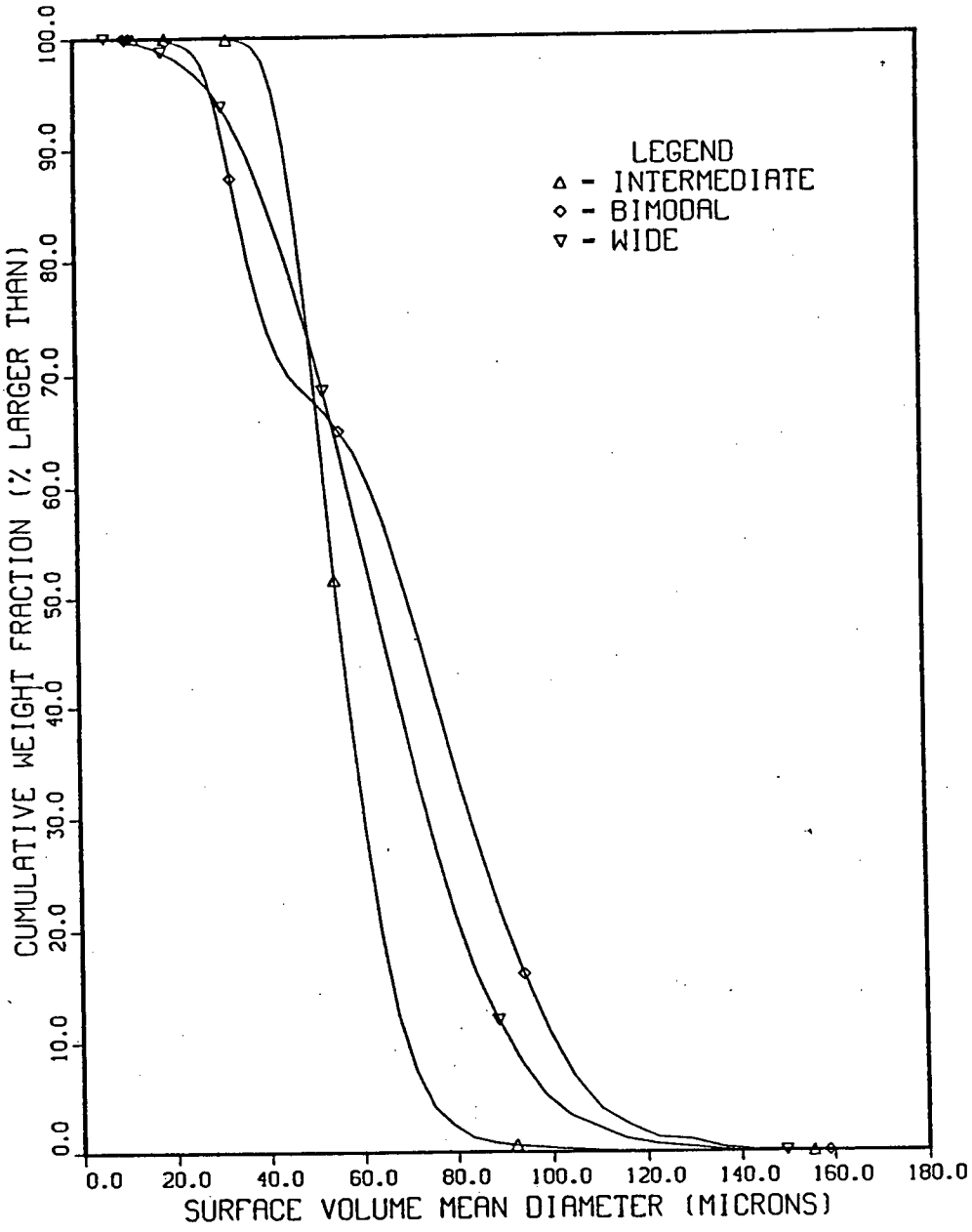

Figure 3.3: Particle Size Distributions for FCC powders with Similar Mean Surface-Volume Mean Particle Diameters.

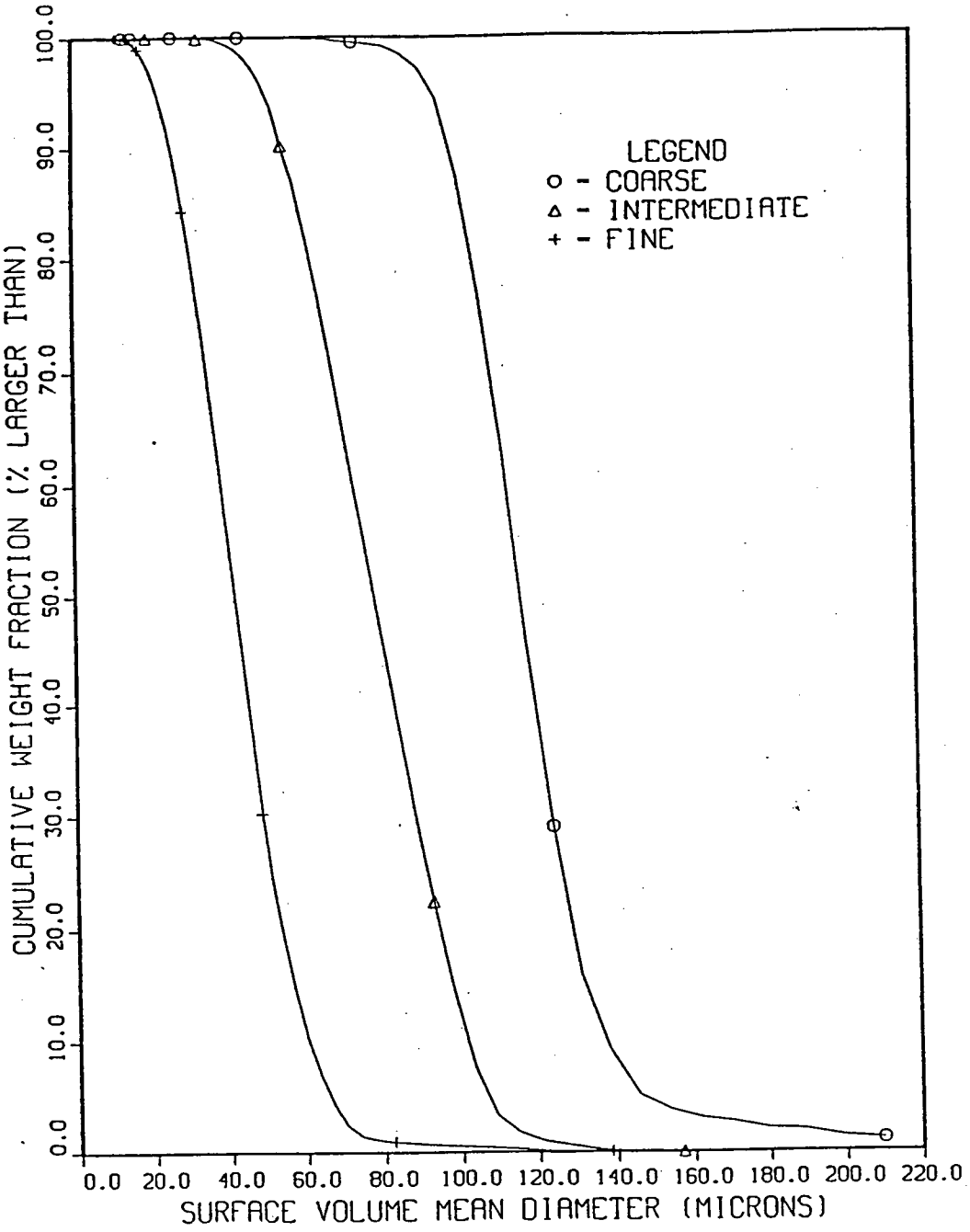

Figure 3.4: Particle Size Distributions for Glass Bead Powders with Narrow Particle Size Distributions.

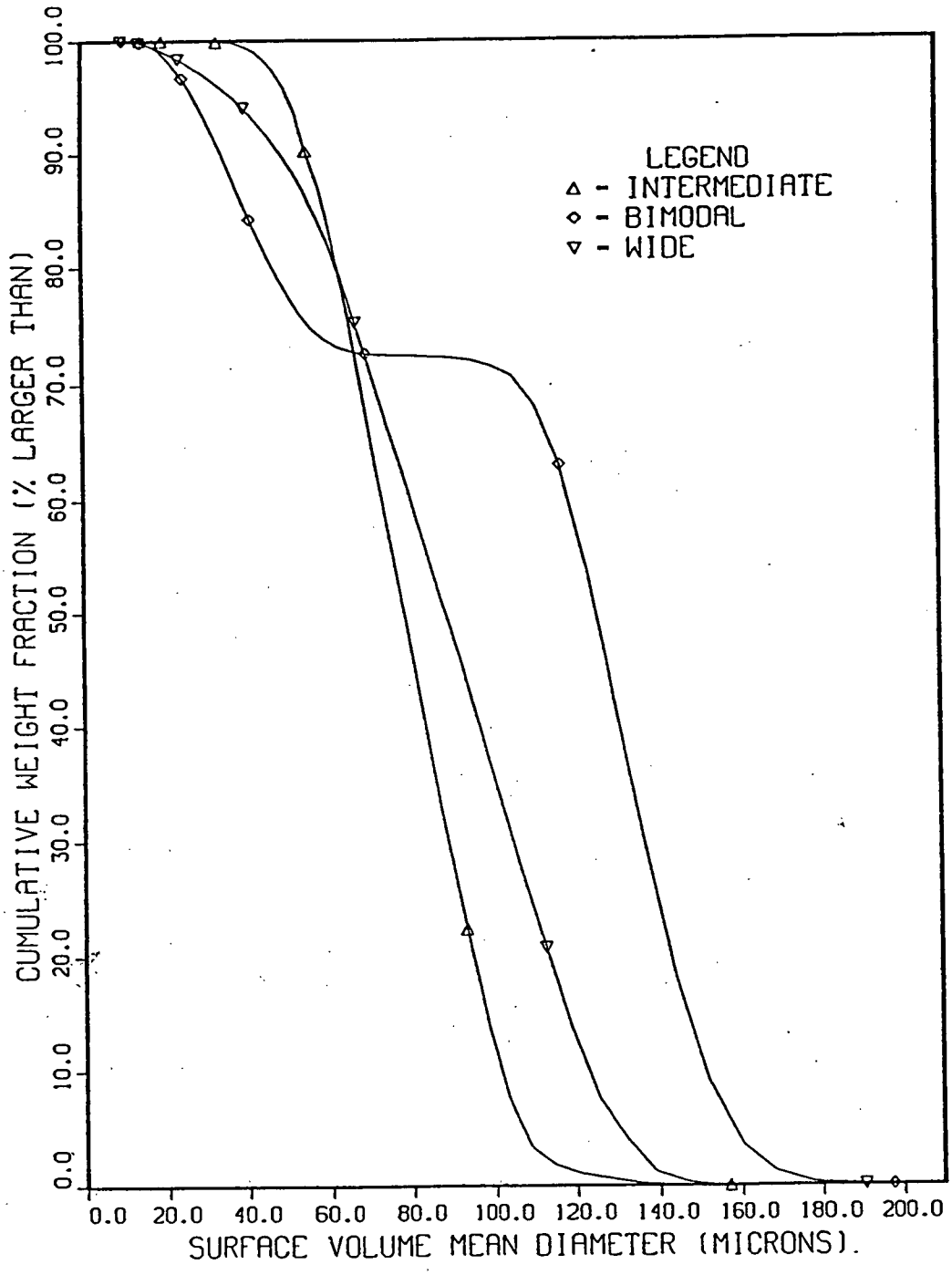

Figure 3.5: Particle Size Distributions for Glass Bead Powder with Similar Mean Surface-volume Mean Particle Diameters.

powder and Group B powder.

Khoe (1988b) found that the particles from all the FCC distributions are quite free-flowing. However, the glass beads appeared to be sticky, especially the intermediate fraction and, even more so, the fine fraction. Khoe examined the powders using microscopy and found that the glass bead particles from the intermediate and fine fractions stuck to each other with a web-like formation. Streaks of particles spread out in all directions. The FCC particles did not show any significant cohesivity when examined under the microscope. Strong interparticle forces are characteristic of Group C powders. This means that the intermediate and fine fractions of glass beads may have some Group C characteristics although they are Group A powders according to Geldart's classification.

3.4 Low Velocity Fluidization

The minimum fluidization and minimum bubbling velocities were measured for each powder. The low flow stream, measured and controlled by 'R2' and 'V2', was used to control the flow of air into the main column. The bed was filled with powder to a certain height which should be constant throughout the experiment. Solenoid valves 'SV1' and 'SV2' were triggered so that they were open and closed respectively. Three-way valve 'V3' was adjusted so that air passed through the low flowrate path. Before any readings were taken, the bed of powder was well mixed for a few minutes with the air flowrate well beyond that corresponding to the minimum bubbling point. The air supply was then shut off. The bed settled to a static bed height. The air flow was then increased in small increments. For each flowrate, about two minutes were allowed to ensure a steady air flow through the column before readings were taken. The following readings were taken when steady state was reached: rotameter 'R2' reading, gauge pressure inside the plenum chamber, pressure drop across the bed and bed height. The rotameters were calibrated

under atmospheric pressure. The actual volumetric gas flowrate was calculated using the plenum chamber pressure and bed pressure. The dry bulb and wet bulb temperatures of air inside the system were measured at a location between 'R2' and 'SV1' and the relative humidity was close to 50% throughout the experiments. The ambient pressure was also recorded. The point where bubbles first appear was noted. The first part of these experiments was finished when the air velocity reached two to three times the minimum bubbling velocity.

The second part of the experiments was basically the same as the first one, except that it was performed by decreasing the air velocity. Between data points, the bed of powder was well mixed at a superficial velocity about twice the minimum bubbling velocity. The same set of measurements was made for each air flowrate. The point where bubbles were last seen was noted.

The results were used to generate plots of bed pressure drop and bed height versus air velocity for both increasing and decreasing air velocity. The minimum fluidization point was obtained from the plot of bed pressure drop versus decreasing air velocity. The plot should contain two linear sections as shown in Figure 1.3, the intersection of these linear sections giving the minimum fluidization point. The minimum bubbling point is taken as the average of the points where bubbles first appeared (increasing velocity) and where bubbles were last seen (decreasing velocity), these points were in general within 6% of each other.

3.5 Collapse Test

Collapse tests were performed with a wide range of superficial gas velocity: from about 1.5 mm/s to 40 mm/s.

As in the previous experiment, the powder was well mixed before each run. The

gas flowrate was then adjusted to the desired value. For air velocities below 10 mm/s, rotameter 'R2' served as the flow indicator. For higher flowrates, 'R2' was bypassed and 'R1' became the flowrate indicator. The gauge pressure inside the plenum chamber was recorded. At the start of the collapse test, the operator turned off both solenoid valves. Hence no more air could go through 'SV1' and into the main column while 'SV2' was open. The air flow from the plenum chamber through 'SV2' to the outside was controlled by adjusting valve 'V5'. The operator adjusted 'V5' in order to minimize the pressure difference across the distributor. This pressure drop was indicated on a water manometer. The purpose of this was to limit the airflow through the distributor during the collapse test. This procedure was repeated three or four times for each gas flowrate.

The course of the bed collapse was recorded using a Sony Betamax videocamera. A stopwatch and a metric tape were placed on the side of the main column to indicate the time and the bed height.

3.6 Pressure Fluctuations

The instantaneous pressure was measured at a height 27 mm above the distributor for a total bed height of about 0.5 m. The reference point for the pressure measurements was in the expansion zone. The pressure was measured using the DISA pressure transducer. The results were recorded on a chart recorder at a paper speed of 6.7 or 13.3 mm/s. Pressure fluctuations were measured for the following FCC size distributions - original, wide, intermediate and bimodal. Four different superficial velocities ranging from 0.036 to 0.259 m/s were used for each distribution of powder.

Similar measurements were made at a location 0.18 m above the distributor. For these measurements, a separate glass section of height 0.15 m and diameter 0.10 m was added to the bottom of the main column. The results were also recorded on videotape

for future reference. Pressure measurements were not made at other bed levels because of the difficulty in drilling holes in the glass column.

3.7 Sources of Experimental Errors

The daily variations of air temperature and relative humidity were less than 2°C and 5%, respectively, throughout the experiments. The temperature of air leaving the fluidization column was within 1°C of that entering the column. No significant change (less than 5%) in the relative humidity of air was noticed when it was passed through the fluidized bed.

Ideal collapse tests require an instantaneous stoppage of fluid flow into and out of the grid the moment the test starts. However, in these experiments, a small amount of gas flow through the distributor occurred for a short period of time after the bed collapse had started. It usually took the operator about 1 s to equalize the pressure across the distributor. The 'bubble escape stage' usually lasted for 2 to 4 s and the usual collapse times were about 5 to 10 s for the glass beads and 10 to 20 s for the FCC powders. Hence the error introduced was probably small.

Additional errors might be introduced by the DISA pressure tranducer and the chart recorder when the fluidized bed pressures were measured. The instruments were calibrated regularly before the start of each experiment. The calibration curves showed changes of less than 4%. The linearity of the instruments was excellent with coefficient of correlation of at least 0.999 in the calibration curves.

Chapter 4

Results and Discussion: Low Velocity Fluidization

4.1 Minimum Fluidization Velocity

The experimental results for minimum fluidization velocity are shown in this section. Minimum fluidization plots for individual size distributions are given in Appendix A. Results for different static bed heights are compared. Empirical correlations are examined to test their validity. Appendix B shows the predicted terminal settling velocities which are needed to predict some fluidization properties of the powders.

4.1.1 Fluid Cracking Catalyst

The minimum fluidization points for all the FCC distributions were clear and reproducible. Though the surface-volume mean particle diameters for some powders examined were smaller than those used by most other workers, problems in defining the minimum fluidization conditions were never encountered in our experiment. Instead, there was always a clear transition on the plots of bed pressure drop versus gas velocity with two distinctly linear regions when the gas flow was increased or decreased.

The experiments with the original and intermediate powders were repeated a few times over a period of three months. For both distributions, the variations of minimum fluidization velocity and voidage were less than $\pm 1.5\%$ and $\pm 0.6\%$ of their respective means. These variations might have been introduced by simple experimental errors such as minor fluctuations of fluid flow and errors in the bed height measurement due to

uneven bed surface.

Increasing the mean particle diameter increased the minimum fluidization velocity of the powder as expected. The minimum fluidization voidage was found to increase as the mean particle diameter decreased as shown in Tables 4.1 and 4.2. Among the three size distributions having essentially the same mean particle diameter (labelled 'intermediate', 'wide' and 'bimodal'), the surface-volume mean diameter and the particle density differ by as much as 1.7% ($0.9\mu m$) and 2.2%, respectively, which can theoretically result in about 5% changes in U_{mf} (estimated using equations 1.4-1.6). The variation of particle density and mean particle diameter can also cause minimum fluidization voidage to change by about 5% which is evaluated from the theoretical variation of U_{mf} using Ergun's equation (1.1). The particle size distribution was found to affect U_{mf}. The wide distribution has significantly lower U_{mf} (7-13%) than the bimodal distribution and the intermediate fraction with the latter two having roughly the same U_{mf} (less than 3% difference). The minimum fluidization voidages for all three size distributions differ by less than 4.5% which is not significant.

Static bed height is not a factor in the determination of minimum fluidization velocity. When the bed height to diameter ratio changes from 3.3 to about 4.4, there is no definite shift in the U_{mf} of FCC powders and the difference in U_{mf} is mostly less than 3%. Frantz (1966) claimed that the bed height does not affect U_{mf} as long as the bed height to diameter ratio is larger than two.

In a packed bed, the bed pressure drop increases as superficial velocity increases. At minimum fluidization, the weight of the bed should be completely supported by the air flow. Table 4.1 shows that the bed pressure drop at minimum fluidization is within 2% of the predicted value for FCC. Static bed height is not a factor. Generally, a fluidized bed is regarded to having uniform gas distribution when the experimental bed pressure drop is within 5% of the pressure exerted by the weight of powders on the distributor

Table 4.1: Minimum Fluidization Data for Fluid Cracking Catalyst. Static bed heights are 3.3 and 4.4 times the bed diameter

Size Distribution	$H_o = 3.3D$		$H_o = 4.4D$	
	Experimental U_{mf} (m/s)	$\frac{exp'l \Delta P_{mf}}{pred. \Delta P_{mf}}$	Experimental U_{mf} (m/s)	$\frac{exp'l \Delta P_{mf}}{pred. \Delta P_{mf}}$
Original	0.00208	0.99	0.00214	0.99
Coarse	0.00553	1.00	0.00585	0.99
Intermediate	0.00285	0.99	0.00275	0.98
Fine	0.00151	1.00	0.00153	1.00
Wide	0.00250	0.99	0.00257	0.99
Bimodal	0.00287	0.99	0.00282	0.99

Table 4.2: Experimental Values of Minimum Fluidization Voidage for FCC at Different Static Bed Heights

Size Distribution	Experimental ϵ_{mf}		
	$H_o = 3.3D$	$H_0 = 4.4D$	Difference due to Change in H
Original	0.497	0.491	-1.2%
Coarse	0.478	0.473	-1.0%
Intermediate	0.501	0.497	-0.8%
Fine	0.554	0.546	-1.4%
Wide	0.479	0.475	-0.8%
Bimodal	0.483	0.483	0.0%

plate. No channels were visible during fluidization of FCC powders. Bubbles were fairly uniformly distributed as they reached the bed surface. The cardboard distributor plate provided better gas distribution than other types of distributor such as the metal screen or perforated plate.

Among the correlations for U_{mf} considered here, the one proposed by Baeyens and Geldart (1973) gave the best results. As shown in Table 4.3, Baeyens and Geldart's prediction is less than 20% different from the actual values of U_{mf}. Other correlations produced predictions that differ from the experimental data by as much as 150%.

All the correlations for minimum fluidization velocity predict that U_{mf} is proportional to about the square of the mean particle diameter for small particles. When all the size distributions of FCC used in the experiment are included, the following relationship is obtained:

$$U_{mf} \quad \alpha \quad d_{sv}^{1.46} \tag{4.1}$$

If only the powders with larger mean particle size (i.e. coarse, intermediate, original, bimodal and wide distributions) are considered, then:

$$U_{mf} \quad \alpha \quad d_{sv}^{1.62} \tag{4.2}$$

This indicates that the dependence of minimum fluidization velocity is reduced for smaller particles, similar to the findings of Simone and Harriott (1980) who explained that the large deviation for the smallest size was largely due to the higher minimum fluidization voidage for the fine powder (Table 4.2).

A low dependence of minimum fluidization velocity on the surface-volume mean particle diameter has also been obtained by Frantz (1966). He argued that the deviation was caused by the use of powders with wide size distributions. Most of the correlations previously shown were developed for narrow size distribution powders. His argument is not substantiated by the results collected here. When only the coarse, intermediate and

Table 4.3: Predicted Minimum Fluidization Velocities for FCC Powders. Bracketted Values are the Ratio of Predicted to Experimental Values.

Size Distribution	Predicted U_{mf} (m/s)			
	Ergun (1952)	Wen and Yu (1966)	Baeyens and Geldart (1973)	Davies and Richardson (1966)
Original	0.00178 (0.85)	0.00182 (0.87)	0.00191 (0.91)	0.00273 (1.31)
Coarse	0.00584 (1.06)	0.0133 (2.43)	0.00554 (0.97)	0.00623 (1.10)
Intermediate	0.00250 (0.87)	0.00502 (1.77)	0.00259 (0.92)	0.00267 (0.95)
Fine	0.00110 (0.72)	0.00167 (1.10)	0.00124 (0.80)	0.00117 (0.75)
Wide	0.00244 (0.97)	0.00278 (1.11)	0.00253 (1.01)	0.00260 (1.02)
Bimodal	0.00255 (0.88)	0.00318 (0.87)	0.00264 (1.04)	0.00272 (1.07)

fine fractions are considered, then:

$$U_{mf} \quad \alpha \quad d_{sv}^{1.45} \tag{4.3}$$

The index actually drops when only the narrow size distributions are considered. It should be recalled that the particle density of FCC changes from one size fraction to another. This could also contribute to the difference between the theoretical and experimental degrees of dependence.

4.1.2 Glass Beads

The minimum fluidization properties for glass beads are shown in Table 4.4. The minimum fluidization points were also very easy to identify from the plots of bed pressure drop versus superficial velocity. With decreasing mean particle diameter, U_{mf} decreased and ϵ_{mf} increased. ϵ_{mf} is generally smaller for glass beads than for the corresponding FCC fractions. The particle size distribution of the glass beads had a significant influence on U_{mf}. Among the intermediate, wide and bimodal distributions, the difference in surface-volume mean diameter was 1.7% which can theoretically cause 3.4% change in U_{mf} and 5% in ϵ_{mf}. However, the difference in U_{mf} was as much as 68%, with the intermediate fraction having the highest and the bimodal distribution the lowest values of U_{mf}. The minimum fluidization voidage follows the same pattern. These are very significant differences, and they cannot be accounted for by the small difference in mean particle diameter.

The uniformity of the gas distribution in the fluidized bed was more of a problem for the glass beads. The difference between the experimental bed pressure drop at minimum fluidization and the predicted value was as much as 5% which was still acceptable. Some channels, 30 mm long at most, were occasionally visible when the glass beads were fluidized. The bubble distribution was fairly uniform on the bed surface for the bubbling

Table 4.4: Experimental Minimum Fluidization Data for Glass Beads

Size Distribution	ϵ_{mf}	U_{mf} (m/s)	$\frac{exp'l \Delta P_{mf}}{pred. \Delta P_{mf}}$
Coarse	0.442	0.0118	0.99
Intermediate	0.479	0.00588	0.99
Fines	0.495	0.00164	0.95
Wide	0.444	0.00501	1.00
Bimodal	0.406	0.00350	1.00

regime. Hence the gas distribution was satisfactory for the fluidization of glass beads. The difference between the two types of material studied is the low ϵ_{mf} of the glass beads bed compared to the FCC. The particle density of the glass beads is also about 80% higher than that of the FCC. The glass bead fractions also showed some stickiness as observed by Khoe (1988), making the powder harder to fluidize and more prone to channelling.

The correlations for U_{mf} do not do as well for the glass beads as for FCC. As shown in Table 4.5, all but one of the predictions are at least 28% off the experimental values. None of the correlations provides satisfactory predictions for all distributions of glass beads.

The dependence of U_{mf} on surface-volume mean particle diameter is significantly higher for the glass beads than for the FCC. The following relationship is obtained when all the size distributions of glass beads are considered:

$$U_{mf} \quad \alpha \quad d_{sv}^{1.75} \tag{4.4}$$

There is no significant difference when only the narrow size fractions (coarse, intermediate and fine) are included:

$$U_{mf} \quad \alpha \quad d_{sv}^{1.79} \tag{4.5}$$

The index goes up to beyond 2 when the size fraction with the smallest mean particle diameter is excluded:

$$U_{mf} \quad \alpha \quad d_{sv}^{2.09} \tag{4.6}$$

Simone and Harriott's explanation (1980) that the smallest particles are mainly responsible for lowering the dependence of U_{mf} on the surface-volume mean diameter appears to be correct for glass beads. It should be pointed out that the lowest mean particle size among the glass bead fractions was 71 μm when the fine distribution is excluded while

Table 4.5: Predicted Minimum Fluidization Velocities for Glass Bead Powders. Bracketted values are the ratio of predicted to experimental values.

Size Distributions	Predicted U_{mf} (m/s)			
	Ergun (1952)	Wen and Yu (1966)	Baeyens and Geldart (1973)	Davies and Richardson (1966)
Coarse	0.0190 (1.63)	0.0200 (1.72)	0.0164 (1.41)	0.0203 (1.75)
Intermediate	0.00787 (1.37)	0.00568 (0.98)	0.00740 (1.28)	0.00840 (1.46)
Fine	0.00208 (1.28)	0.00084 (0.51)	0.00224 (1.38)	0.00222 (1.37)
Wide	0.00771 (1.56)	0.00622 (0.65)	0.00725 (1.46)	0.00821 (1.66)
Bimodal	0.00795 (2.33)	0.00643 (1.87)	0.00747 (2.18)	0.00849 (2.49)

it was 53 μm for the FCC. Even the intermediate fraction of FCC is probably too fine to have the expected dependence of U_{mf} on the mean particle size.

4.2 Bubble-Free Bed Expansion

4.2.1 Fluid Cracking Catalyst

Bubble-free bed expansion data are shown in Table 4.6. The correlations provided by Abrahamsen and Geldart (1980a) (equation 1.9) indicated that decreasing the mean particle size should increase the maximum bubble-free expansion, ϵ_{mb}, of a batch of powder. The narrow size distribution fractions are considered first. Going from the coarse ($d_{sv} = 83\mu m$) to the intermediate ($d_{sv} = 53\mu m$) to the fine ($d_{sv} = 34\mu m$) fractions, the maximum bubble-free voidage increases by 10% and 12% respectively. The maximum variation of maximum bubble-free bed voidage when experiments were replicated was $\pm 0.4\%$ of the mean. Hence the effect of mean particle diameter on ϵ_{mb} is very significant. Changing the static bed height does not seem to affect the maximum bubble-free bed voidage significantly.

As mentioned in Section 1.2.2, the bubble-free bed expansion may depend on the elasticity coefficient which in turn depends on the number of contact points among particles. For the same volume of powder, the number of contact points for the fine fraction is obviously more than for the coarse fraction. Therefore the powder with a smaller surface-volume mean particle size expands more than that with a larger mean particle size.

Mutsers and Rietema (1977) mentioned that powder of wide size distribution has more contact points per unit volume than a powder with a narrow size distribution. Hence the wide distribution powder is expected to expand more homogenously than the intermediate distribution. In our experiments, while the maximum bubble-free voidages

Table 4.6: Bed Voidages at Minimum Bubbling and Corresponding Fractional Bubble-Free Bed Expansion Data for Different FCC Size Distributions at Different Static Bed Heights.

Size Distribution	Minimum Bubbling Voidage (ϵ_{mb})		Fractional Bed Expansion ($\frac{\epsilon_{mb}-\epsilon_{mf}}{\epsilon_{mf}}$)	
	$H_o = 3.3D$	$H_o = 4.4D$	$H_o = 3.3D$	$H_o = 4.4D$
Original	0.558	0.550	0.123	0.120
Coarse	0.505	0.500	0.056	0.057
Intermediate	0.549	0.548	0.096	0.100
Fine	0.617	0.613	0.114	0.123
Wide	0.528	0.530	0.102	0.116
Bimodal	0.528	0.529	0.093	0.095

(ϵ_{mb}) of the wide and bimodal FCC powders differed by only 0.4% from each other, they were about 3.6% less than that of the intermediate distribution. However, these three distributions have slightly different mean particle diameters (1.7%) and particle densities (2.2%) which, in theory (estimated using equation 1.12), can result in a 3% change in ϵ_{mb}. Since the variation of ϵ_{mb} determined in replicated measurements was 0.4%, the difference in ϵ_{mb} has to be at least 3.5% in order to be significant. Hence, increasing the spread of particle size distribution significantly lowers the minimum bubbling voidage.

The wide distribution actually had significantly higher fractional bed expansion (6-16%) than the intermediate FCC powder. The ratio of interparticle void volume to bulk volume of solids is normally higher for a powder with narrow size distribution. Even though the fractional bed expansion may be larger for the wide distribution powder, it may not be enough to make up the difference in static bed voidage so that the wide distribution has a higher maximum bubble-free voidage than the intermediate fraction.

The bimodal powder contains 67.5% by weight of coarse fraction and 32.5% of fine fraction. Compared to the wide FCC distribution, the bimodal distribution has higher fines fraction which promotes bubble-free bed expansion. On the other hand, the higher coarse content in the bimodal distribution powder discourages such expansion. The overall result is that the coarse powder predominates and the bimodally distributed powder has significantly lower fractional bubble-free expansion when compared with the wide fraction of FCC.

The wide distribution powder expands 4-6% less than the original FCC powder. The principal difference between these two powders is the higher coarse particle content in the wide distribution. Bubble-free expansion is reduced with the addition of coarse powder. Of course, one has to be careful in comparing these two powders because the wide distribution has a somewhat higher mean particle diameter than the original material.

4.2.2 Glass Beads

With the glass beads, the minimum bubbling voidage and the fractional bubble-free bed expansion again increase as the mean particle size decreases (Table 4.7). Though the coarse fraction falls barely into the Geldart's Group B powder category, it still expands to a small but significant extent. This simply shows that the change in fluidization behavior from Group A to Group B powders is gradual rather than stepwise. The difference in maximum bubble-free bed expansion between the coarse and the intermediate fractions is much less than that for FCC. This trend persists when the intermediate and the fine fractions are compared. This may be caused by the change in particle density, ϵ_{mf} and U_{mf}. In general, the mean particle sizes of the corresponding FCC fractions are smaller than those of the respective fractions of glass beads. It is therefore natural that the former would expand more before reaching U_{mb} than the latter. However, it should also be noted that the intermediate and fine fractions of the glass beads appeared to be quite sticky. The interparticle forces for these fractions may be greater than the forces the fluid can exert on the particles. Hence some channelling occurs when fluidizing these glass bead fractions and the powders do not expand as much as expected.

The intermediate, bimodal and wide distributions differ in mean particle diameter by 1.7% which can theoretically cause a deviation with the same magnitude in ϵ_{mb} among the three powders. This plus the experimental variations from replicated measurements imply that the difference in ϵ_{mb} for these size distributions must be at least 2.5% in order to be significant. The intermediate powder was found to have a significantly higher maximum bubble-free bed expansion (3.7%) than the wide distribution though the latter had a higher fractional bed expansion as predicted by Mutsers and Rietema (1977). Again this is due to the much higher ϵ_{mf} of the intermediate compared to the wide distribution powders. The bimodal distribution had a ϵ_{mb} value 3% less than for the wide

Table 4.7: Bed Voidage at Minimum Bubbling and Corresponding Fractional Bubble-Free Bed Expansion for Glass Bead Powders.

Size Distribution	ϵ_{mf}	Minimum Bubbling Voidage (ϵ_{mb})	Fractional Bed Expansion $(\frac{\epsilon_{mb}-\epsilon_{mf}}{\epsilon_{mf}})$
Coarse	0.442	0.452	0.023
Intermediate	0.479	0.492	0.027
Fine	0.495	0.516	0.042
Wide	0.444	0.474	0.068
Bimodal	0.406	0.460	0.133

distribution, and this difference is also significant. However, the bimodally distributed glass beads expanded fractionally about 100% more than the wide distribution and that is different from the results for FCC. The relative trend of fractional bed expansion between the wide and narrow size distributions appears to be generally true for Group A powders. However, the fractional bubble free expansion of the bimodal distribution relative to the other fractions should be treated cautiously. The bimodal distribution is made up of two other size fractions whose proportions change according to the desired mean particle diameter. For some systems, the coarse particles predominate as in the case of FCC and the overall result is that the bed expands fractionally less than a wide and continuous size distribution powder with the same mean particle diameter. For other systems, the fine fraction predominates as in the case of glass beads, and the mixture expands fractionally more than the corresponding wide size distribution powder. The order of maximum bubble-free bed voidage (ϵ_{mb}) for different size distributions also should not be generalized because it depends very much on the difference in static bed voidage as well as fractional bed expansion among the various size distributions.

Another interesting point is that both the wide and the bimodal distributions of glass beads expand fractionally more than the fine fraction by a significant 50-200%. The mean particle diameters of the wide and bimodal distribution powders are almost twice that of the fine fraction so that one would expect the fine fraction to expand more. However, the interparticle forces are so strong in the fine fraction that channelling occurs. When a small amount of fines is added to a powder of much larger particle diameter, the fines fill up the interparticle spaces between the larger particles. The overall attraction forces among the particles in this powder are then stronger than among big particles only, but weaker than among fine particles only. This makes the powder less sticky than the fine fraction so that channelling is less likely to occur. The powder then has a chance to expand evenly. The stronger attraction forces of the wide size spectrum powder enable

a higher degree of expansion compared to a powder of similar mean particle size but narrow size spectrum.

4.3 Minimum Bubbling Properties

4.3.1 Fluid Cracking Catalyst

Minimum bubbling velocities for FCC are shown in Table 4.8. The minimum bubbling points for the FCC were very easy to identify. At gas velocities just below U_{mb}, numerous tiny air jets could be seen on the bed surface resembling the appearance of volcanoes. This must not be mistaken as the minimum bubbling point. At the minimum bubbling point, gross bubbling appeared at three or more areas on the bed surface. The bubble distribution was uniform and widespread with no gas maldistribution. The maximum fluctuations in U_{mb} and ϵ_{mb} determined in replicated measurements were $\pm 3\%$ and $\pm 0.4\%$ of their respective means.

As the mean particle diameter decreased from 83μm (coasrse fraction) to 34μm (fine fraction), the minimum bubbling velocity decreased by 62%. However, the minimum bubbling voidage (see Table 4.6) was found to increase by 22%.

The minimum bubbling properties were affected by the particle size distribution. Theoretically, the differences in mean particle size and particle density among the intermediate, wide and bimodal distributions can cause changes of 2% in U_{mb} and 3% in ϵ_{mb} (estimated using equations 1.10 and 1.12). That means the difference in U_{mb} has to be over 5% in order to be significant since the maximum variation of U_{mb} was 3% when experiments with the same powder were replicated. The bimodal distribution has significantly higher U_{mb} than the intermediate fraction (9-11% difference). However, the U_{mb} of the wide distribution does not differ significantly from either the intermediate (narrow) or the bimodal distributions. It was pointed out in Section 4.2 that increasing

Table 4.8: Experimental Minimum Bubbling Properties for Different FCC Size Distributions.

Size Distribution	$U_{mb}(m/s)$		Effect of Increase in Static Bed Height	
	$H_o = 3.3D$	$H_o = 4.4D$	ΔU_{mb}	$\Delta \epsilon_{mb}$
Original	0.00456	0.00449	-1.6%	-1.4%
Coarse	0.00890	0.00857	-3.7%	-1.0%
Intermediate	0.00503	0.00514	2.2%	-0.2%
Fine	0.00371	0.00383	3.2%	-1.0%
Wide	0.00531	0.00533	0.4%	0.4%
Bimodal	0.00550	0.00570	3.6%	0.2%

the spread of particle size distribution significantly lowers the minimum bubbling voidage of FCC powders. Changing the static bed height does not seem to have a definite effect on the minimum bubbling velocity or minimum bubbling voidage.

Except for the fluidization of Group C powders, increasing the ratio of U_{mb}/U_{mf} is generally considered to result in an improvement in the quality of fluidization, meaning smaller pressure fluctuations and smaller gas bubbles. Larger ratios signify more importance of the bubble-free regime.

Table 4.9 shows that the velocity ratio is well over one for all the FCC powders. When the mean particle size decreases, the quality of fluidization becomes better. Particle size distribution also affects the quality of fluidization. It is normally expected that the addition of fines results in smoother fluidization by reducing gas maldistribution and enhancing dense phase gas flow . The velocity ratio for the wide size distribution is significantly higher (11-20%) than for the intermediate (narrow cut) distribution. Correspondingly, the fluidization is generally better in powders with wide size spectra than in those of narrow particle size spread. There is no significant difference in U_{mb}/U_{mf} between the bimodal distribution and either the intermediate or the wide distributions even though the the bimodal distribution has a distinctly higher U_{mb} than the intermediate fraction.

The predicted minimum bubbling properties are shown in Table 4.10. The simpler correlation for U_{mb} (equation 1.10, Geldart and Abrahamsen (1978)) gives much better predictions than the more complicated (equation 1.11, Abrahamsen and Geldart (1980a)). Ironically, the latter which takes the fines fraction into consideration produces the worst prediction for the fine fraction of the FCC. These results do not support Abrahamsen and Geldart's (1980a) belief that the more extensive correlation should be used when the weight fraction of powder with particle diameter of less than 45 μm exceeds 15%. In general, the simple correlation predicted U_{mb} to within 10% of the actual value. Foscolo's

Table 4.9: Ratios of Minimum Bubbling Velocities to Minimum Fluidization Velocities for Different FCC Size Distributions.

Size Distribution	$\frac{U_{mb}}{U_{mf}}$	
	$H_o = 3.3D$	$H_o = 4.4D$
Original	2.19	2.10
Coarse	1.61	1.46
Intermediate	1.76	1.87
Fine	2.46	2.50
Wide	2.12	2.07
Bimodal	1.92	2.02

Table 4.10: Predicted Values of Minimum Bubbling Velocities and Voidages for Different Size Distributions of FCC. Bracketted values are the ratios of the predicted to the experimental values.

Size Distribution	F_{22}	F_{45}	U_{mb} (m/s)		ϵ_{mb}
			Geldart and Abrahamsen (1978)	Abrahamsen and Geldart (1980a)	Foscolo (1983)
Original	0.0087	0.357	0.00450 (0.99)	0.00619 (1.37)	0.507 (0.92)
Coarse	0.0000	0.0124	0.00833 (0.96)	0.00887 (1.02)	0.393 (0.71)
Intermediate	0.0000	0.0992	0.00532 (1.05)	0.00612 (1.21)	0.465 (0.85)
Fine	0.0031	0.885	0.00341 (0.90)	0.00694 (1.85)	0.572 (0.93)
Wide	0.0050	0.188	0.00531 (1.00)	0.00652 (1.22)	0.470 (0.91)
Bimodal	0.0003	0.294	0.00540 (0.97)	0.00712 (1.28)	0.463 (0.88)

(1983) correlation for ϵ_{mb} (equation 1.12) worked well for powders of small mean particle diameter giving predictions within 15% of the true values. For the coarse fraction, the predictions are out by as much as 29%.

4.3.2 Glass Beads

The minimum bubbling results for the glass beads are given in Table 4.11. The minimum bubbling points for most size distributions were again quite distinct except for the fine fraction where localized bubbles appeared at gas velocities just beyond U_{mf}. The strong interparticle forces between these fine particles makes bubble-free bed expansion uneven. The values of minimum bubbling velocity and voidage given here correspond to where bubbles were seen over most of the bed surface. This involved some subjective judgement so that the results for this fraction should be treated with caution.

As for FCC, the minimum bubbling velocity of the glass beads goes down while the minimum bubbling voidage (see Table 4.7) goes up with decreasing mean particle size. The theoretical variations of U_{mb} caused by small difference in mean particle diameter among the intermediate, wide and bimodal distributions are less than 1.7%. For the distributions with similar mean particle diameter, the minimum bubbling velocities of the bimodal and wide distributions differ by 2.2% which is not significant because it has the same magnitude as the maximum fluctuations of U_{mb} determined in replicated measurements. However, the bimodal and wide distributions have minimum bubbling velocities of 13-15% lower than the intermediate (narrow) fraction and that is significant. This differs from the results for FCC. The minimum bubbling velocity of wide FCC powder is higher than that of the corresponding intermediate fraction. As described in Section 1.2.3, the effects of particle size distribution on the U_{mb} is controversial. It seems that U_{mb} may also depend on other particle properties such as particle shape and particle density. Some particles are porous while others are not. The minimum bubbling voidage

Table 4.11: Experimental Minimum Bubbling Data Glass Beads.

Size Distribution	U_{mb} (m/s)	$\frac{U_{mb}}{U_{mf}}$
Coarse	0.0141	1.19
Intermediate	0.00883	1.50
Fine	0.00572	3.49
Wide	0.00769	1.53
Bimodal	0.00752	2.15

may also be a factor. As shown in Section 4.2.2, the wide and bimodal distributions also have significantly lower ϵ_{mb} than the intermediate fraction.

The trends in the U_{mb}/U_{mf} ratio are also different for both materials. Table 4.11 shows that the intermediate (narrow) and the wide distributions of glass beads have essentially the same U_{mb}/U_{mf} ratio (2% difference). The highest ratio occurred for the bimodal distribution of the glass beads rather than the wide distribution as for the FCC. According to Abrahamsen and Geldart (1980b), the U_{mb}/U_{mf} ratio depends on the fines fraction, F_{45}. Since the intermediate fraction has fewer fines than the other distributions, it is expected that it should also have a low U_{mb}/U_{mf} ratio. From this, one would expect a low U_{mb} for the intermediate fraction. However, the intermediate fraction also has the highest U_{mf} and this more than compensates for the effect of the low level of fines. This produces a high U_{mb} for the intermediate fraction. The bimodal distribution has a higher U_{mb}/U_{mf} ratio than the wide distribution. This suggests that the fines portion of the bimodally distributed glass beads prevails.

The predicted minimum bubbling properties of the glass beads (see Table 4.12) are generally not as good as for the FCC (see Table 4.10). The simpler correlation (equation 1.10) for U_{mb} provides predictions that differ by as much as 35% from the experimental values. Foscolo's (1980) predictions of ϵ_{mb} with equation (1.12) are in error by as much as 48%. However, the correlation that takes the fines fraction into consideration provides much better predictions for glass beads than for FCC. The maximum difference between the experimental and predicted values is only 21%. For glass beads with narrow size distribution, this correlation is better than the simple correlation for U_{mb}.

Table 4.12: Predicted Minimum Bubbling Velocities and Voidages for Different Size Distributions of Glass Beads. Bracketted values are the ratios of the predicted to the experimental values.

Size Distribution	F_{22}	F_{45}	U_{mb} (m/s)		ϵ_{mb}
			Geldart and Abrahamsen (1978)	Abrahamsen and Geldart (1980a)	Foscolo and Gibilaro (1983)
Coarse	0.0000	0.000	0.0113 (0.81)	0.0120 (0.86)	0.233 (0.52)
Intermediate	0.0001	0.017	0.00727 (0.84)	0.00784 (0.90)	0.319 (0.65)
Fine	0.102	0.587	0.00374 (0.65)	0.00606 (1.07)	0.466 (0.90)
Wide	0.0114	0.090	0.00719 (0.95)	0.00888 (1.18)	0.321 (0.68)
Bimodal	0.0300	0.184	0.00731 (0.99)	0.00888 (1.21)	0.318 (0.69)

4.4 Summary

With increasing surface-volume mean particle size, U_{mf} increases and ϵ_{mf} decreases. Increasing the spread of particle size distribution with constant mean particle diameter decreases the minimum fluidization voidage and velocity for glass beads. The wide FCC powder has lower U_{mf} than the bimodal and intermediate distributions although all three distributions have similar ϵ_{mf}. Static height does not affect the minimum fluidization properties. The dependence of U_{mf} on the mean particle diameter is stronger for coarser powders (FCC and glass beads). The correlation of Baeyens and Geldart (1973) for U_{mf} is the best for FCC powders.

Both the minimum bubbling voidage and the fractional bubble-free bed expansion increase with decreasing mean particle size. With the mean particle size kept constant, the wide distribution powder has higher fractional bed expansion than with narrow cut (intermediate) fraction although the latter has a higher minimum bubbling voidage.

Different materials have different minimum bubbling properties. Decreasing the mean particle size decreases the minimum bubbling velocity, increases the minimum bubbling voidage and leads to smoother fluidization unless the powder becomes too cohesive. The U_{mb} depends on factors other than the mean particle size and particle size distribution. Increasing the spread of particle size distribution while maintaining a constant mean particle size decreases ϵ_{mb} of both glass beads and FCC.

Chapter 5

Results and Discussion: Dense Phase Properties

As mentioned previously, collapse tests were performed to measure the dense phase properties of some powder fractions. An example of bed height versus time plot from the collapse test of a powder studied in our experiment is shown in Figure 5.1. The linear part in the middle denotes the 'hindered sedimentation stage'. The dense phase bed height is the intercept of this linear portion and the ordinate axis. The superficial collapse velocity is the slope of the linear section of the collapse curve. Since the air pressure above and below the distributor plate are equalized throughout the course of bed collapse, no gas could flow through the distributor in either direction. Thus the bed collapse velocity is essentially the superficial dense phase gas velocity (Geldart and Wong, 1984).

The results were anslyzed with confidence level of 95%. As an example, error bars are shown on the plots for the dense phase properties of FCC with the static bed height 4.4 times bed diameter.

The de-aeration rate of the FCC powders was in general slower than the glass beads, i.e. the former has a longer period of hindered sedimentation. It is sometimes more difficult to identify the linear section on the bed height versus time plot for some glass bead fractions. This creates more uncertainty in the determination of dense phase properties. Three to four runs were performed to minimize the experimental errors and improve the reliability of the data.

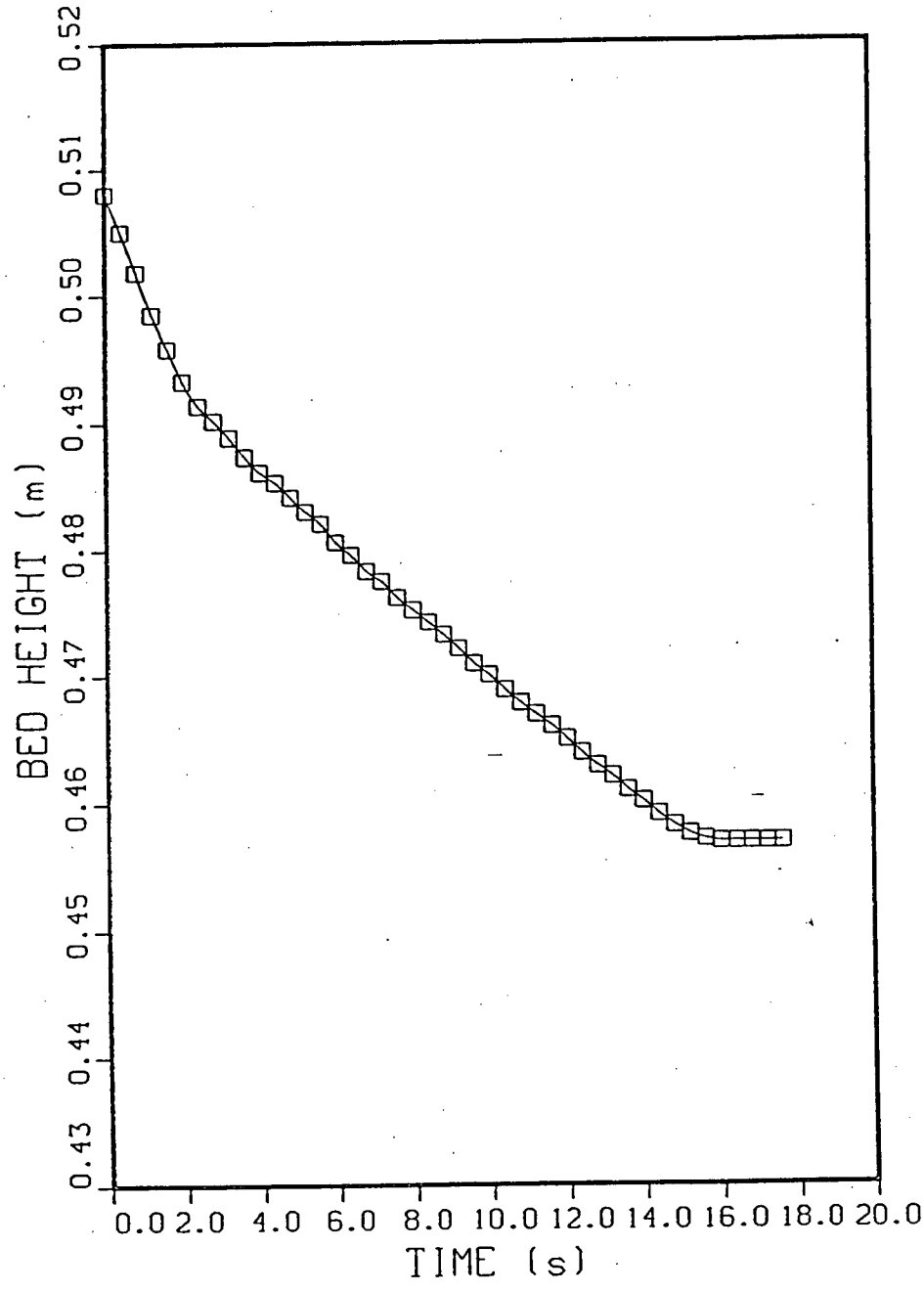

Figure 5.1: Sample Plot of Bed Height Versus Time for Intermediate FCC Powder with Initial Superficial Velocity of 0.0086 m/s.

5.1 Effect of Mean Particle Diameter of Fluid Cracking Catalyst

The collapse test results for the fluid cracking catalyst powder with different surface-volume mean particle diameters are shown in Figures 5.2-5.5. The dense phase superficial velocity and voidage at minimum fluidization are given on the plots as reference points. For all the size distributions of FCC, the dense phase voidage increases as expected when the superficial velocity is increased from U_{mf} to U_{mb}. During this stage, gas flows through the dense phase only.

At about the minimum bubbling point, both the superficial dense phase gas velocity and the dense phase voidage reach their peaks. The interparticle gaps are at their largest. When the superficial velocity is increased beyond this point, bubble-free expansion is no longer possible and bubble formation occurs. Gas is now carried and passed through the bubble phase. This means a drop in superficial dense phase gas velocity. Since the dense phase voidage is related to the dense phase gas flow, both the dense phase gas flow and voidage keep on dropping. Eventually, the values of these two dense phase properties level off and reach limiting values. The amount of dense phase contraction in response to a certain increase in gas velocity depends on the mean particle size when the narrow size fractions (coarse, intermediate and fine) are considered. The extent of contraction increases with decreasing mean particle size. The limiting dense phase voidage and gas flow are also functions of mean particle size, both being higher for larger particles.

The superficial gas velocity was increased to about 38 mm/s which is well beyond U_{mb} for any size fraction. At this flowrate, the dense phase gas velocity and bed voidage hardly changed with increasing gas flow. Therefore the dense phase properties measured at U = 38 mm/s can serve as good estimations for much higher superficial velocities (in the bubbling regime) at which most industrial processes are operated.

The dense phase voidage at high gas flows (Table 5.1) is roughly the same as the

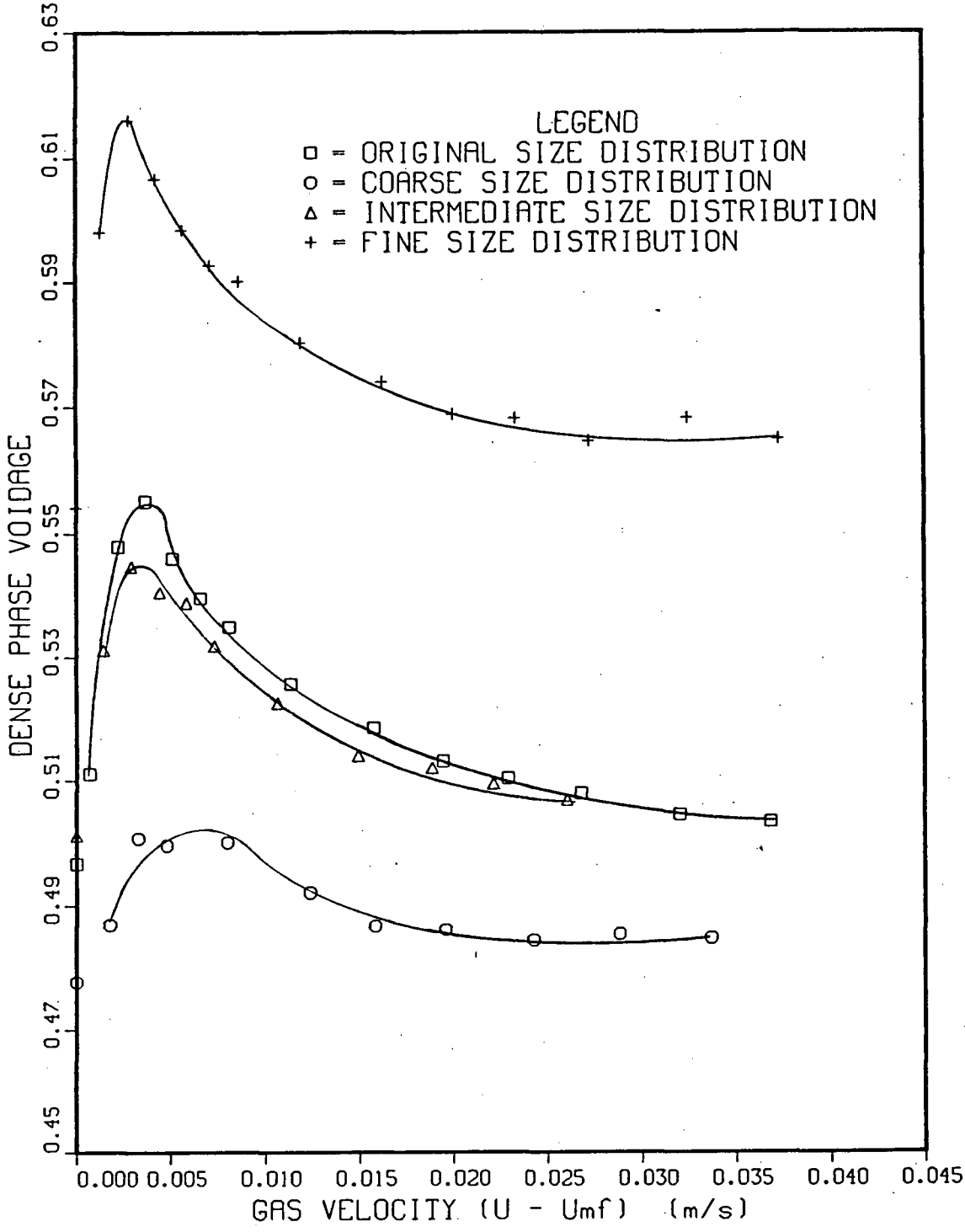

Figure 5.2: Dense Phase Voidages for FCC Powders with Different Surface-Volume Mean Particle Diameters. Static bed height is 3.3 times bed diameter.

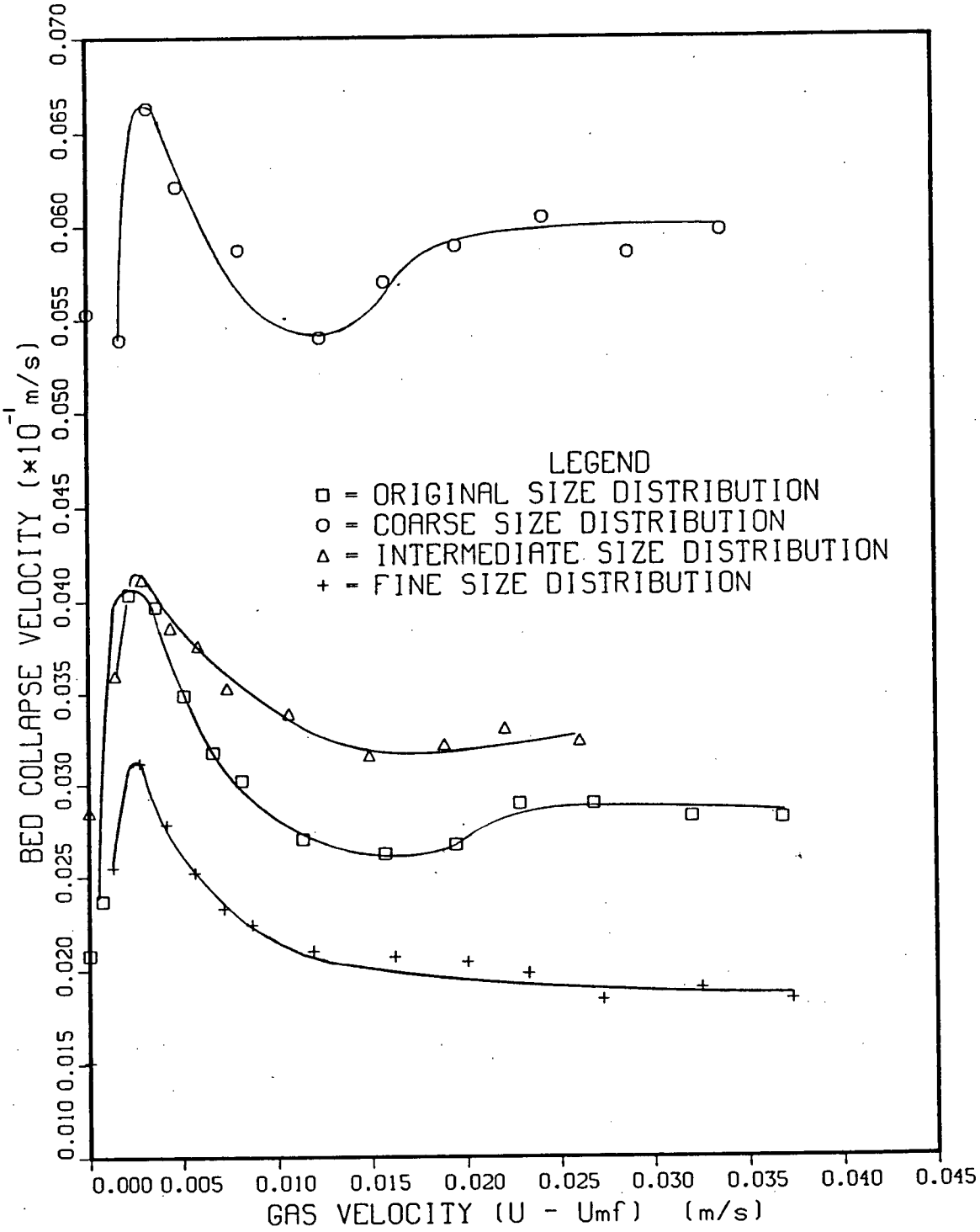

Figure 5.3: Bed Collapse Velocities for FCC Powders with Different Surface-Volume Mean Particle Diameters. Static bed height is 3.3 times bed diameter.

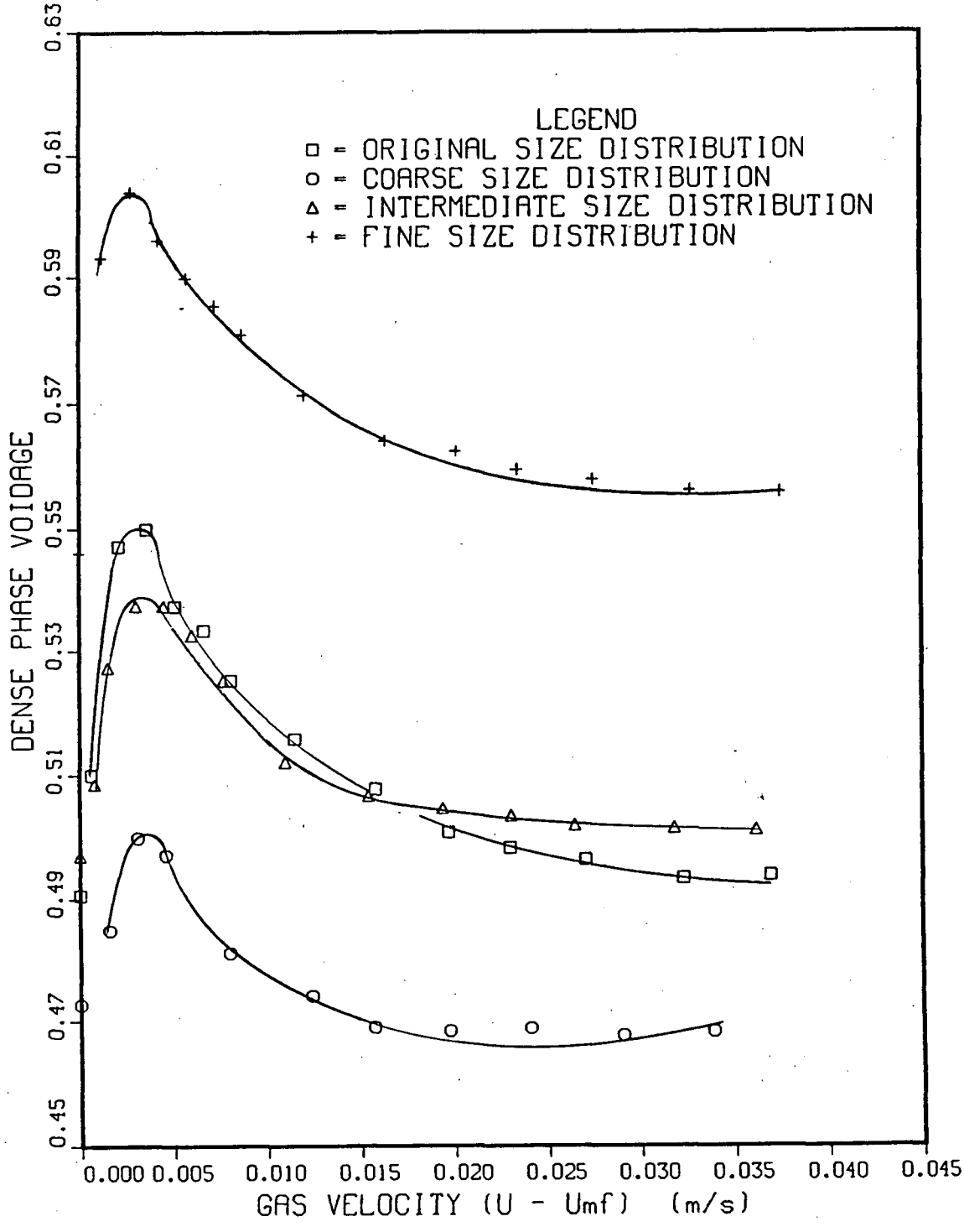

Figure 5.4: Dense Phase Voidages for FCC Powders with Different Surface-Volume Mean Particle Diameters. Static bed height is 4.4 times bed diameter.

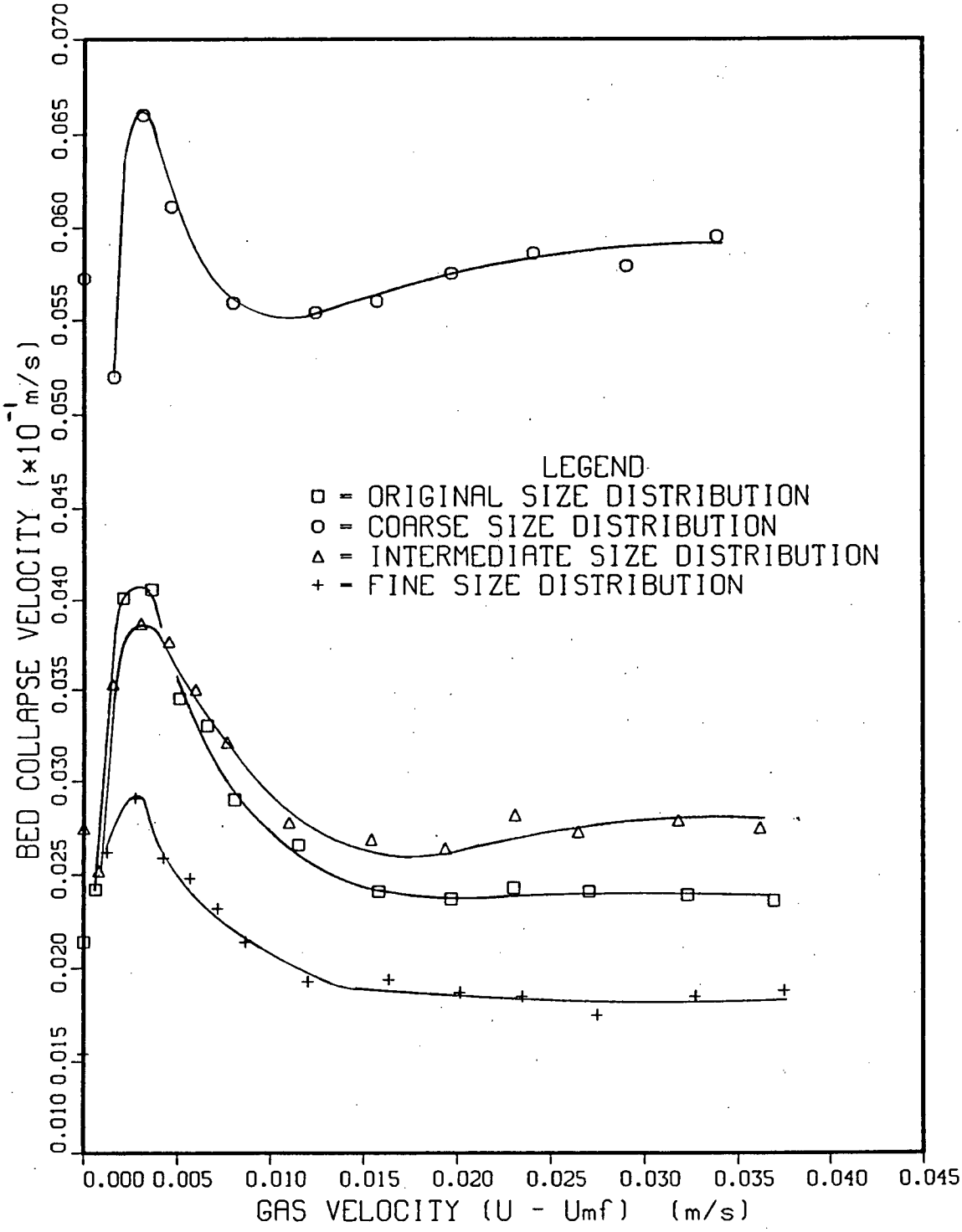

Figure 5.5: Bed Collapse Velocities for FCC Powders with Different Surface-Volume Mean Particle Diameters. Static bed height is 4.4 times bed diameter.

Table 5.1: Dense Phase Properties in Vigorously Bubbling Beds for Different Size Distributions of FCC.

Size Distribution	U_d $(*10^{-3}m/s)$		ϵ_d	
	$H_o = 3.3D$	$H_o = 4.4D$	$H_o = 3.3D$	$H_o = 4.4D$
Original	2.81	2.40	0.503	0.494
Coarse	5.95	5.80	0.485	0.468
Intermediate	3.24	2.80	0.507	0.501
Fine	1.85	1.85	0.566	0.557
Wide	3.45	3.12	0.488	0.478
Bimodal	3.55	3.25	0.492	0.482

ϵ_{mf} for all the FCC size distributions. This probably implies that the powder has little elasticity, regardless of the mean particle size. The superficial dense phase gas velocity increases and the dense phase voidage decreases for powders with smaller mean particle size for both of the bed heights considered. At first sight, it may seem more reasonable to use large particles in a chemical reactor to take advantage of the higher dense phase gas flow. However, larger particles mean smaller surface areas or effectiveness factors of the particles, slowing down the reaction. Hence it is important to increase the dense phase gas flowrate while keeping the particle size small. One way of doing this is by altering the particle size distribution.

5.2 Effect of Particle Size Distribution for Fluid Cracking Catalyst

Collapse tests for three size distributions of FCC with similar mean particle size (intermediate, wide and bimodal) are given in Figure 5.6-5.9. The intermediate size fraction has the smallest capacity to expand during bubble-free bed expansion. The dense phase of the bimodal and wide distributions (both with broader size spectra) are more capable of expanding. Though the intermediate fraction still has the highest peak ϵ_d, the difference between the different size distributions is only a quarter of the difference at minimum fluidization (see Table 4.2).

The difference in U_{mf} among the three size distributions is about 0.3 mm/s while the peak dense phase velocity is about 1 mm/s higher for the wide distribution compared to the intermediate fraction; that of the bimodal distribution is another 0.3 mm/s higher. The slope of the U_d versus $U - U_{mf}$ plot during the bubble-free fluidization stage is the same for all three size distributions. The intermediate fraction obviously cannot accommodate the increase in gas flow as much as the other broader size distributions. The superficial dense phase velocity of the intermediate fraction starts off at a value lower

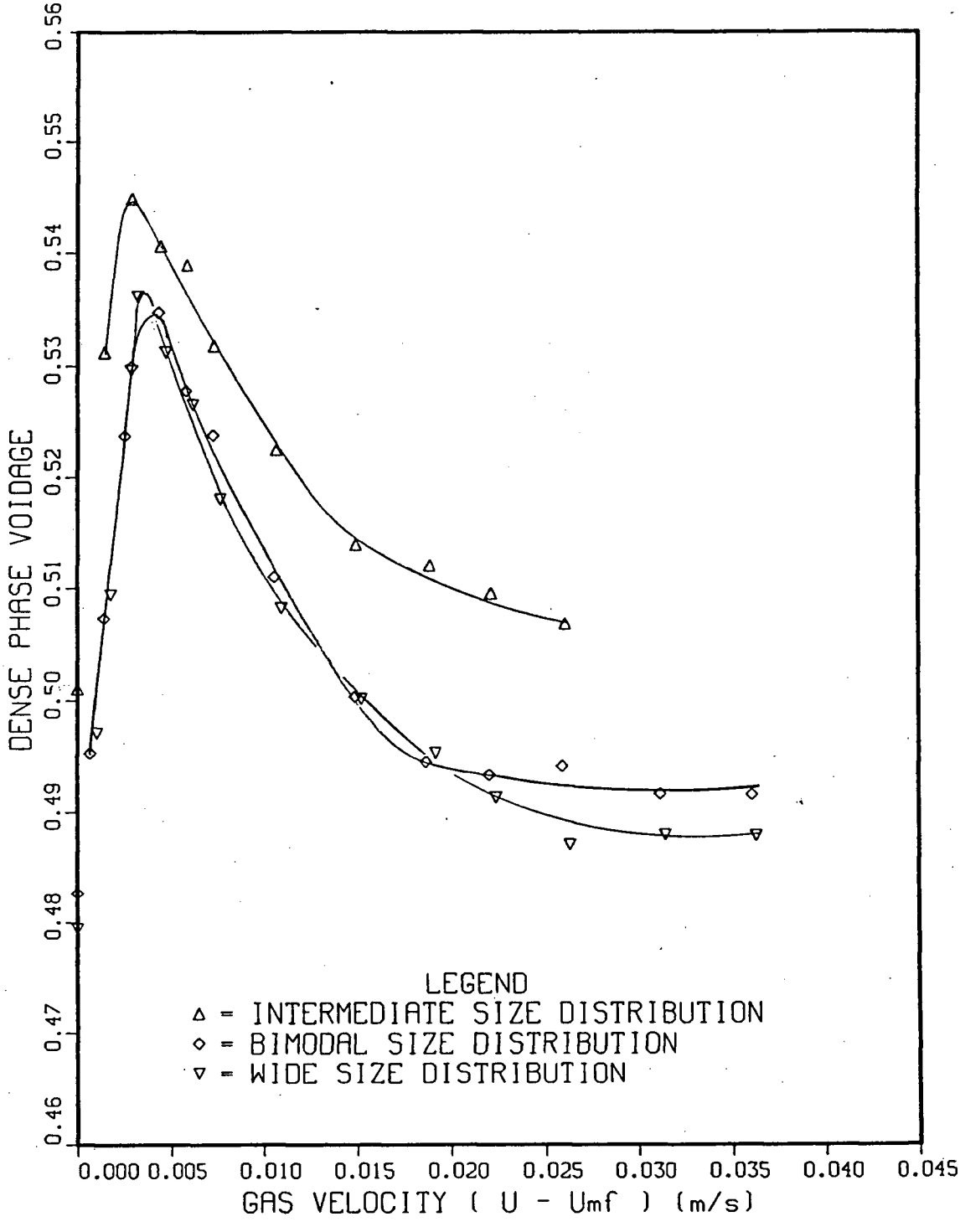

Figure 5.6: Dense Phase Voidages for FCC Powders with Similar Mean Particle Diameters but Different Size Distributions. Static bed height is 3.3 times bed diameter.

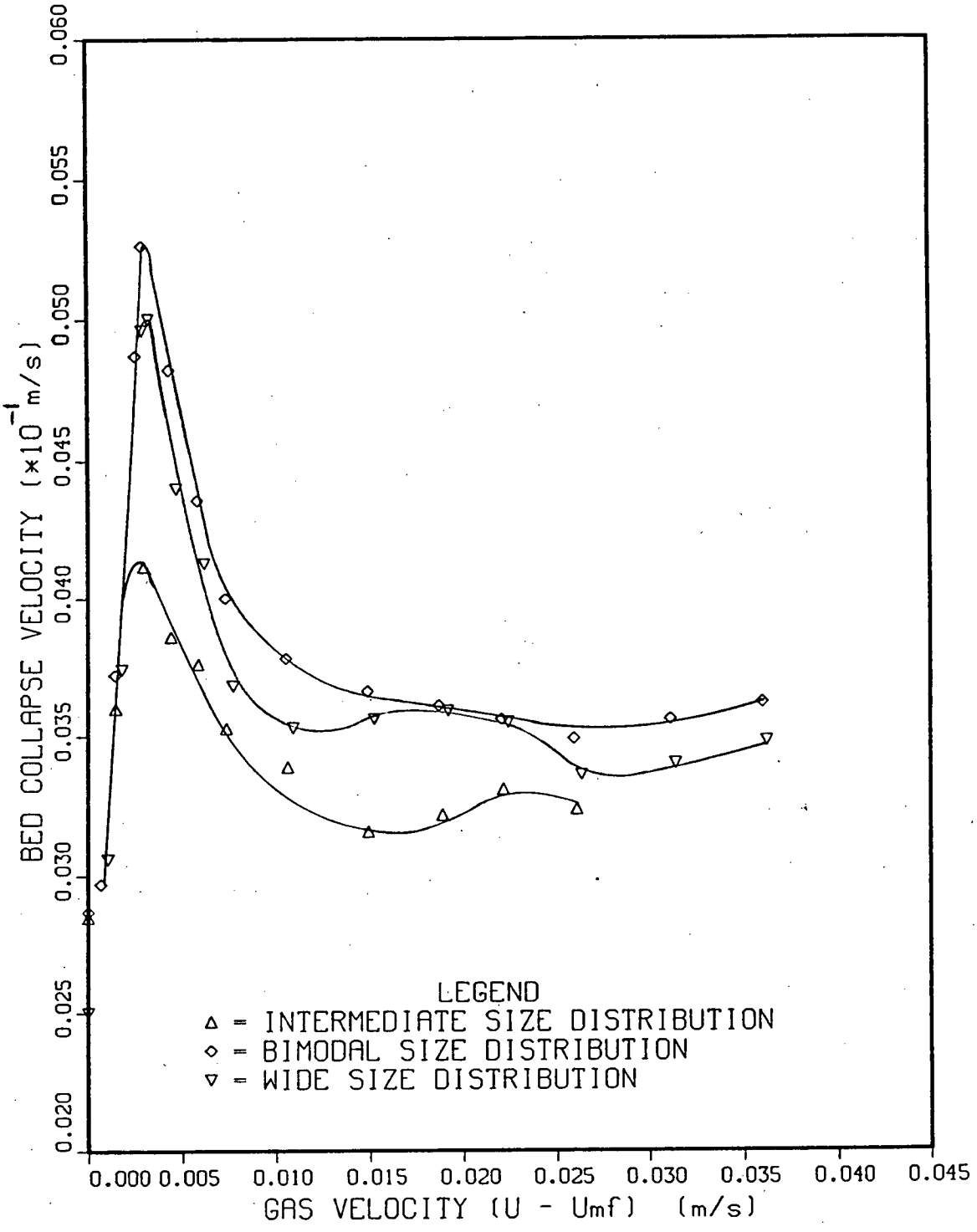

Figure 5.7: Bed Collapse Velocities for FCC Powders with Similar Mean Particle Diameters but Different Size Distributions. Static bed height is 3.3 times bed diameter

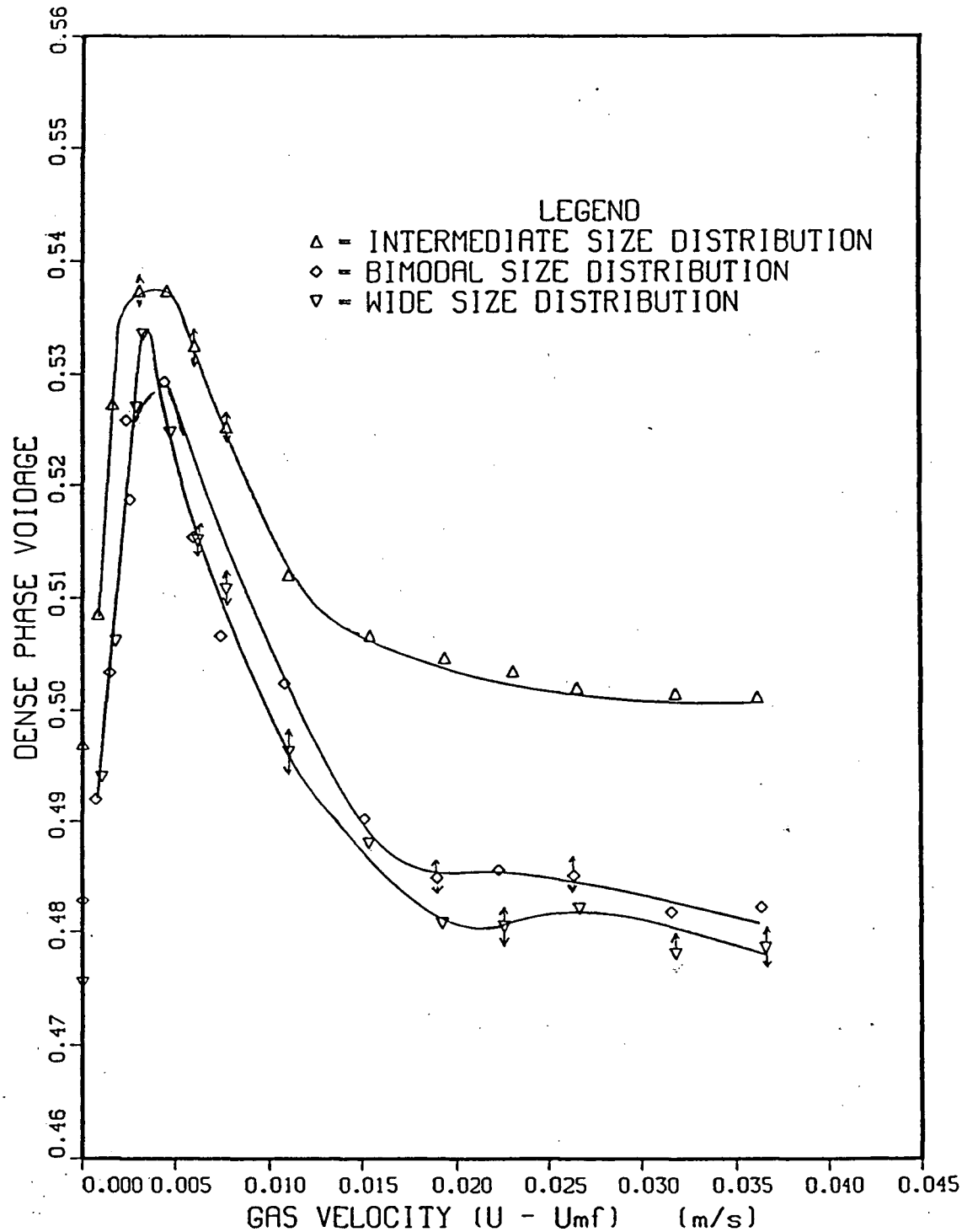

Figure 5.8: Dense Phase Voidages for FCC Powders with Similar Mean Particle Diameters but Different Size Distributions. Static bed height is 4.4 times bed diameter. Error bars are the spread for 95% confidence level.

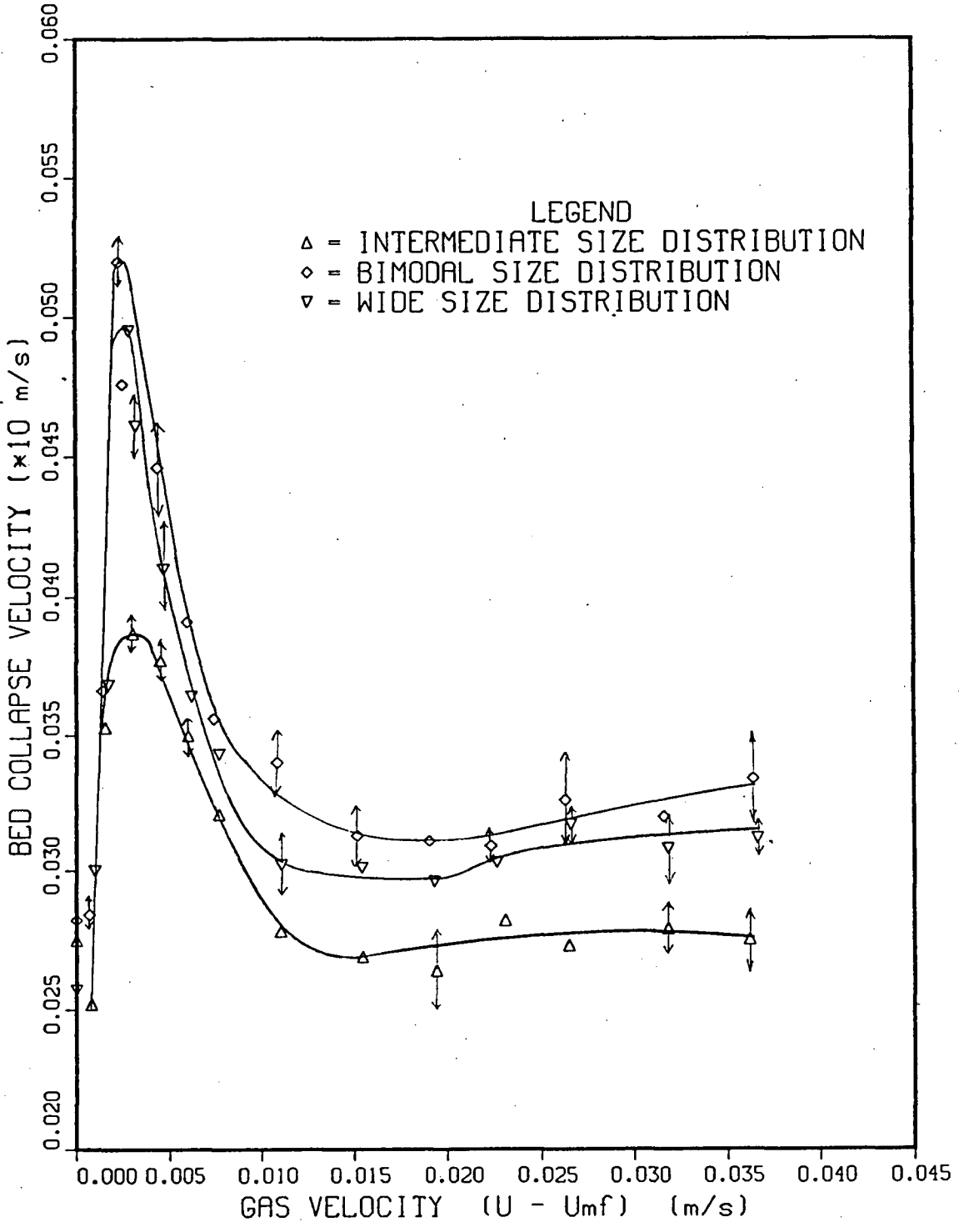

Figure 5.9: Bed Collapse Velocities for FCC Powders with Similar Mean Particle Diameters but Different Size Distributions. Static bed height is 4.4 times bed diameter. Error bars are the spread for 95% confidence level.

than its minimum fluidization velocity as found also by Rowe and Yacono (1976) for a size distribution with very few fines.

At gas velocities roughly beyond U_{mb}, the dense phase contracts and the superficial dense phase gas velocity decreases as with other size distributions of FCC. All three size distributions follow the same pattern. The limiting ϵ_d is significantly higher for the intermediate fraction while those of the other two distributions are quite similar. In fact, the difference in ϵ_d between the intermediate fraction and the distributions with wider size spectra is re-established to its level at minimum fluidization. Hence it would appear that dense phase expansion plays little or no role in a vigorously bubbling bed.

However, higher ϵ_d does not always mean higher dense phase gas flow. The permeability of the dense phase is affected by the particle size distribution of the powder. As shown in Figures 5.7 and 5.9, U_d is highest for the bimodal distribution and lowest for the intermediate fraction. The difference in dense phase properties between the narrow size cut and the broad size powders is significant at the 95% confidence level. This is in the opposite order when compared with the ϵ_d. The increase in dense phase permeability in response to having a wide size spectrum more than compensates for the small dense phase volume in the bimodal and wide distributions. Therefore, they are able to accommodate high dense phase gas flow. Less gas goes through the bubble phase. No clear conclusion can be drawn on the difference in dense phase properties between the bimodal and wide distributions. The dense phase properties did not show consistent and significant changes when going from a bimodal to a wide distribution FCC powder. Hence, dense phase properties cannot be predicted by the fines fraction as the bimodal distribution powder has higher F_{45} but lower F_{22} compared with the wide distribution. The overall size distribution has to be considered.

Increasing the static bed height decreases both the dense phase voidage and the superficial dense phase gas velocity. This is true for all the size distributions studied

here. This is discussed more thoroughly in Section 5.5.

5.3 Effect of Particle Size Distribution for Glass Beads

The collapse test results for the glass beads are shown in Figures 5.10 and 5.11. There is a large deviation in the ϵ_{mf} among the intermediate, bimodal and wide size distributions. The intermediate and the bimodal distributions have the highest and lowest ϵ_d values respectively, even in a bubbling bed. However, the difference is reduced near U_{mb}. This again shows that the dense phase of the powders with wider size spectra have a larger capacity to expand during bubble-free fluidization. This influence of size distribution disappears when there is vigorous bubbling, and the dense phase voidage is re-established roughly to their respective ϵ_{mf}.

The results for the superficial dense phase velocity differ from those of the FCC. When the superficial velocity is increased, U_d for each distribution continues to rise during the bubble-free fluidization stage, dips to a limiting value during the bed contraction stage and then increases very gradually again. The largest difference between the dense phases of the two types of powder occurs during vigorous bubbling as shown in Tables 5.2-5.3. The intermediate and the wide distributions have about the same superficial dense phase velocity. The superficial dense phase velocity of the bimodal distribution is as much as 25% lower, but U_d of the intermediate fraction is about 15% and 33% higher than for the wide and bimodal distributions, respectively, at minimum fluidization. This shrinks to about 1% and 25% at higher gas flow. The change in ϵ_d between the minimum fluidization and vigorous bubbling is similar for all three distributions. Hence the permeability of the dense phase for the bimodal and the wide distributions is higher than that of the intermediate fraction. The increase in dense phase permeability in the wide distribution is barely enough to compensate for the smaller ϵ_d when compared to the intermediate

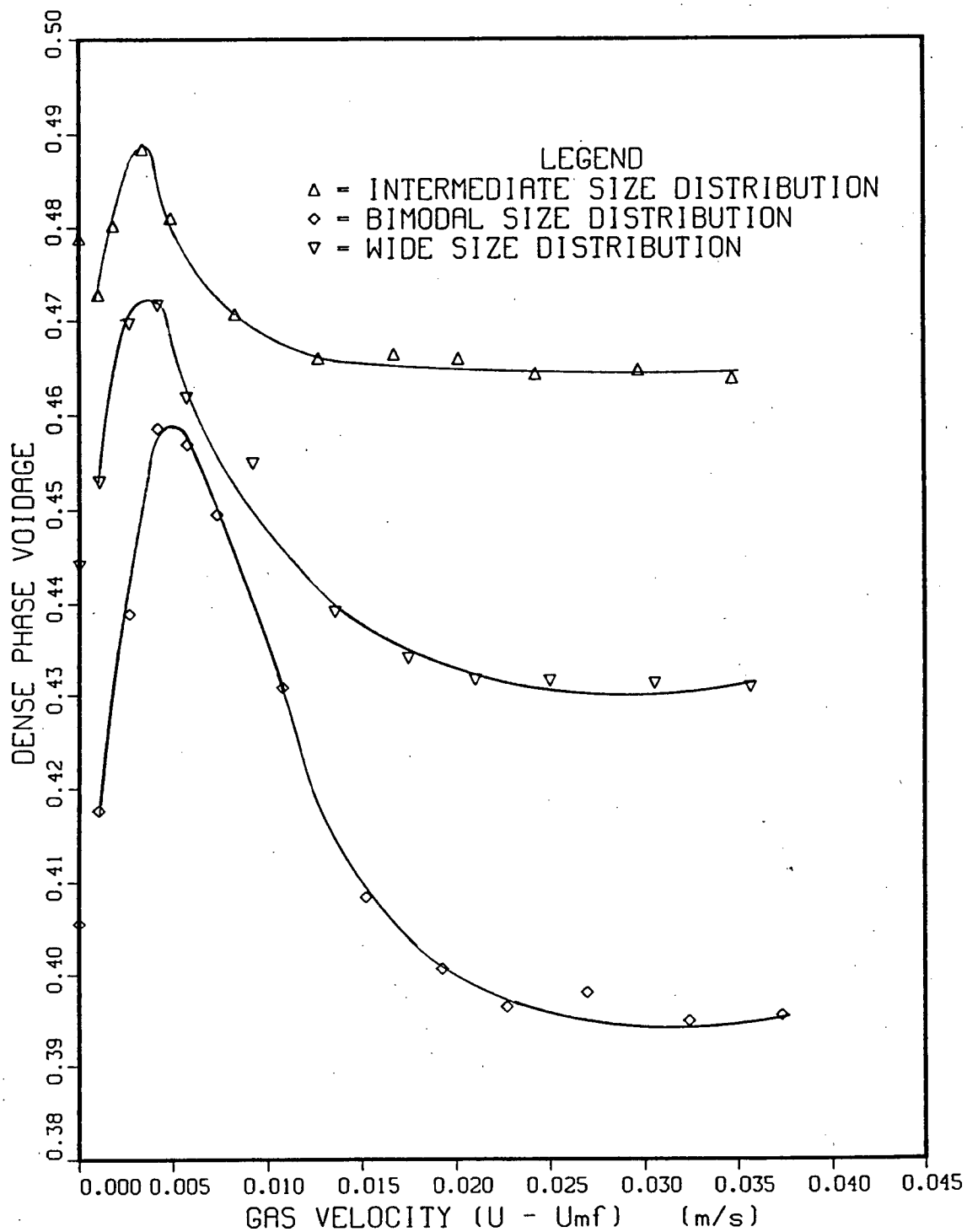

Figure 5.10: Dense Phase Voidages for Glass Bead Powders with Similar Mean Particle Diameter but Different Size Distributions. Static bed height is 4.4 times bed diameter.

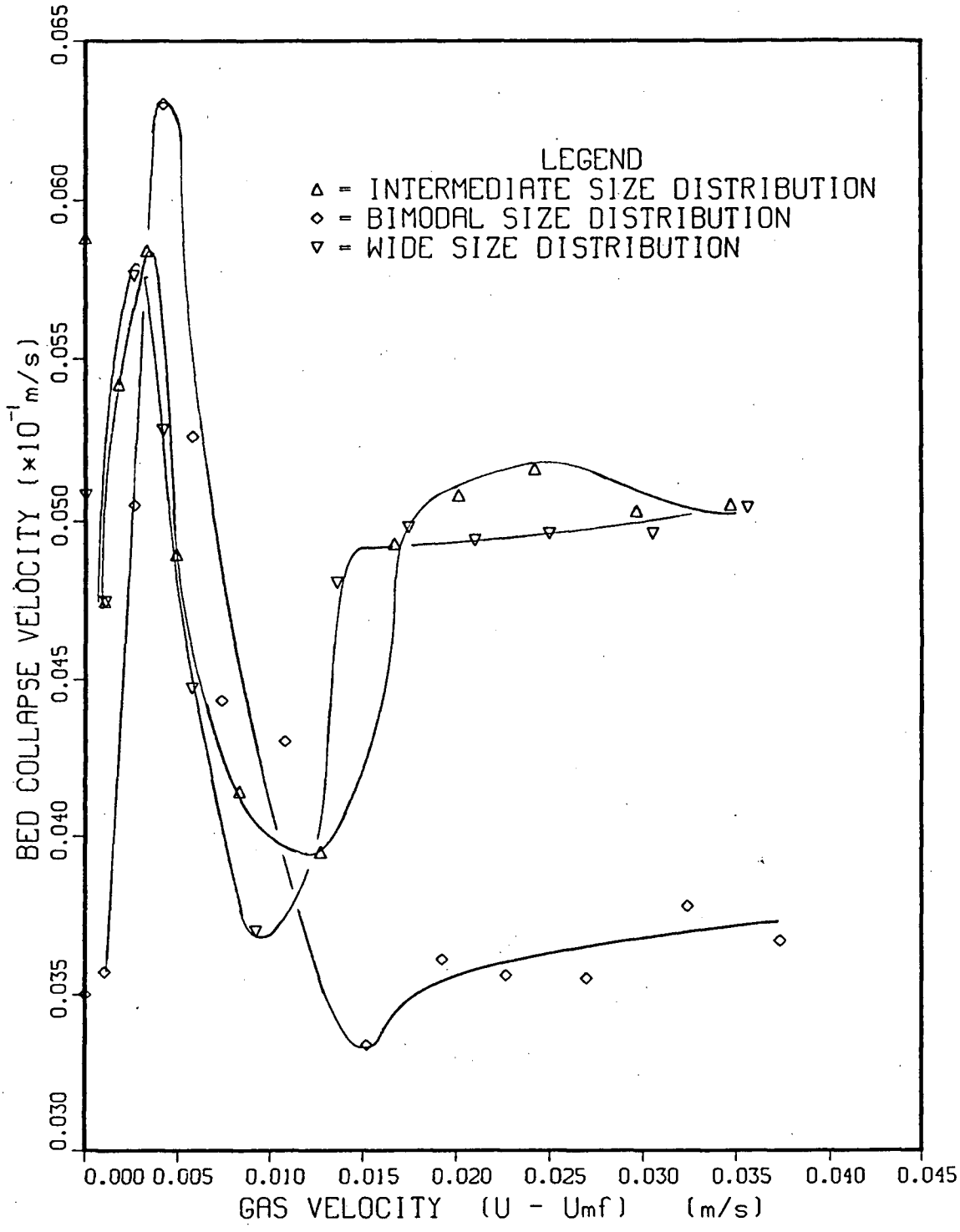

Figure 5.11: Bed Collapse Velocities for Glass Bead Powders with Similar Mean Particle Diameter but Different Size Distributions. Static bed height is 4.4 times bed diameter.

Table 5.2: Experimental and Predicted Dense Phase Voidages in a Vigorously Bubbling Bed for Different Size Distributions of Glass Beads. Bracketted numbers are the ratio of the predicted to the experimetal values.

	ϵ_d					
Size Distribution	Experimental	Abrahamsen and Geldart (1980b)	Dry et al. (1983)	Richardson and Zaki (1954)	Foscolo and Gibilaro (1983)	Kmiec (1982)
Intermediate	0.464	0.470 (1.01)	0.350 (0.75)	0.326 (0.70)	0.390 (0.84)	0.372 (0.80)
Wide	0.431	0.440 (1.02)	0.360 (0.84)	0.328 (0.76)	0.391 (0.91)	0.373 (0.86)
Bimodal	0.395	0.405 (1.03)	0.386 (0.98)	0.300 (0.76)	0.365 (0.92)	0.348 (0.88)

Table 5.3: Experimental and Predicted Superficial Dense Phase Gas Velocities in a Vigorously Bubbling Bed for Different Size Distributions of Glass Beads. Bracketted numbers are the ratio of the predicted to the experimetal values.

	$U_d(*10^{-3}m/s)$					
Size Distribution	Experimental	Abrahamsen and Geldart (1980)	Dry et al. (1983)	Richardson and Zaki (1954)	Foscolo and Gibilaro (1983)	Kmiec (1982)
Intermediate	5.05	4.77 (0.94)	4.26 (0.84)	20.6 (4.08)	11.6 (2.30)	14.3 (2.83)
Wide	5.00	4.10 (0.82)	2.70 (0.54)	15.0 (3.00)	8.02 (1.60)	9.96 (1.99)
Bimodal	3.70	2.93 (0.79)	1.86 (0.50)	11.0 (2.97)	5.42 (1.46)	6.77 (1.83)

fraction. However, the difference in ϵ_d between the intermediate and bimodal distribution is too large (0.06) to be overcome by the larger dense phase permeability of the latter. The difference in U_d between the wide and bimodal distributions is maintained when going from U_{mf} to vigorous bubbling stage. Hence the permeability of the two distributions is about the same and the difference in U_d is caused by the difference in ϵ_d.

5.4 Examination of Correlations for Dense Phase Properties

Correlations for ϵ_d and U_d were described in Section 1.3.2 . They have been compared with our experimental results. Only the correlations from Abrahamsen and Geldart (1980b), equations 1.16-17, take into account the effect of bed height. The results from other correlations are compared with the experimental results averaged from the two bed heights studied. Some correlations have U_d and ϵ_d implicitly depending on each other. In these cases, the experimental value of one parameter is used to predict the other parameter. The results are shown in Tables 5.2 to 5.5.

It can be seen that Abrahamsen's correlations predicts ϵ_d and U_d within 13% and 21% of the experimental values, respectively. This is the best agreement among the five correlations studied here, both for the FCC and the glass beads. Predictions from Dry et al. (1983) are all too low, probably because particle density is excluded in his correlations.

Richardson and Zaki's (1954) predictions of U_d and ϵ_d differ from the experimental values by about 300% and 30%, respectively. A comparsion of the experimental and predicted values of the index n is given in Table 5.6. In general, Richardson and Zaki's predictions of the dense phase properties get better when the predicted index n is close to the experimental value.

The correlations given by Foscolo and Gibilaro (1983), and Kmiec (1982) underestimate the dense phase voidage of the FCC and glass beads by about 10-20%. At the same

Table 5.4: Predicted Dense Phase Voidages in a Vigorously Bubbling Bed for Different Size Distributions of FCC. Bracketted numbers are the ratio of the predicted to the experimental values.

	ϵ_d					
Size Distribution	Abrahamsen and Geldart (1980b)		Dry et al. (1983)	Richardson and Zaki (1954)	Foscolo and Gibilaro (1983)	Kmiec (1982)
	$H_o = 3.3D$	$H_o = 4.4D$				
Original	0.561 (1.12)	0.534 (1.08)	0.357 (0.71)	0.418 (0.84)	0.446 (0.89)	0.441 (0.88)
Coarse	0.504 (1.04)	0.493 (1.05)	0.344 (0.72)	0.386 (0.81)	0.429 (0.90)	0.409 (0.86)
Intermediate	0.548 (1.08)	0.538 (1.07)	0.344 (0.68)	0.399 (0.79)	0.435 (0.78)	0.424 (0.75)
Fine	0.636 (1.12)	0.626 (1.13)	0.348 (0.62)	0.437 (0.78)	0.458 (0.82)	0.454 (0.81)
Wide	0.533 (1.09)	0.524 (1.10)	0.351 (0.73)	0.410 (0.85)	0.441 (0.91)	0.434 (0.90)
Bimodal	0.539 (1.10)	0.533 (1.11)	0.344 (0.71)	0.407 (0.84)	0.440 (0.90)	0.433 (0.89)

Table 5.5: Predicted Superficial Dense Phase Gas Velocities in a Vigorously Bubbling Bed for Different Size Distributions of FCC. Bracketted numbers are the ratios of the predicted to the experimental values.

	$U_d(*10^{-3}m/s)$					
Size Distribution	Abrahamsen and Geldart (1980b)		Dry et al. (1983)	Richardson and Zaki (1954)	Foscolo and Gibilaro (1983)	Kmiec (1982)
	$H_o = 3.3D$	$H_o = 4.4D$				
Original	2.21 (0.79)	2.18 (0.91)	1.40 (0.54)	5.70 (2.18)	4.44 (1.70)	4.67 (1.79)
Coarse	5.90 (0.99)	5.31 (0.92)	9.71 (1.67)	13.8 (2.36)	8.26 (1.41)	12.1 (2.06)
Intermediate	2.99 (0.92)	2.82 (1.01)	3.66 (1.21)	8.41 (2.78)	6.37 (2.11)	6.87 (2.27)
Fine	1.70 (0.92)	1.69 (0.91)	1.24 (0.67)	5.81 (3.14)	4.95 (2.68)	5.07 (2.74)
Wide	2.71 (0.79)	2.60 (0.83)	2.10 (0.64)	6.77 (2.06)	5.07 (1.54)	5.47 (1.66)
Bimodal	3.13 (0.88)	2.74 (0.84)	2.33 (0.69)	7.41 (2.18)	6.17 (1.81)	5.95 (1.75)

Table 5.6: Predicted Values of Index n, a Dense Phase Parameter, in a Vigorously Bubbling Bed for Different Size Distributions of FCC and Glass Beads. Bracketted numbers are the ratios of the predicted to the experimental values.

	index n			
Size Distributtion	FCC		Glass Beads	
	Experimental	Predicted	Experimental	Predicted
Original	5.55	4.43 (0.80)	-	-
Coarse	5.25	4.09 (0.78)	-	-
Intermediate	5.86	4.37 (0.75)	5.81	3.98 (0.69)
Fine	6.49	4.53 (0.70)	-	-
Wide	5.40	4.38 (0.81)	5.29	3.99 (0.75)
Bimodal	5.45	4.37 (0.80)	5.14	3.97 (0.77)

time, they overestimate U_d by factors of two to three.

5.5 Effect of Static Bed Height on Dense Phase Properties

The effects of static bed height on the dense phase properties for FCC are shown in Figures 5.12 and 5.13. The superficial dense phase velocity and dense phase voidage can be correlated with the static bed height by:

$$\epsilon_d \quad \alpha \quad H_o^{\beta} \tag{5.1}$$

$$U_d \quad \alpha \quad H_o^{\gamma} \tag{5.2}$$

The values of β and γ are shown in Table 5.7. One can see that the static bed height has a small effect on the dense phase voidage and a larger influence on the superficial dense phase gas velocity; in both cases, the dependence gets stronger with increasing superficial velocities.

Pyle and Harrison (1967) postulated that there is a gradient of interstitial gas velocity along the height of the bed with the bubble phase underdeveloped in the region close to the distributor. Hence the interstitial velocity is high in this area. The local superficial dense phase gas velocity decreases with increasing height until it finally tapers off at certain bed level. The rate of this decrease of the superficial dense phase gas velocity varies from one type of powder to another.

Rowe and Yacono (1976) drew a similar conclusion from their work. They used silicon carbide powder to make up beds varying from 0.2 to 0.6 m in depth with the mean particle sizes from 40 to 260 μm. They inferred that almost all gas flow occurred interstitially near the distributor. The permeability of the dense phase and the dense phase voidage decreased with increasing height while the interstitial gas flow approached U_{mf} at the bed surface.

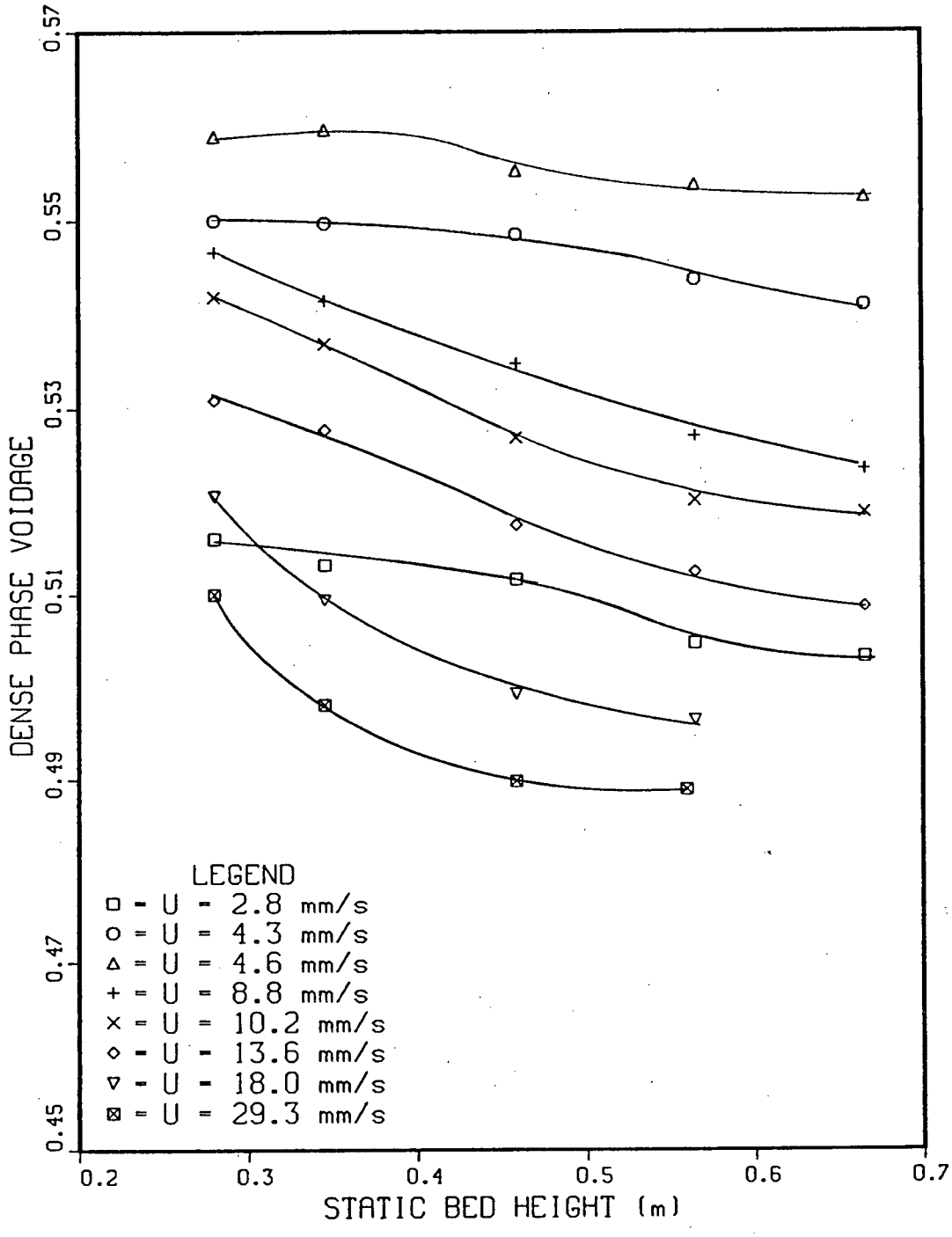

Figure 5.12: Effect of Static Bed Heights on Dense Phase Voidages of Original FCC Distribution.

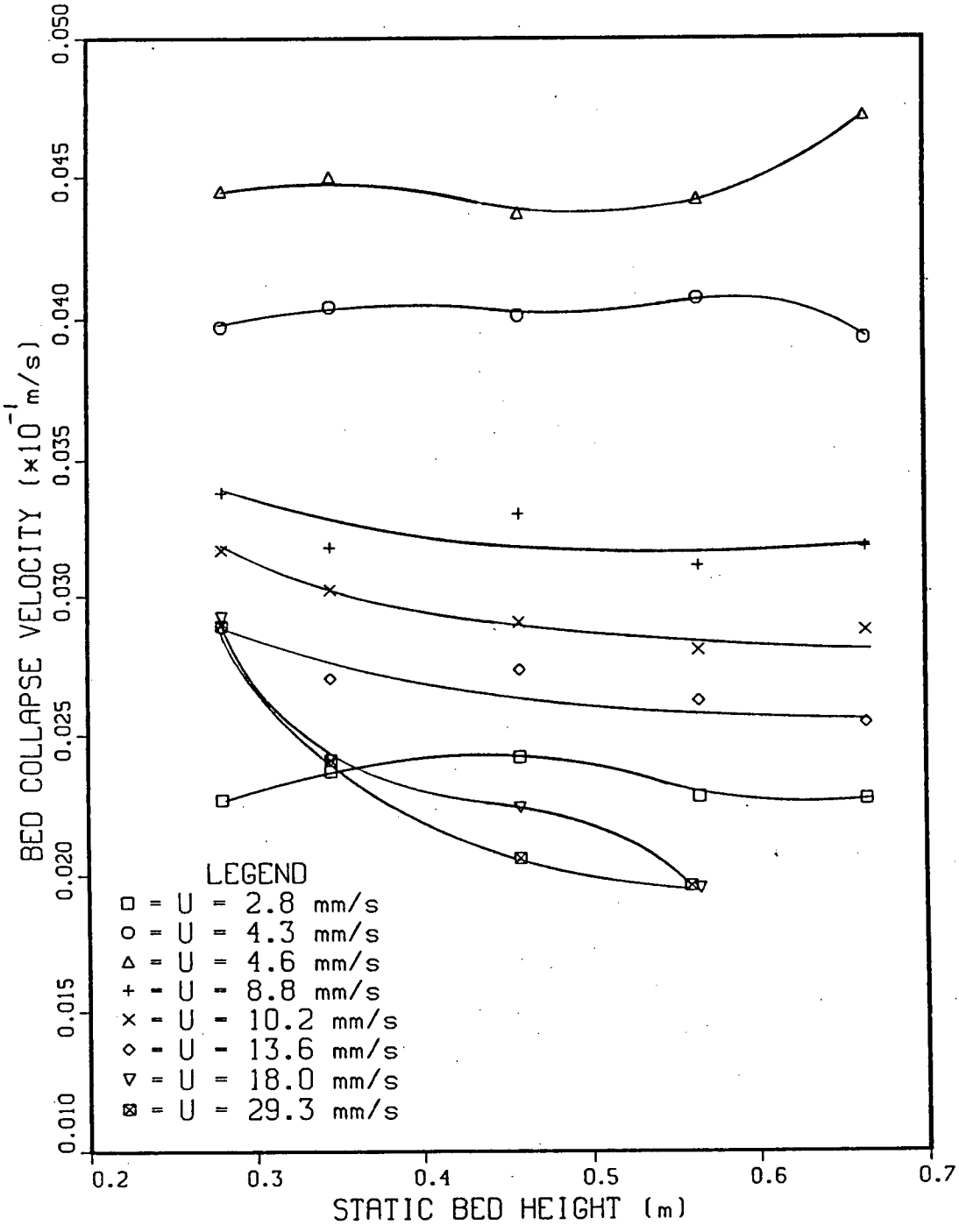

Figure 5.13: Effect of Static Bed Heights on Bed Collapse Velocities of Original FCC Distribution.

Table 5.7: Indices for Variation of Dense Phase Voidage (β) and Superficial Dense Phase Velocity (γ) on Static Bed Height at Different Gas Flowrates.

U ($*10^{-3}$m/s)	β	γ
2.80	-0.0299	-0.0140
4.30	-0.0204	-0.00375
4.60	-0.0155	-0.0384
8.80	-0.0513	-0.0638
10.2	-0.0543	-0.127
13.6	-0.0521	-0.123
18.0	-0.0754	-0.537
29.3	-0.0677	-0.614

These past findings can perhaps help to explain the results from our experiments. During the bubble-free expansion stage, no bubble phase is present in the fluidized bed. There is only a small gradient in U_d caused by the hydrostatic pressure change along the bed. In the bed contraction stage, bubbles are present in the bed although not in large number. There is probably a certain gradient of U_d along the height of the bed. The powder retains some elasticity. An increase in the interstitial velocity brings about an increase in dense phase voidage. The gradient in ϵ_d at this stage is possibly larger than during bubble-free expansion. Hence the dependence of ϵ_d and U_d on the static bed height is stronger.

When the superficial velocity is increased further, the effect of the underdeveloped bubble phase at the lower portion of the bed may become more significant. The superficial dense phase velocity immediately above the distributor is quite high, and a velocity gradient may be present along a larger portion of the bed. The superficial dense phase velocity may not have levelled off even at the surface of some of the shallow beds used here. The dependence of the dense phase properties on the static bed height becomes even stronger.

The degree of dependence in a vigorously bubbling bed is approximately as follows:

$$\epsilon_d \quad \alpha \quad H_o^{-0.07} \tag{5.3}$$

$$U_d \quad \alpha \quad H_o^{-0.6} \tag{5.4}$$

The dependence of ϵ_d on the static bed height is much lower than that of the superficial dense phase velocity. Hence only a small fraction of the decrease in U_d can be accounted for by the decrease in ϵ_d with increasing static bed height. It is also known from the collapse test results that in a vigorously bubbling bed, the dense phase voidage stays at the limiting value in spite of the increase in superficial dense phase velocity with

increasing superficial velocity. Hence, the dependence of the dense phase voidage on the static bed height is relatively weak.

The dependence of ϵ_d and the U_d on the static bed height are both two to three times higher than reported by Abrahamsen and Geldart (1980b) and Dry et al. (1983). Abrahamsen and Geldart used beds of about 0.3 to 0.9 m in depth while Dry et al. investigated beds more than 2 m deep. The bed depths in our experiments are only in the range of 0.28 to 0.67 m. The gradient in dense phase properties may have become negligible somewhere along the height of the deeper beds used by other workers. However, it is possible that the gradient is still present even at the surface of our more shallow beds. Therefore, a high degree of dependence is reported from our experiment.

5.6 Summary

The dense phase properties depend on mean particle size, particle size distribution, superficial velocity, static bed height and physical properties of the powders. The dense phase of the powders with wide size spectra expands proportionally more during bubble-free fluidization than those with a narrow distribution. The dense phase voidage of any size distribution in a vigorously bubbling bed is roughly the same as the minimum fluidization voidage; the latter is in turn controlled by the overall particle size distribution of the powder. The permeability of the dense phase is enhanced by having a broad size spectrum. The dense phase permeability and the dense phase voidage both affect the superficial dense phase gas velocity. The balance of these two factors determines which size distribution produces the highest dense phase gas flow. Decreasing the mean particle size within Group A increases ϵ_d and decreases U_d. The effect of static bed height is stronger on U_d than on ϵ_d.

Chapter 6

Results and Discussion: Pressure Fluctuations

The final part of the experiments was intended to study pressure fluctuations in the bubbling and slugging flow regimes. The results were analyzed with 95% confidence level.

The minimum slugging velocity for our powders is about 0.046 m/s (Stewart and Davidson, 1967). The fluidized bed should be in the bubbling regime for U = 0.037 m/s and in the slugging flow regime when U = 0.095, 0.175 and 0.267 m/s. Other criteria for the occurrence of slugging (Grace, 1982) were also met. The static bed height to diameter ratio was about five which is larger than the 3.5 required (Darton et al., 1977). The maximum stable bubble size for the powders studied is at least 0.07 m which is larger than 60% of the bed diameter (Grace, 1982). The transition velocity to turbulent fluidization is about 1.1 m/s in our system (Yerushalmi and Cankurt, 1979), much larger than the maximum superficial velocity employed here. It was confirmed visually that our fluidized bed was bubbling for U = 0.037 m/s and slugging for U = 0.095m/s and higher. The slugging pattern was axisymmetric for all size distributions.

6.1 Mean Pressure in the Fluidized Bed

The mean pressure, calculated as the average of the instantaneous pressures recorded at a tap 27 or 180 mm above the distributor over a 20-second period, is given in Tables 6.1 and 6.2. The effects of superficial velocity and mean particle diameter on the mean pressure depend on whether the pressure measurement was taken in the 'freely bubbling

Table 6.1: Mean Pressure from Fluidization of Different Size Distributions of FCC. Pressure Tap is 27 mm above the Distributor. Bracketted values are the deviations from the mean for 95% confidence level.

Size Distribution	Mean Pressure At Different Superficial Gas Velocity (* 10^3 kPa)			
	U=0.037m/s	U=0.095m/s	U=0.175m/s	U=0.267m/s
Original	3.87 (±0.01)	3.87 (±0.01)	3.85 (±0.01)	3.81 (±0.03)
Intermediate	3.89 (±0.01)	3.89 (±0.01)	3.89 (±0.02)	3.91 (±0.02)
Wide	3.89 (±0.01)	3.88 (±0.01)	3.87 (±0.02)	3.81 (±0.03)
Bimodal	3.87 (±0.01)	3.85 (±0.02)	3.86 (±0.02)	3.84 (±0.02)

Table 6.2: Mean Pressure from Fluidization of Different Size Distributions of FCC. Pressure Tap is 180 mm above the Distributor. Bracketted values are the deviations from the mean for 95% confidence level.

Size Distribution	Mean Pressure At Different Superficial Gas Velocity (* 10^3 kPa)			
	U=0.037m/s	U=0.095m/s	U=0.175m/s	U=0.267m/s
Original	2.68 (±0.01)	2.74 (±0.02)	2.80 (±0.04)	2.82 (±0.03)
Intermediate	2.71 (±0.01)	2.75 (±0.02)	2.84 (±0.04)	2.91 (±0.03)
Wide	2.65 (±0.01)	2.70 (±0.01)	2.77 (±0.04)	2.88 (±0.01)
Bimodal	2.70 (±0.01)	2.73 (±0.01)	2.79 (±0.04)	2.88 (±0.03)

zone' or the 'slugging zone', i.e. the lower or upper portions of the bed, respectively.

In the 'freely bubbling zone', a small change in the mean particle size had no discernible effect on the mean pressure. Significant changes in mean pressure in response to the rise in superficial velocity was found for wide distribution and original FCC powders. The three distributions of similar mean particle diameter (intermediate, bimodal and wide) did not show significant difference in mean pressure except perhaps when the superficial velocity was 0.259 m/s.

When the bed pressure is measured higher up the column, the mean pressure increases significantly with the superficial velocity as predicted by Svoboda et al. (1984) and Fan et al. (1981) for every FCC size distribution studied. The mean pressure measured when fluidizing the original distribution was significantly higher than that of the wide distribution when the superficial velocities were 0.037 and 0.095 m/s. This difference became insignificant when the superficial velocity increased to 0.175 or 0.267 m/s. It seems that by increasing the surface-volume mean particle size, the change in mean pressure in response to a change in superficial velocity goes up. The particle size distribution again did not seem to affect the mean pressure in a consistent manner.

6.2 Magnitude of Pressure Fluctuations

The magnitude of the pressure fluctuation can be represented by the root mean square deviation from the mean pressure. Figures 6.1 and 6.2 show the magitude of pressure fluctuations at different bed levels when fluidizing different FCC distributions. The magnitude of pressure fluctuation increases significantly with superficial velocity. When the bed was merely bubbling, the amplitude and frequency of the pressure waveform were quite irregular as shown in Figure 6.3. The amplitudes of the pressure fluctuations were insensitive to changes in particle size distribution and small changes in mean particle

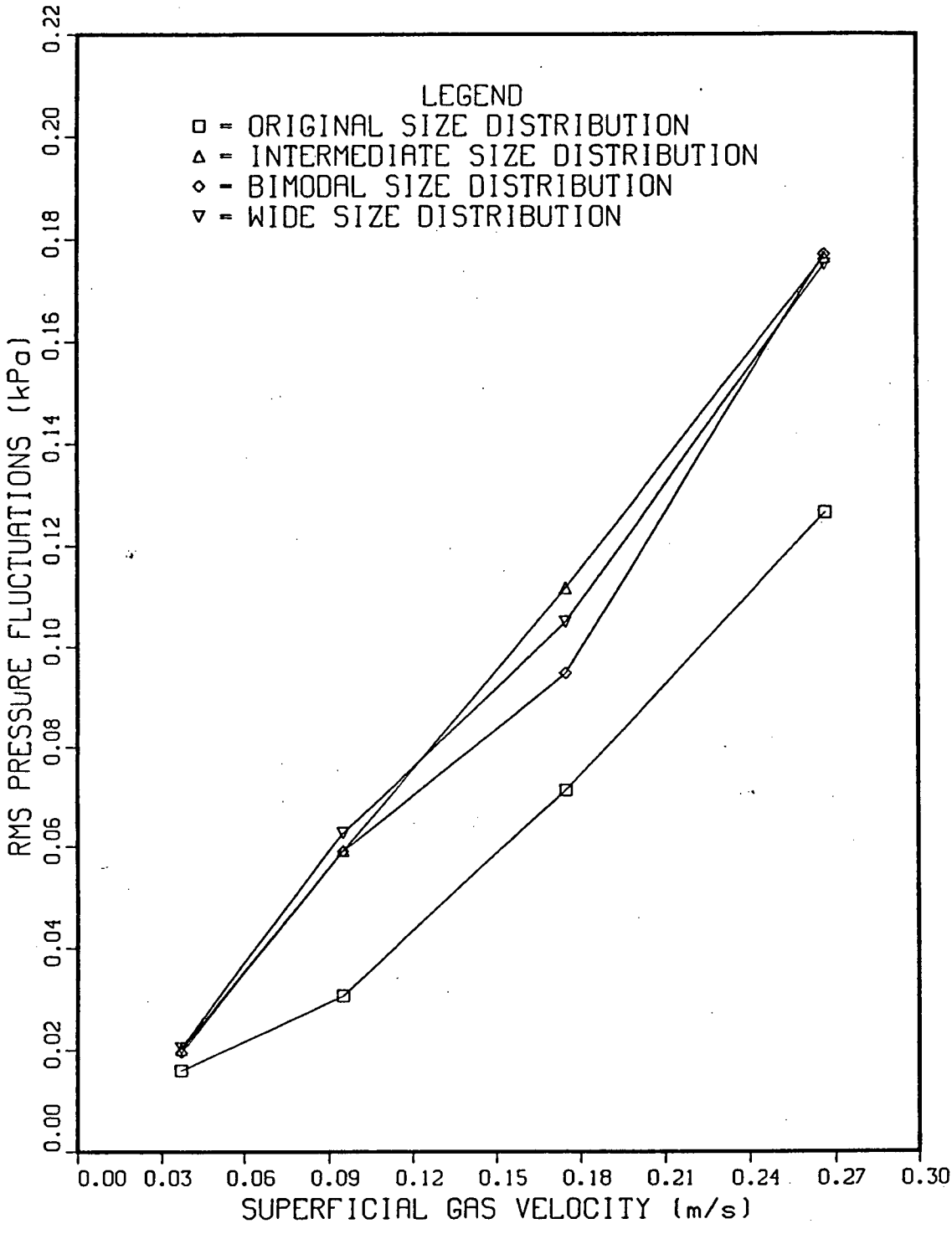

Figure 6.1: Pressure Fluctuations when Fluidizing Different FCC Powders Measured 27 mm above the Distributor.

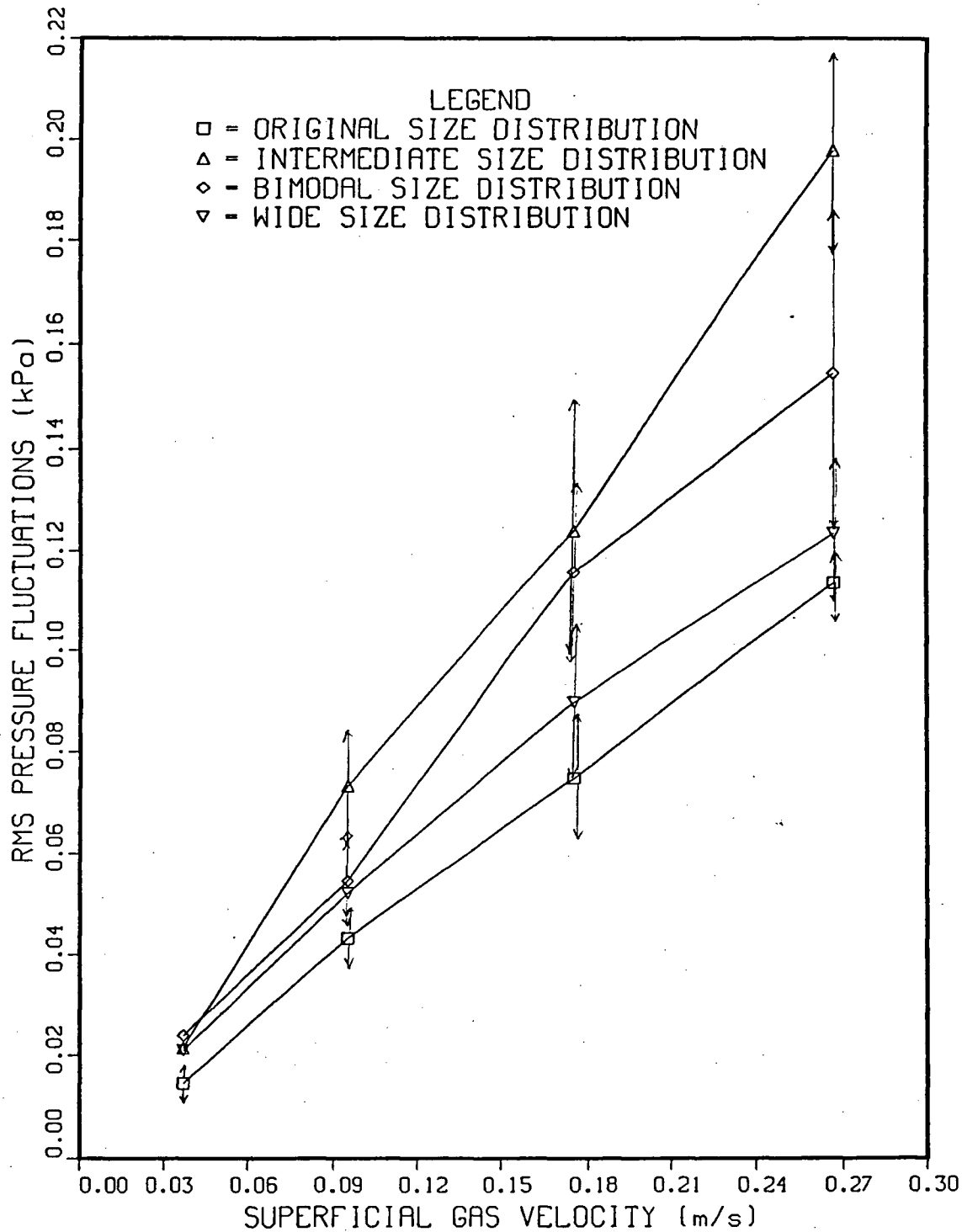

Figure 6.2: Pressure Fluctuations when Fluidizing Different FCC Powders Measured 180 mm above the Distributor. Error bars are the spread for 95% confidence level

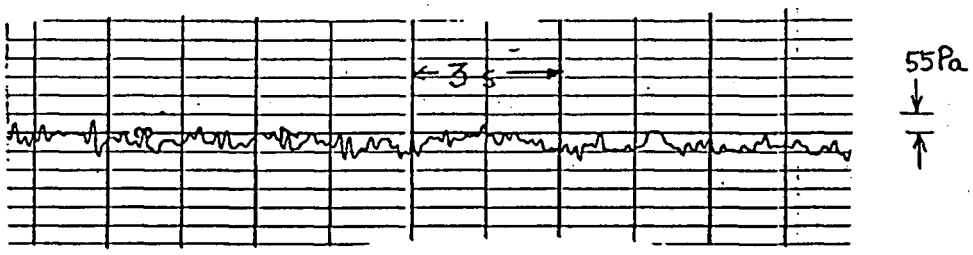

(a) Bubbling Regime; Probe at 27 or 180 mm above Distributor.

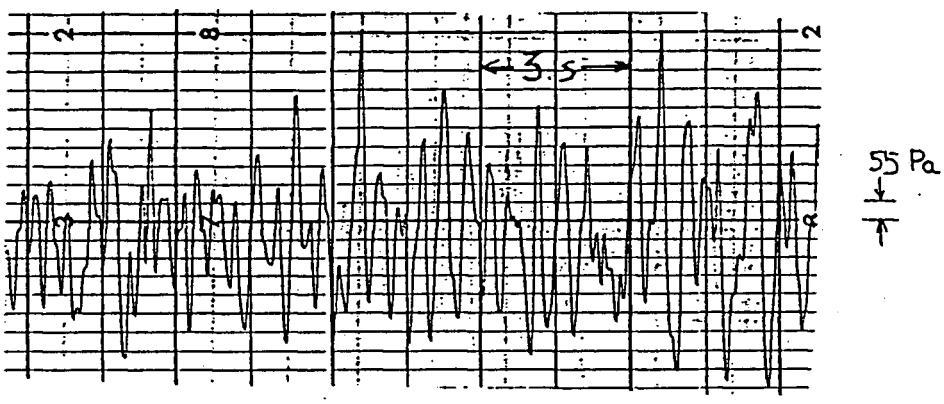

(b) Slugging regime; Probe at 27 mm above Distributor.

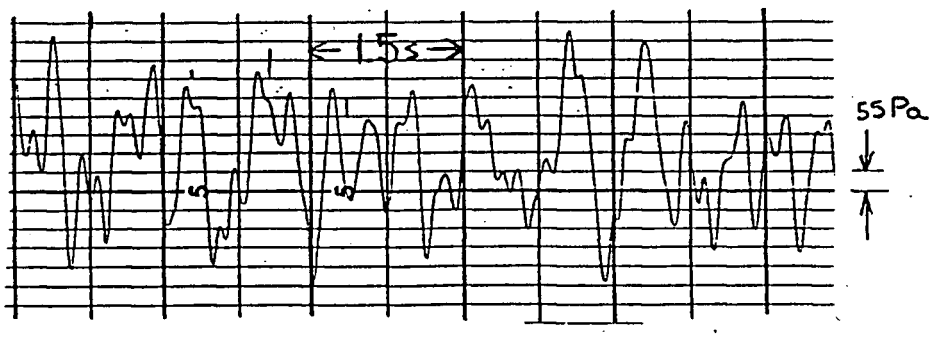

(c) Slugging Regime; Probe at 180 mm above Distributor.

Figure 6.3: Typical Fluidized Bed Pressure Waveforms for FCC Distributions at Different Bed Levels. Each vertical interval represents a pressure of about 55 Pa.

size.

However, the magnitude of the pressure fluctuations did depend on the particle size distribution and mean particle size in the slugging regime. The pressure waveforms also became more regular. The principal differences in size distribution between the wide and the original FCC powders were the higher fines content and larger mean particle diameter of the latter. Decreasing the mean particle diameter significantly lowered the magnitude of fluctuation in a slugging bed when the probe was 27 mm above the distributor. This difference did not persist when the pressure probe was placed at 180 mm above the distributor.

Changing the particle size distribution affected the magnitude of the pressure fluctuation only when the pressure probe was placed higher up the column. When the pressure tap was very close to the distributor, it seems that only the mean particle size was important in determining the amplitude of the pressure fluctuation. When the probe was placed 0.18 m above the distributor, the particle size distribution became important. At this height, the bubbles had a chance to grow and bring about slugging. A powder that had a narrow particle size distribution produced a significantly higher amplitude of pressure fluctuation than the wide distribution. The magnitude of pressure fluctuations for the bimodal distribution did not differ significantly from that for either the intermediate fraction or the the wide distribution. So a powder with a wide and continuous size spectrum provides the least chance of structual damage to the fluidized bed as a result of pressure fluctuations in a slugging bed.

6.3 Frequency of Pressure Fluctuation

The frequency of pressure fluctuation does not seem to be influenced by the mean particle size, the particle size distribution, the placement of the pressure probe or the superficial

gas velocity (see Tables 6.3 and 6.4). The frequency was about 1.4 Hz under all the conditions used in this work. There was no definite shift in the frequency of the pressure fluctuation when the pressure probe was moved away from the distributor.

6.4 Summary

The mean pressure in the slugging zone increases with increasing superficial velocity. Changing the particle size distribution does not have a definite effect on the mean pressure. In the bubbling regime, the magnitude of pressure fluctuation is relative small and is not affected by particle size distribution and small changes in mean particle size. In a slugging bed, the magnitude of pressure fluctuation in the 'slugging zone' is lower for a powder with a wide and continuous particle size distribution than one with a narrow size spectrum. The magnitude of pressure fluctuation increases with superficial velocity regardless of the bed level and particle size distribution. The frequency of the pressure fluctuation did not depend on any of these factors.

Table 6.3: Frequency of Pressure Fluctuation for Fluidization of Different Size Distributions of FCC. Pressure Tap is 27 mm above the Distributor.

Size Distribution	Frequency of Pressure Fluctuation (Hz)			
	U=0.037m/s	U=0.095m/s	U=0.175m/s	U=0.267m/s
Original	1.47	1.33	1.80	1.58
Intermediate	1.43	1.40	1.43	1.47
Wide	1.27	1.67	1.43	1.57
Bimodal	1.80	1.57	1.70	1.47

Table 6.4: Frequency of Pressure Fluctuation for Fluidization of Different Size Distributions of FCC. Pressure Tap is 180 mm above the Distributor.

Size Distribution	Frequency of Pressure Fluctuation (Hz)			
	U=0.037m/s	U=0.095m/s	U=0.175m/s	U=0.267m/s
Original	1.40	1.33	1.53	1.43
Intermediate	1.40	1.47	1.47	1.40
Wide	1.47	1.40	1.53	1.43
Bimodal	1.50	1.33	1.47	1.50

Chapter 7

Conclusions and Recommendations

A summary on the effects of particle size distribution on fluidization properties is given in Table 7.1. The glass bead and FCC powders have very different fluidization hydrodynamics from minimum fluidization to vigorous bubbling regimes. For both types of powder, when the mean particle size increases, the U_{mf}, U_{mb}, U_d and fractional bubble free bed expansion increase, but the ϵ_{mf}, ϵ_{mb} and ϵ_d decrease. Compared to a narrow size cut fraction, a broad size cut decreases ϵ_{mb}, increases fractional bubble-free bed expansion and affects U_{mb}. A broad size spectrum FCC powder has higher U_d and lower ϵ_d than a narrow fraction. No significant difference in dense phase properties is found between the bimodal and wide FCC distributions. The effect of particle size distribution on the dense phase properties of glass beads is unclear because of the large difference in ϵ_{mf} among the size distributions studied.

Increasing the static bed height did not have any significant effects on the minimum fluidization or the minimum bubbling properties. However, it decreased the superficial dense phase velocity and the dense phase voidage of FCC.

With increasing superficial velocity, the mean pressure in the slugging zone of a fluidized bed increased. The magnitude of pressure fluctuations in the slugging regime increased with increasing superficial velocity and for powders of narrow size cut.

Further studies should be conducted to attain deeper understanding of the hydrodynamics of fluidization involving fine particles. It was found that the physical characteristics of powder play a role in the determination of certain fluidization properties.

Table 7.1: Summary for the Effect of Particle Size Distribution on the Fluidization Properties of FCC and Glass Beads.

	FCC			Glass Beads		
	Interm.	Wide	Bimodal	Interm.	Wide	Bimodal
U_{mf}	H (=Bimodal)	L	H (=Interm)	H	M	L
ϵ_{mf}	same	same	same	H	M	L
ϵ_{mb}	H	L (=Bimodal)	L (=Wide)	H	M	L
$\frac{\epsilon_{mb}-\epsilon_{mf}}{\epsilon_{mf}}$	L (=Bimodal)	H	L (=Interm)	L	M	H
U_{mb}	L	same	H	H	L (=Bimodal)	L (=Wide)
U_{mb}/U_{mf}	L	H	same	L (=Wide)	L (=Interm)	H
U_d	L	H (=Bimodal)	H (=Wide)	H (=Wide)	H (=Interm)	L
ϵ_d	H	L (=Bimodal)	L (=Wide)	H	M	L
ΔP_{rms} at bubbling zone	same	same	same	-	-	-
ΔP_{rms} at slugging zone	H	L	same	-	-	-

Interm - Intermediate (Narrow Cut)
H - High
M - Medium
L - Low
same - no statistically significant difference compared with the other two distributions

Other powders such as alumina can be used in order to investigate the patterns that these fluidization properties may follow. The experiments here were performed under ambient conditions which were fairly constant throughout the course of investigation. Most industrial fluidized beds are run under different conditions. It would be worthwhile to repeat these experiments at different pressure, temperature and humidity.

Only the bubble-free fluidization, bubbling and slugging regimes have been studied in this work. Further experiments should be performed to study the hydrodynamics of fine particle fluidization in the turbulent regime or in a circulating bed. Another fluidization column of different material for the fluidized bed should be built so that the pressure fluctuations can be studied at different levels of the bed.

Nomenclature

Ar - Archimedes number.

D - Bed diameter, m.

d_p - Mean particle diameter obtained from standard sieve analysis, m.

d_{pi} - Mean opening diameter of adjacent sieves, m.

d_{sv} - Surface-volume mean particle diameter, m.

d_v - Number-volume mean particle diameter, m.

E - Elasticity coefficient.

F_{22} - Mass fraction of powder with particle diameter less than 22μm.

F_{45} - Mass fraction of powder with particle diameter less than 45μm.

g - Gravitational constant, 9.8 m/sec^2.

h - Bed Level, m.

H - Bed Height, m.

H_d - Dense phase bed height,m.

H_{mf} - Bed height at minimum fluidization, m.

H_{mb} - Bed Height at minimum bubbling, m.

H_o - Static bed height, m.

Re_p - Particle Reynolds number.

Re_t - Terminal particle Reynolds number.

U - Superficial gas velocity, m/s.

U_d - Superficial dense phase gas velocity, m/s.

U_{mf} - Minimum fluidization velocity, m/s.

U_{mb} - Minimum bubbling velocity, m/s.

U_t - Particle terminal settling velocity, m/s.

x - Volume of water to cake 1 kg of powder, m^3/kg.

x_i - Weight fraction of powder collected in sieve i.

β - Exponential proportionality factor.

γ - Exponential proportionality factor.

ϵ - Bed voidage.

ϵ_d - Dense phase voidage.

ϵ_{mb} - Minimum bubbling voidage.

ϵ_{mf} - Minimum fluidization voidage.

μ - Gas viscosity, $kg/(m*s^2)$.

ρ_g - Gas density, kg/m^3.

ρ_p - Particle density, kg/m^3.

ρ_s - Skeletal density, kg/m^3

τ - Shear stress.

References

Abrahamsen, A. R., and D. Geldart, Behaviour of gas-fluidized beds of fine powders part I: homogenous Expansion, *Powder Technology*, 26 (1980) 35-46.

Abrahamsen, A. R., and D. Geldart, Behaviour of gas-fluidized beds of fine powders part II: voidage of dense phase in bubbling beds, *Powder Technology*, 26 (1980) 47-55.

Baeyens, J., and D. Geldart, Predictive calculations of flow parameters in gas fluidized beds and fluidization behaviour of various powders, **La Fluidisation et ses Applications**, 263-273, Societe Chimie Industrielle, Toulouse, 1973.

Barreto, G. F., J. G. Yates and P. N. Rowe, The effect of pressure on the flow of gas in fluidized beds of fine powders, *Chemical Engineering Science*, 38 (1983) 1935-1945.

Bohle, W., and W. P. M. Swaay, The fluidization of gas adsorption on mass transfer and gas mixing in a fluidized bed, **Fluidization - Proceedings of the Second Engineering Foundation Conference**, eds. J. F. Davidson and D. L. Keairns, 166-172, Cambridge University Press, Cambridge, 1978.

Clift, R., Particle-Particle Interactions in Gas-Particles Systems, *Institution of Chemical Engineers Symposium Series*, 91 (1986) 27-43.

Darton, R. C., R. D. Lanauze, J. F. Davidson and D. Harrison, Zubble growth due to coalescence in fluidized bed, *Trans. Inst. Chem. Eng.*, 55 (1977) 274-280.

Davidson, J. F., and D. Harrison, **Fluidised Particles**, Cambridge University Press, 1963.

Davies, L., and J. F. Richardson, Gas interchange between bubbles and the continuous phase in a fluidised bed, *Trans. Inst. Chem. Eng.*, 44 (1966) T293-T305.

Diekman, R., and W. L. Forsythe, Laboratory prediction of flow properties of fluidized solids, *Industrial and Engineering Chemistry*, 45 (1953) 1174-1177.

Donsi, G., B. Formisani, R. Valentino and G. Volpicelli, The measurement of characteristic angles of powders in their prediction in the gas fluidized state, *powder Technology*, 37 (1984) 39-47.

Dry, R. J., M. R. Jugg and T. Shingles, Bubble velocities in fluidized beds of fine dense powders, *Powder Technology*, 34 (1983) 213-223.

Dry, R. J., I. N. Christensen and G. C. Thomas, The effect of naturally-occurring interparticle forces on the fluidisation characteristics of fine iron-oxide powders, *Chemical Engineering Science*, 43 (1987) 1033-1038.

Ergun, S., Fluid flow through packed column, *Chemical Engineering Progress*, 48 (1952) 89-94.

Ergun, S., Determination of particle density of crushed porous solids, *Analytical Chemistry*, 23 (1951) 151.

Fan, L. T., T. Ho, S. Hiraoka and W. P. Walawender, Pressure fluctuation in a fluidized bed, *AIChE Journal*, 27 (1981) 388-396.

Fan, L. T., T. Ho and W. P. Walawender, Measurements of the rise velocities of bubbles, slugs and pressure waves in a gas-solid fluidized bed using pressure fluctuation

signals, *AIChE Journal*, 29 (1983) 33-39.

Foscolo, P. U., L. G. Gibilaro and S. P. Waldram, A unified model for particulate expansion of fluidised beds and flow in fixed porous media, *Chemical Engineering Science*, 38 (1983) 1251-1260.

Foscolo, P. U., and L. G. Gibilaro, A fully predictive criterion for the transition between particulate and aggregate fluidization, *Chemical Engineering Science*, 39 (1984) 1667.

Frantz, J. F., Minimum fluidization velocities and pressure drop in fluidized beds, *Chemical Engineering Progress Symposium Series*, No. 62, 62 (1966) 21-31.

Geldart, D., The effect of particle size and size distribution on the behaviour of gas-fluidised beds, *Powder Technology*, 6 (1972) 201-205.

Geldart, D., Types of gas fluidization, *Powder Technology*, 7 (1973) 285-292.

Geldart, D., and A. R. Abrahamsen, Homogenous fluidization of fine powders using various gases and pressures, *Powder Technology* 19 (1978) 133-136.

Geldart, D., N. Harnby and A. C. Wong, Fluidization of cohesive powders, *Powder Technology*, 37 (1984) 25-37.

Geldart, D., and A. C. Y. Wong, Fluidization of powders showing degrees of cohesiveness - II: experiments on rate of de-aeration. *Chemical Engineering Science* 40 (1985) 653-661.

Geldart, D. ed., **Gas Fluidization Technology**, Wiley, New York, 1986.

Grace, J. R., Chapter 8 in **Handbook of Multiphase System**, ed. G. Hetsroni, Hemisphere Press, 1982.

Grace, J. R., Contacting modes and behaviour classification of gas-solid and other two-phase suspension, *Canadian Journal of Chemical Engineering*, 64 (1986) 353-363.

Groot, de, Scaling-up of gas-fluidized bed reactors, **Proceedings on International Symposium of Fluidization**, ed. A. A. H. Drinkenberg, Netherlands University Press, Eindhoven, 348-361,1967.

Jacob, K. V., and A. W. Weimer, High pressure synthesis gas fluidization of fine carbon carbon powders: particle expansion and bubbling, *AIChE Journal*, 33 (1987) 1698-1706.

Jong, J. A. H. de, and J. F. Nomden, Homogenous gas-solid fluidization, *Powder Technology*, 9 (1974) 91-97.

Kang W. K., J. P. Sutherland and G. L. Osberg, Pressure fluctuations in a fluidized bed with and without screen cylindrical packings, *Industrial and Engineering Fundamentals*, 6 (1967), No. 4, 499-504.

Kehoe, P. W. K., and J. F. Davidson, Continuously slugging fluidised beds, *Institution of Chemical Engineering Symposium Series*, 33 (1970) 97-116, Butterworth of Australia.

Khoe, G. K., T. Ip and J. R. Grace, The influence of fine particles on the rheology and fluidization behaviour of powders, **Proceedings of the 1988 Conference on Measurement and Control of Granular Material**, Shenyong, China, 1988.

Khoe, G. T., Private communication, 1988.

Kmiec, A., Equilibrium of forces in a fluidized bed - experimental verification, *Chemical Engineering Journal*, 23 (1982) 133-136.

Kunz, R. G., Minimum fluidization velocities: Fluid cracking catalyst and spherical glass beads, *Powder Technology*, 4 (1970) 156-162.

Lirag, R. C., and H. Littman, Statistical study of the pressure fluctuations in a fluidized bed, *AIChE Symposium Series*, No. 116, 67 (1970) 11-22.

Littman, H., and G. A. Homolka, *Chemical Engineering Progress Symposium Series*, No. 105, 60 (1970) 37.

Matheson, G. L., W.A. Herbst and P. H. Holt, Characteristics of fluid-solid system, *Industrial and Engineering Chemistry*, 41 (1949) 1099-1104.

May, W. G., Fluidized-bed reactor studies, *Chemical Engineering Progress*, 55 (1959) No. 12, 49-56.

Massimilla, L., G. Donsi and C. Zucchini, The structure of bubble-free gas fluidized beds of fine fluid cracking catalyst particles, *Chemical Engineering Science*, 27 (1972) 2005-2015.

Massimilla, L., and G. Donsi, Cohesive forces between particles of fluid-bed catalysts, *Powder Technology*, 15 (1976) 253-260.

Mori, S., and C. Y. Wen, Estimation of bubble diameter in gaseous fluidized beds, *AIChE Journal*, 21 (1975) 109-115.

Morse, R. D., and C.O. Ballou, The uniformity of fluidization - its measurement and use, *Chemical Engineering Progress*, 47 (1951) 199-204.

Murfitt, P. G., and P. L. Bransby, Deaeration of powders in loppers, *Powder Technology*, 27 (1980) 149-162.

Mutsers, S. M. P., and K. Rietema, The effect of interparticle forces on the expansion of a homogenous gas-fluidized bed, *Powder Technology*, 18 (1977) 239-248.

Noodergraaf, I. W., A. van Dijk and C. M. van den Bleek, Fluidization and slugging in large-particle systems,. *Powder Technology*, 52 (1987) 59-68.

Pyle, D. L., and D. Harrison, An experimental investigation of the two- phase theory of fluidization, *Chemical Engineering Science*, 22 (1967) 1199-1207.

Richardson, J. F., and W. N. Zaki, Sedimentation and fluidization: part I, *Trans. Instn. Chem. Engrs.*, 32 (1954) 35-53.

Richardson, J. F., Chapter 2 in J. F. Davidson and D. Harrison (Eds.), **Fluidization**, Academic Press, London, 1971.

Rietema, K., Application of Mechanical Stress Theory to Fluidization, **Proceedings of International Symposium on Fluidization**, ed. A. A. H. Drinkenberg, 154-175, Netherlands University Press, Eindhoven, 1967.

Rietema, K., Powders, what are they, *Powder Technology*, 37 (1984) 5-23.

Rowe, P. N., and C. X. R. Yacono, The bubbling behaviour of fine powders when fluidized, *Chemical Engineering Science*, 31 (1976) 1179-1192.

Rowe, P. N., L. Santoro and J. G. Yates, The division of gas between bubble and interstitial phases in fluidised beds of fine powders, *Chemical Engineering Science*, 33 (1978) 133-140.

Sadasivan, S., D. Bareteau and C. Laguerie, Studies on frequency and magnitude of fluctuations of pressure drop in gas-solid fluidised beds, *Powder Technology*, 26 (1980) 67-74.

Satija, S., and L. Fan, Characteristics of slugging regime and transition to turbulent regime for fluidized beds of large coarse particles, *AIChE Journal*, 31 (1985) 1554-1562.

Simone, S., and P. Harriott, Fluidization of fine powders with air in the particulate and the bubbling regions, *Powder Technology*, 26 (1980) 161-167.

Stewart, P. S. B., and J. F. Davidson, Slug flow in fluidised beds, *Powder Technology*, 1 (1967) 61-80.

Stockham, J. D., and E. G. Fochtman, **Particle Size Analysis**, Ann Arbor Science, Ann Arbor, 1978.

Svoboda, K., J. Cermak, M. Hartman, J. Drahos and K. Selucky, Influence of particle size on the pressure fluctuations and slugging in a fluidized bed, *AIChE Journal*, 30 (1984) 513-517.

Toomey, R. D., and H. F. Johnstone, Gaseous fluidization of solid particles, *Chemical Engineering Progress*, 48 (1952) 220-226.

Tung Y., Z. Ziping, Y. Xia, W. Zheng, Y. Yang and M. Kwauk, Assessing fluidizing characteristics of powders, in **Fluidization**, eds. J. R. Grace and L. W. Shemilt, Engineering Foundation, New York, 1989.

Verloop, J., and P. M. Heertjes, Periodic pressure fluctuation in fluidized beds, *Chemical Engineering Science*, 29 (1974) 1035-1042.

Volk, W., C. A. Johnson and H. H. Stotler, Effect of reactor internals on quality of fluidization, *Chemical Engineering Progress* 58 (1962) 38-41.

Vries, R. J. de, W. P. M. van Swaaij, C. Mantovani and A. Heijkoop, **Proceedings of Fifth European / Second International Symposium on Chemical Reaction Engineering**, B9-B59, Elsevier Publishing Company, Amsterdam, 1972.

Wen, C. Y., and Y. H. Yu, *Chemical Engineering Progress Symposium Series*, 62 (1966) 100.

Wen, C. Y., and Y. H. Yu, A generalized method for predicting the minimum fluidization velocities, *AIChE Journal*, 12 (1966) 610.

Yershalmi, J., and N. T. Cankurt, Further studies of the regimes of fluidization, *Powder Technology*, 24 (1979) 187-205.

Appendix A.

Minimum Fluidization Plots

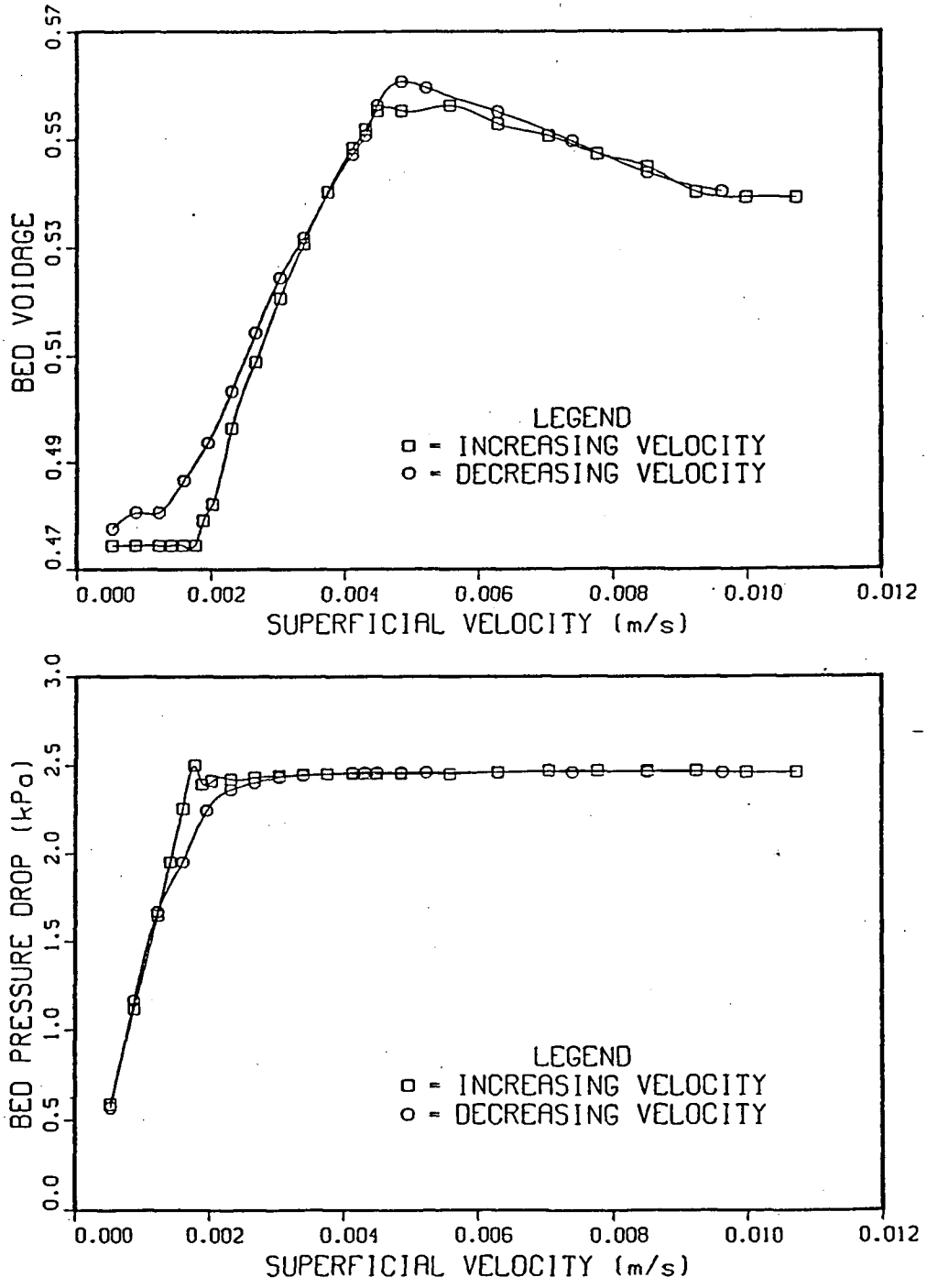

Figure A.1: Minimum Fluidization Plots for Original Distribution of FCC. Static bed height is 3.3 times bed diameter.

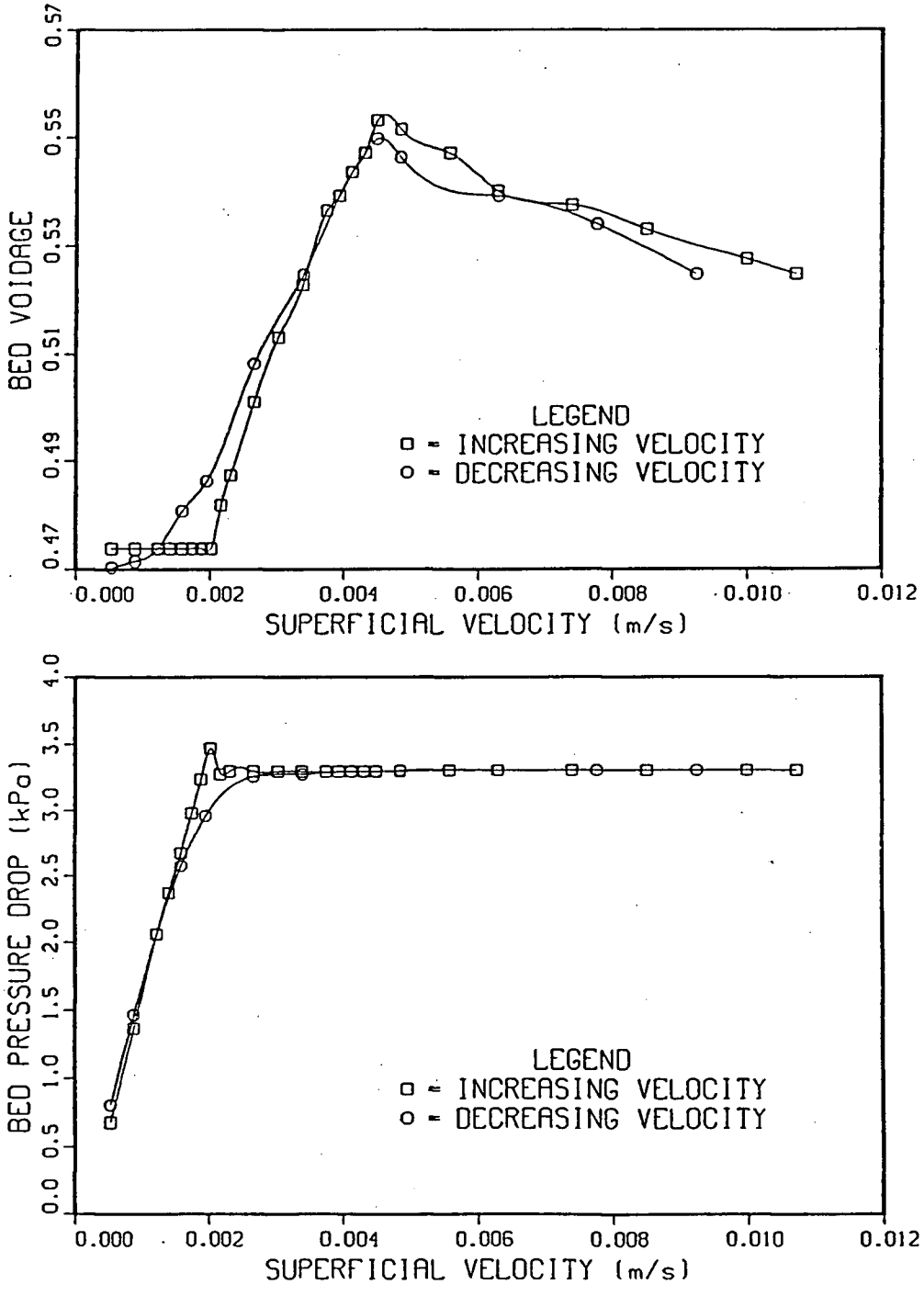

Figure A.2: Minimum Fluidization Plots for Original Distribution of FCC. Static bed height is 4.4 times bed diameter.

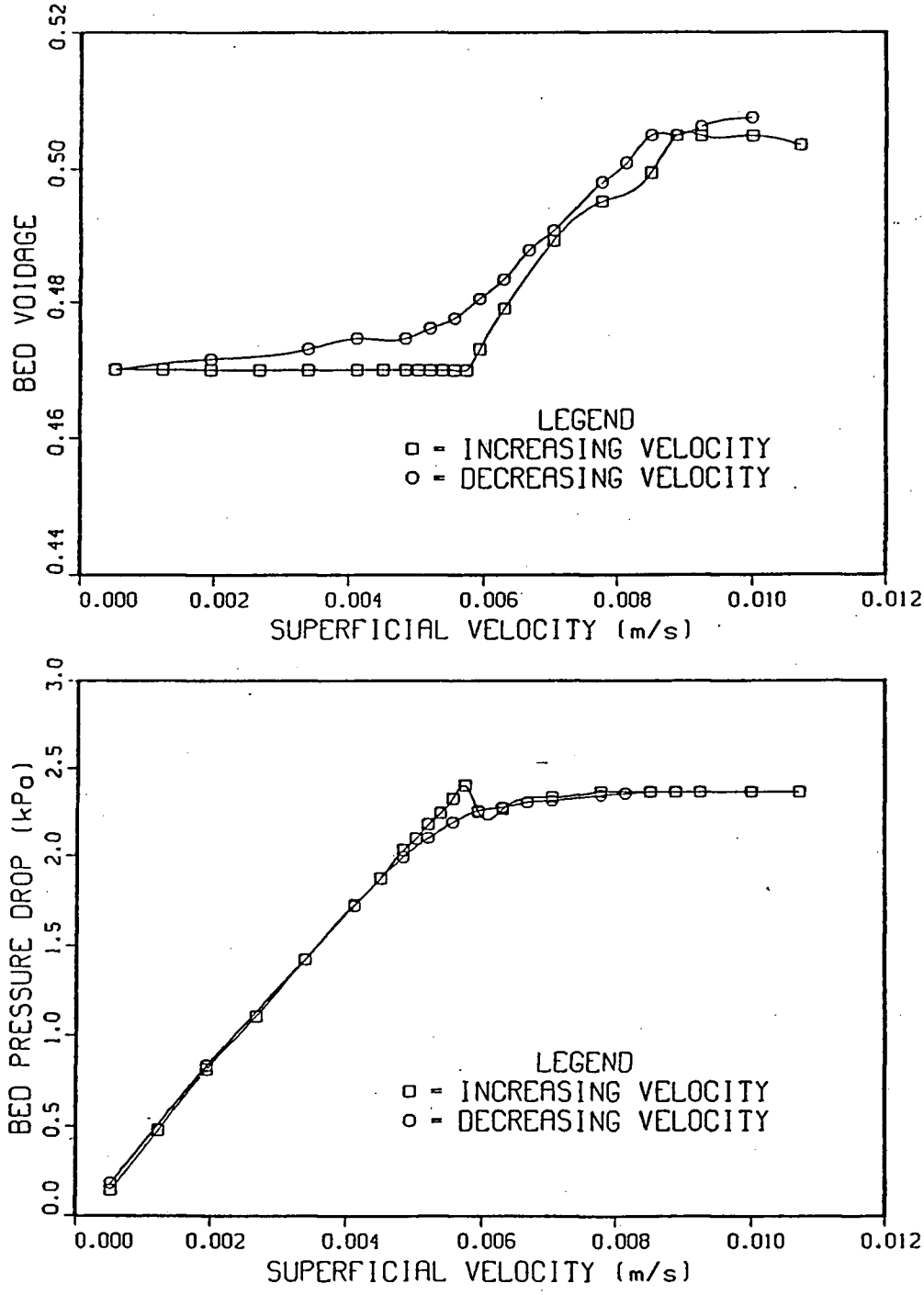

Figure A.3: Minimum Fluidization Plots for Coarse Distribution of FCC. Static bed height is 3.3 times bed diameter.

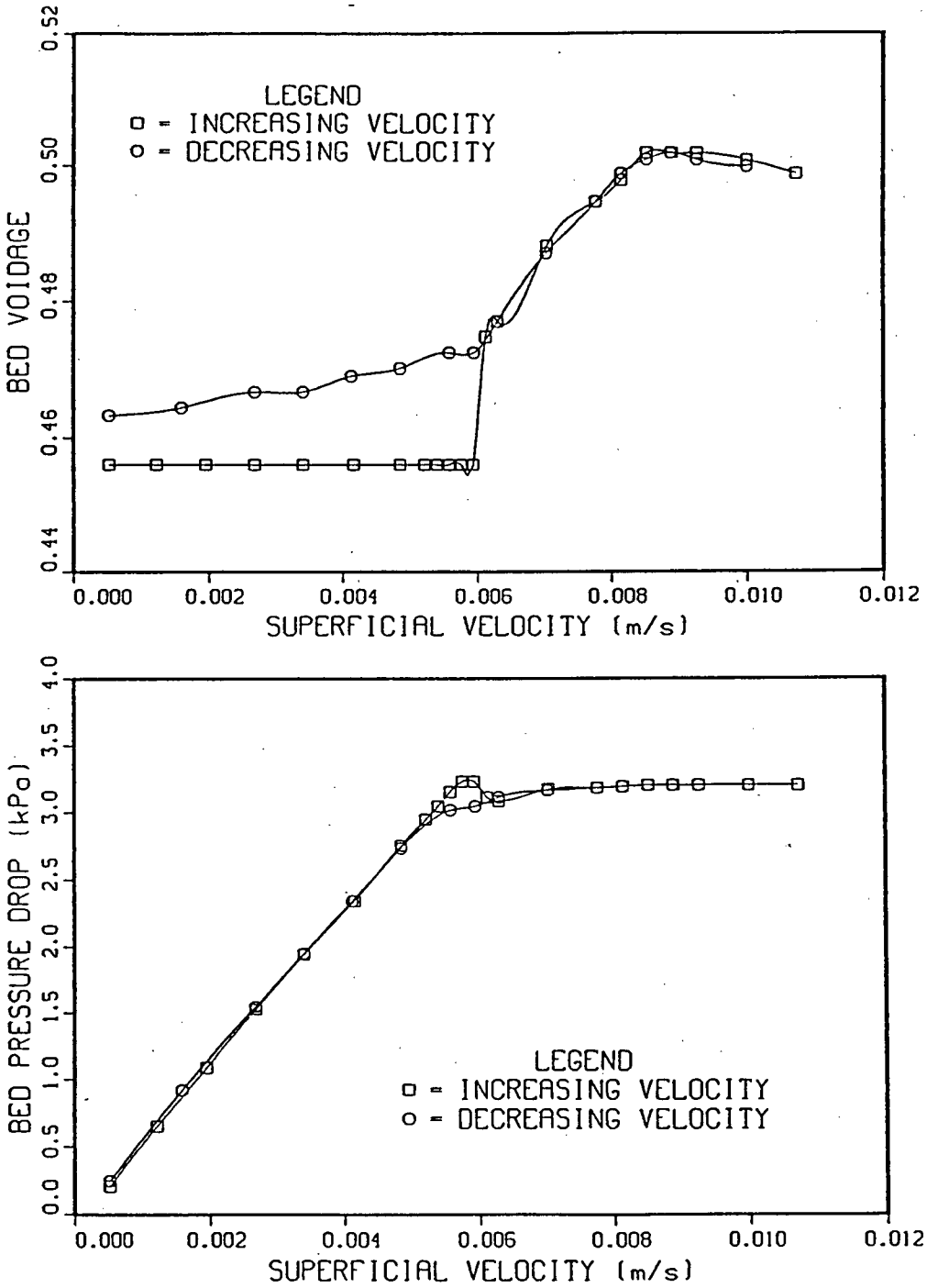

Figure A.4: Minimum Fluidization Plots for Coarse Distribution of FCC. Static bed height is 4.4 times bed diameter.

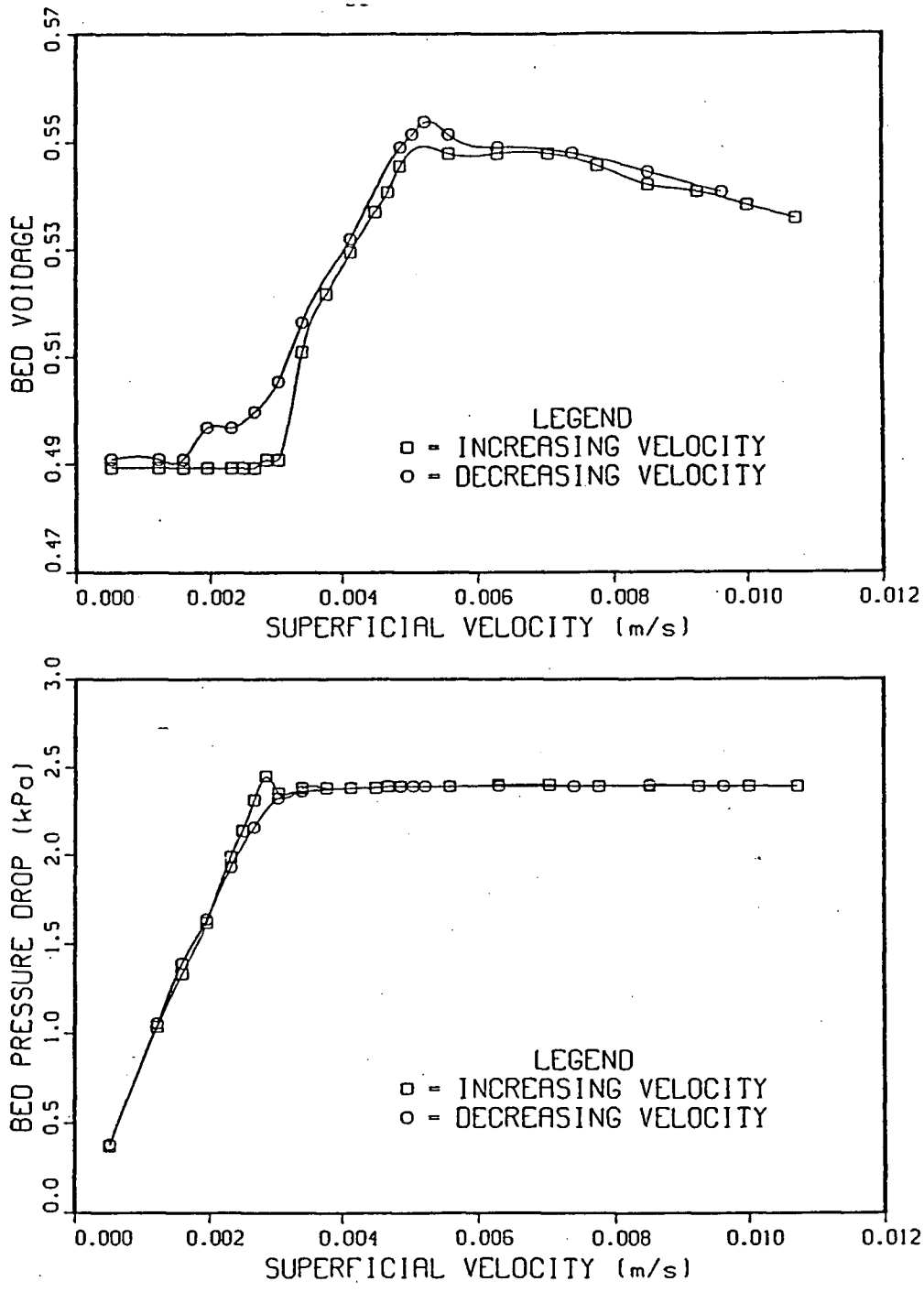

Figure A.5: Minimum Fluidization Plots for Intermediate Distribution of FCC. Static bed height is 3.3 times bed diameter.

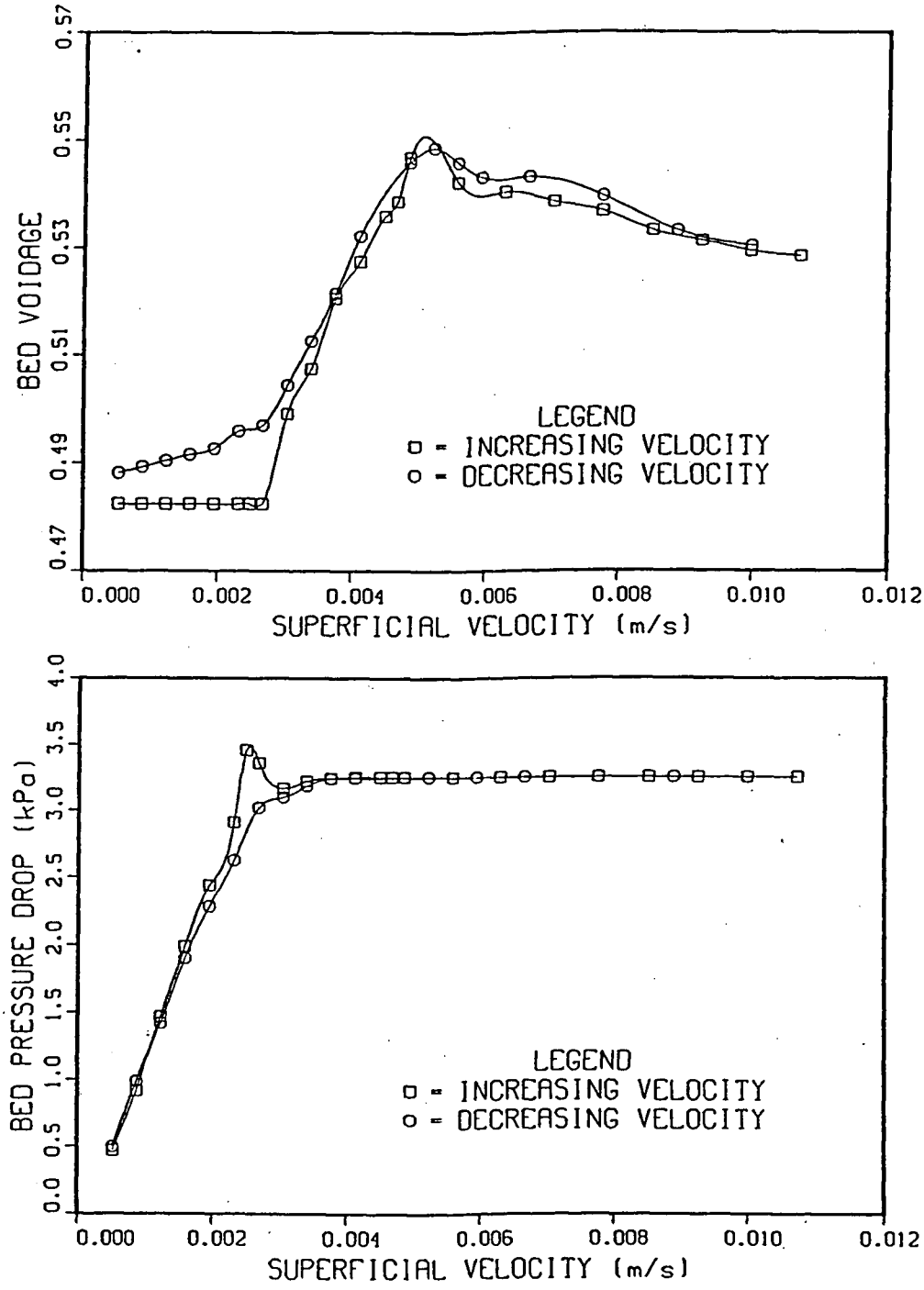

Figure A.6: Minimum Fluidization Plots for Intermediate Distribution of FCC. Static bed height is 4.4 times bed diameter.

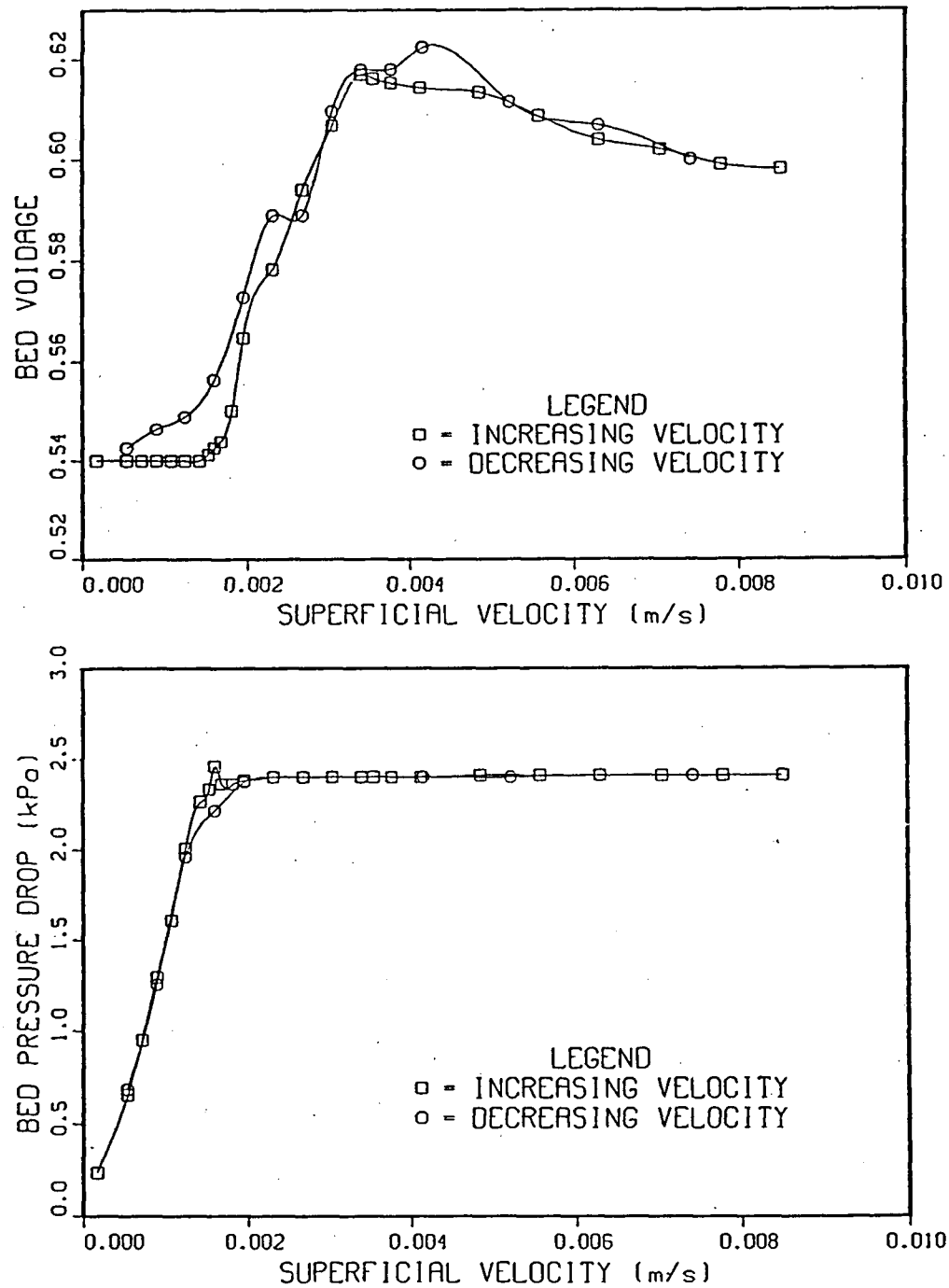

Figure A.7: Minimum Fluidization Plots for Fine Distribution of FCC. Static bed height is 3.3 times bed diameter.

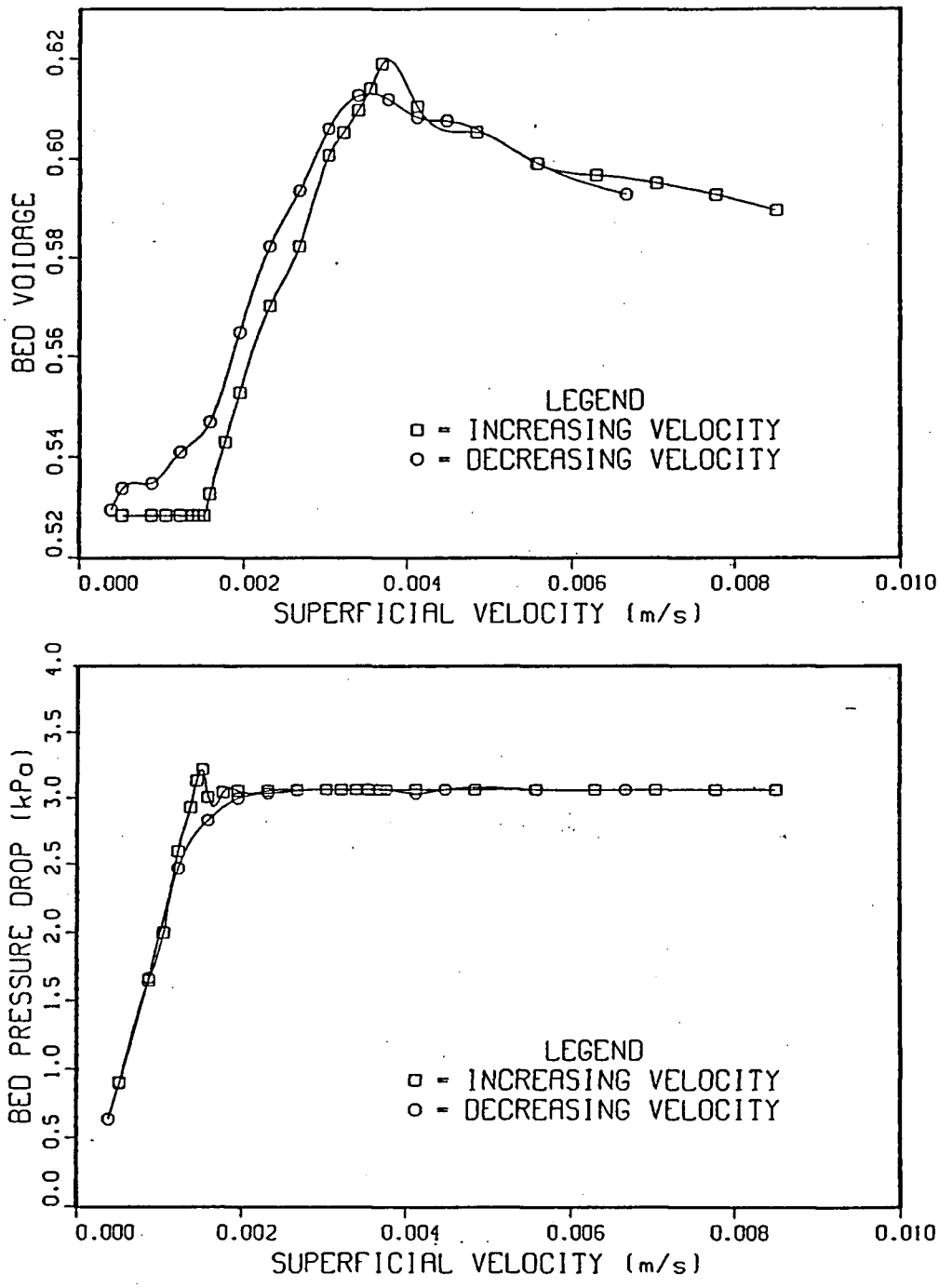

Figure A.8: Minimum Fluidization Plots for Fine Distribution of FCC. Static bed height is 4.4 times bed diameter.

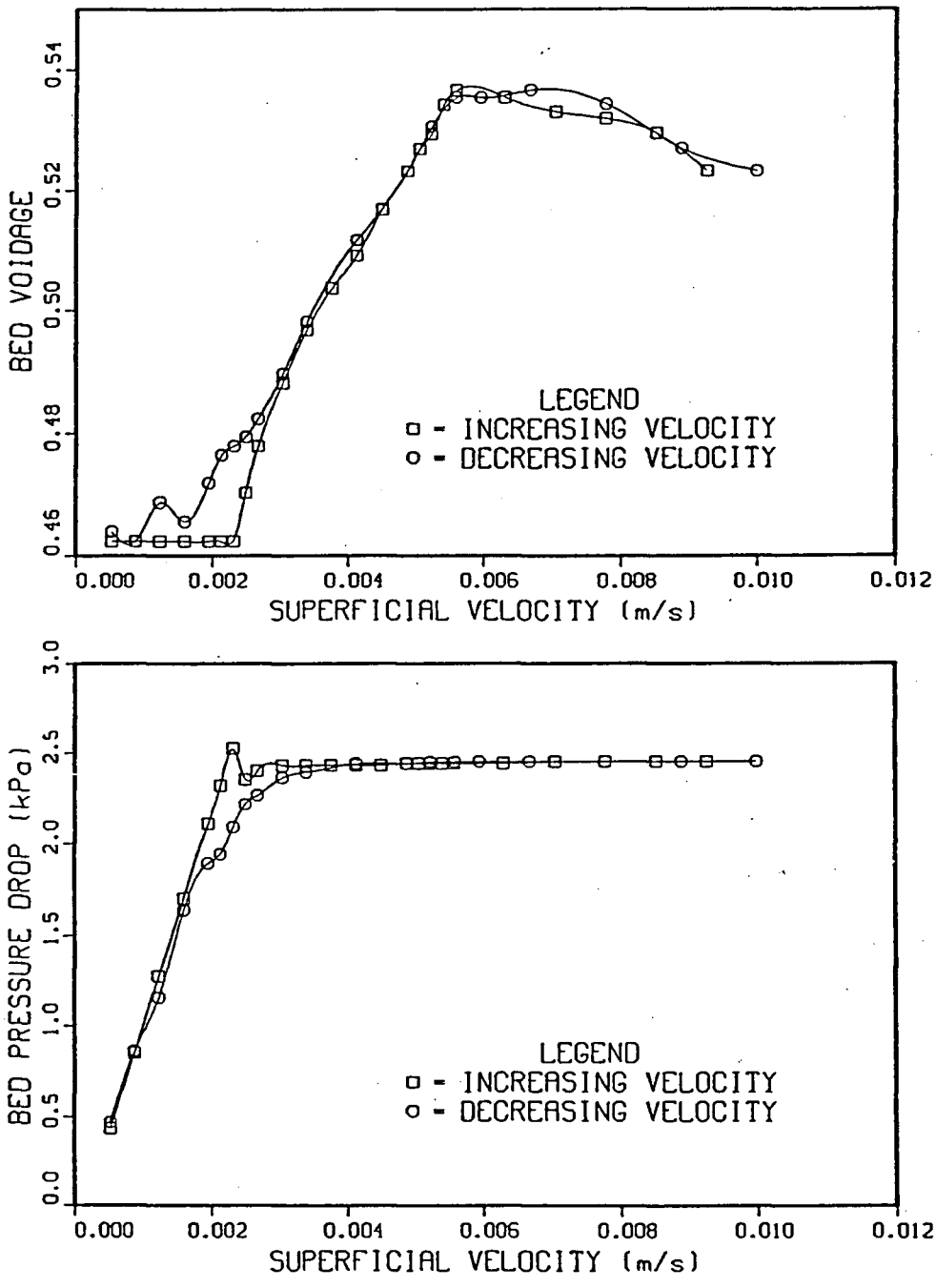

Figure A.9: Minimum Fluidization Plots for Wide Distribution of FCC. Static bed height is 3.3 times bed diameter.

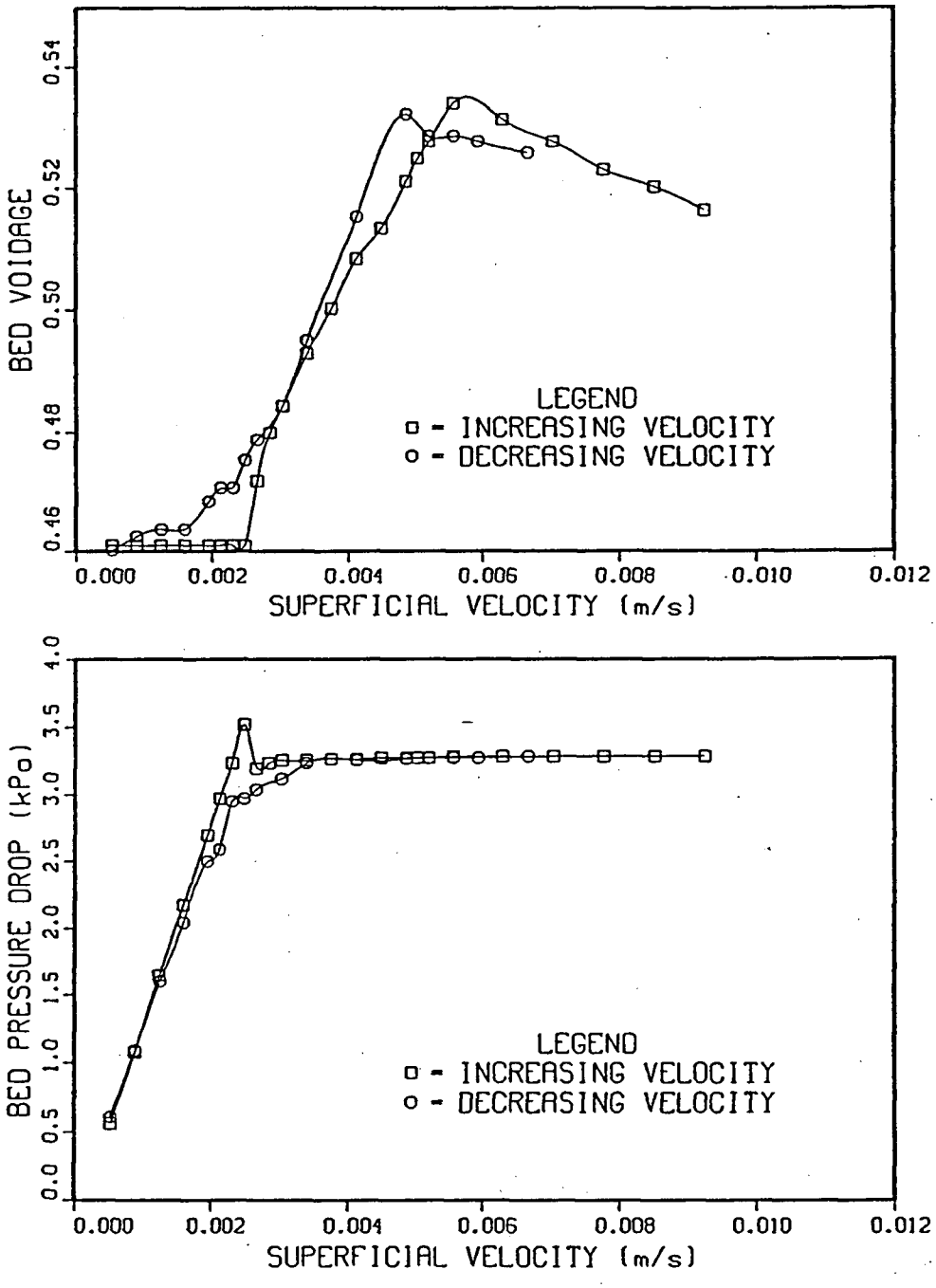

Figure A.10: Minimum Fluidization Plots for Wide Distribution of FCC. Static bed height is 4.4 times bed diameter.

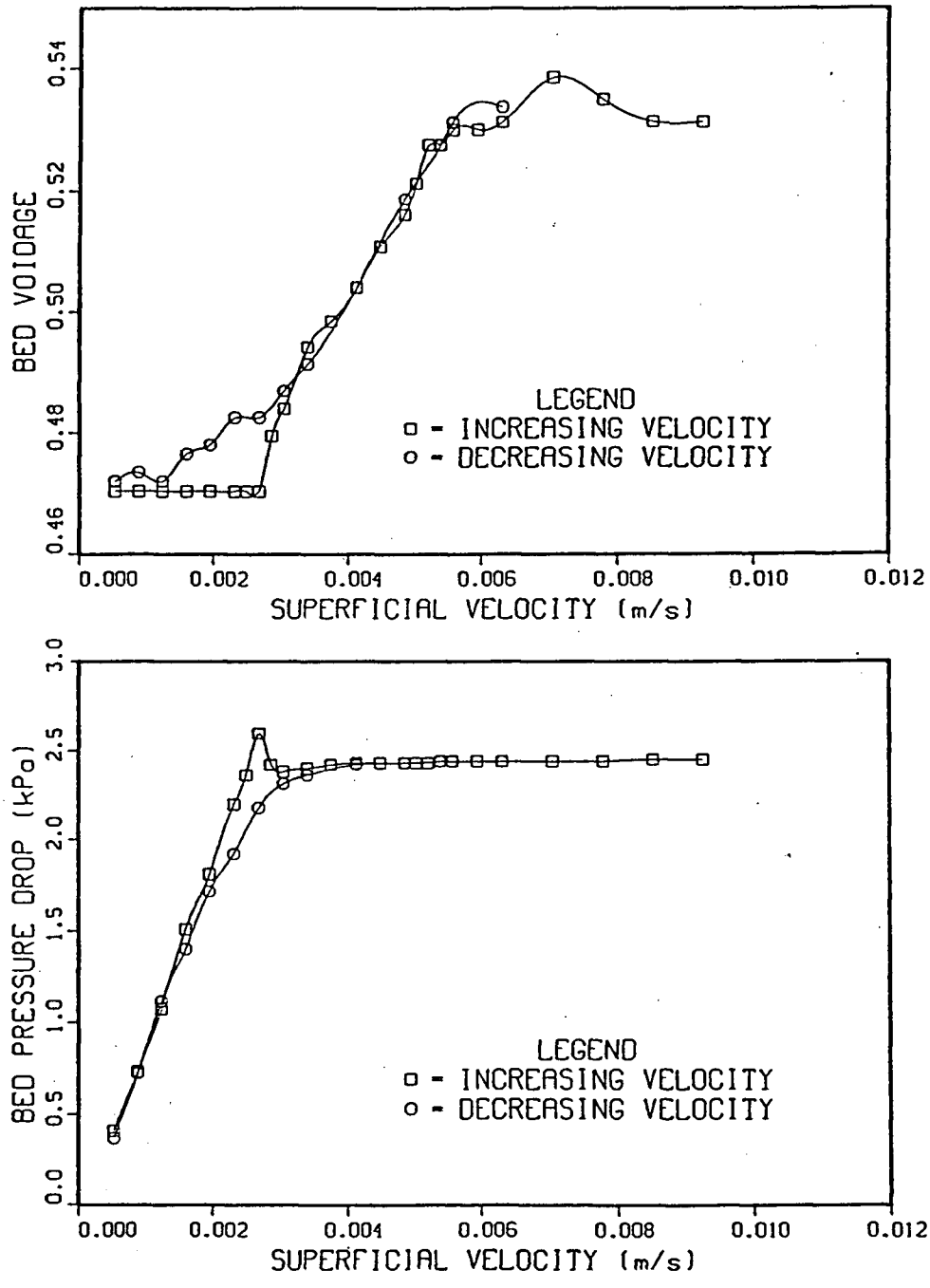

Figure A.11: Minimum Fluidization Plots for Bimodal Distribution of FCC. Static bed height is 3.3 times bed diameter.

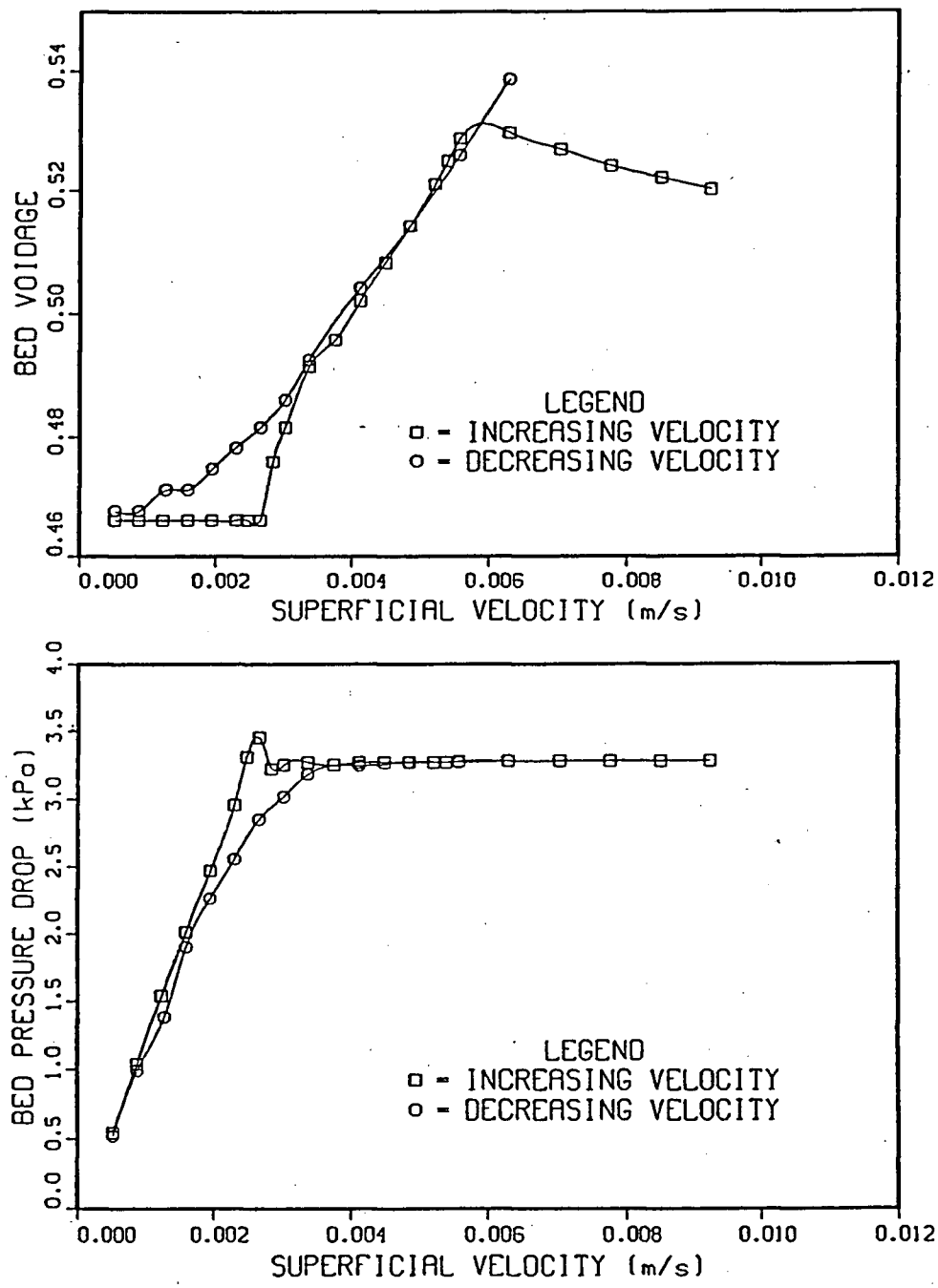

Figure A.12: Minimum Fluidization Plots for Bimodal Distribution of FCC. Static bed height is 4.4 times bed diameter.

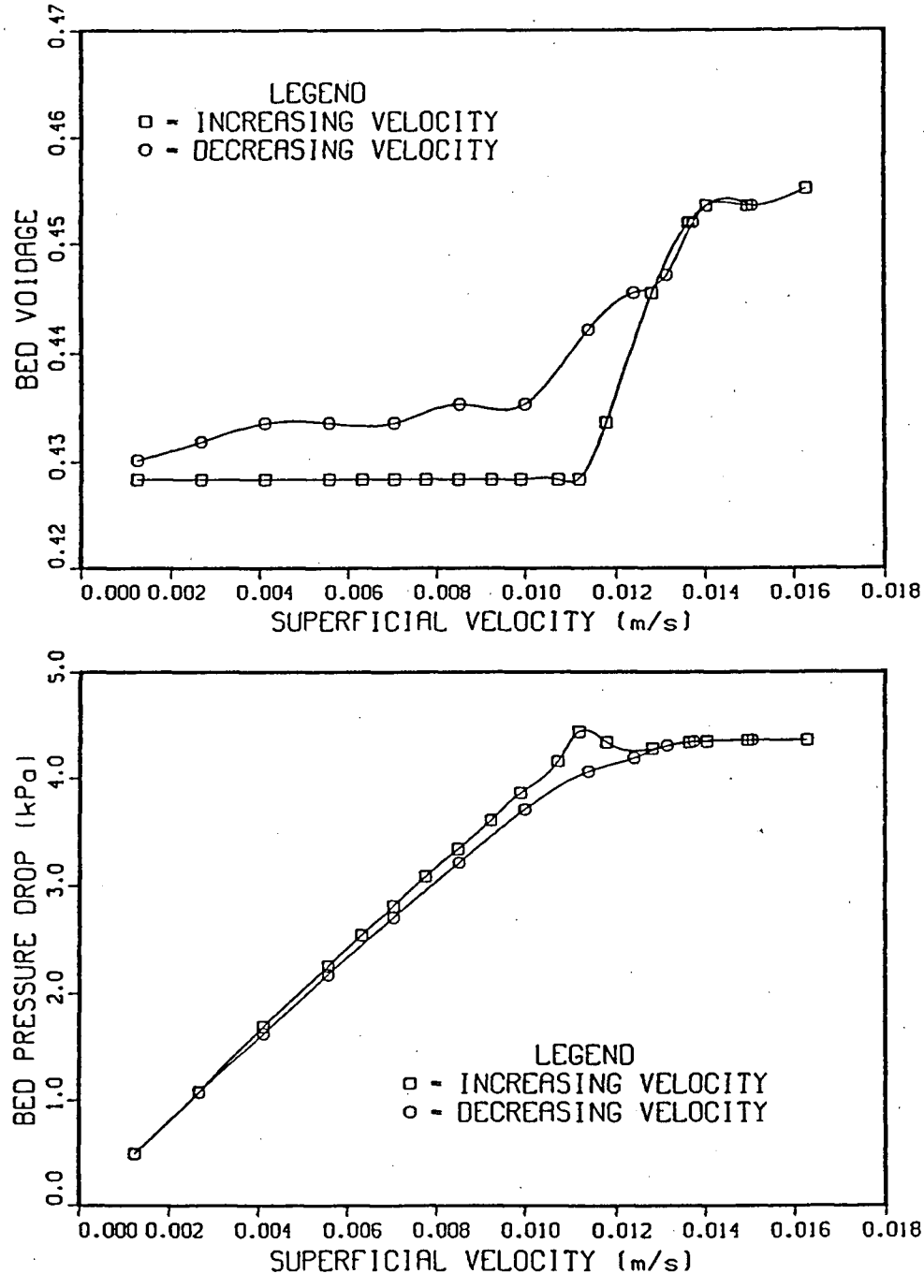

Figure A.13: Minimum Fluidization Plots for Coarse Distribution of Glass Beads. Static bed height is 3.3 times bed diameter.

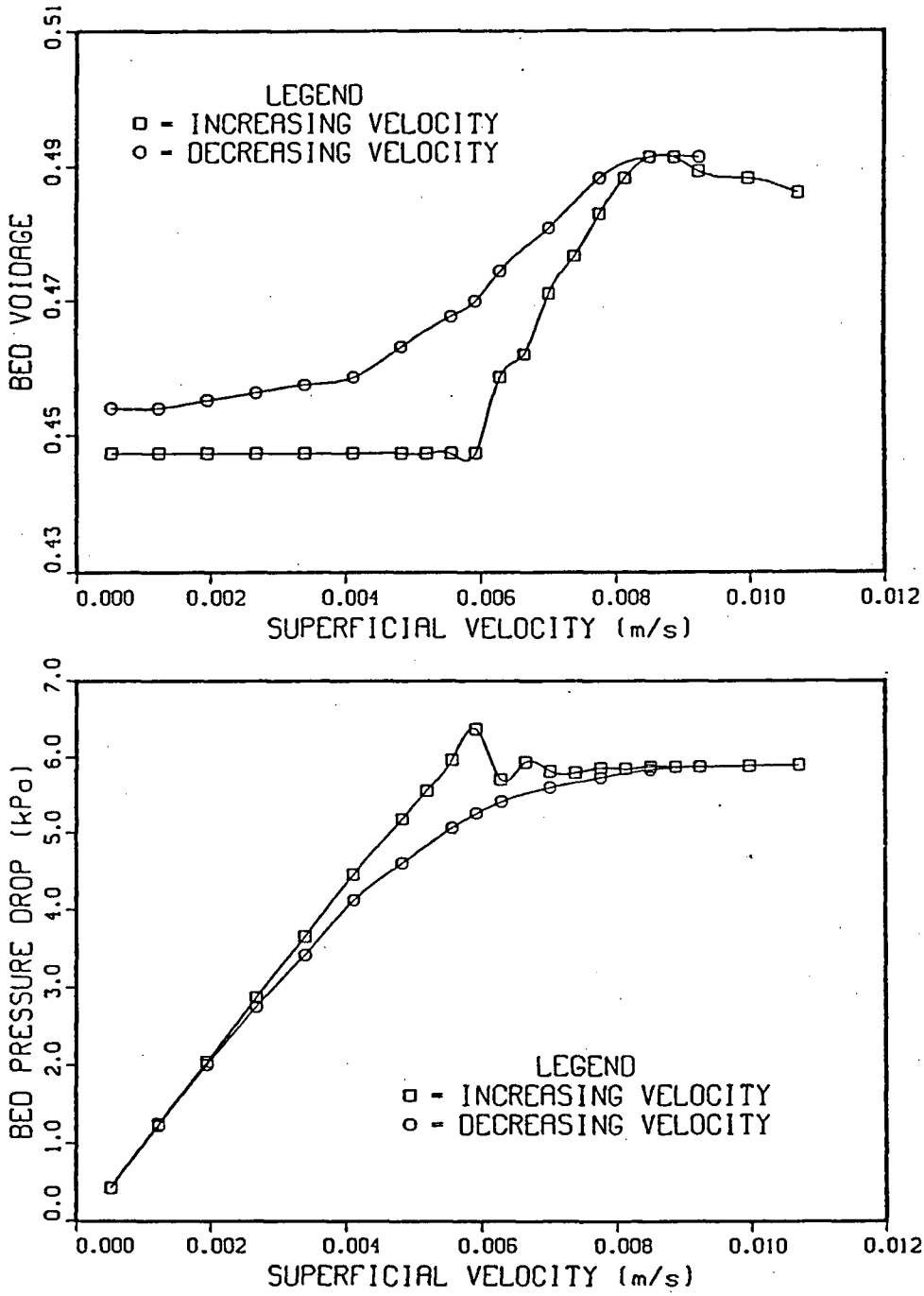

Figure A.14: Minimum Fluidization Plots for Intermediate Distribution of Glass Beads. Static bed height is 4.4 times bed diameter.

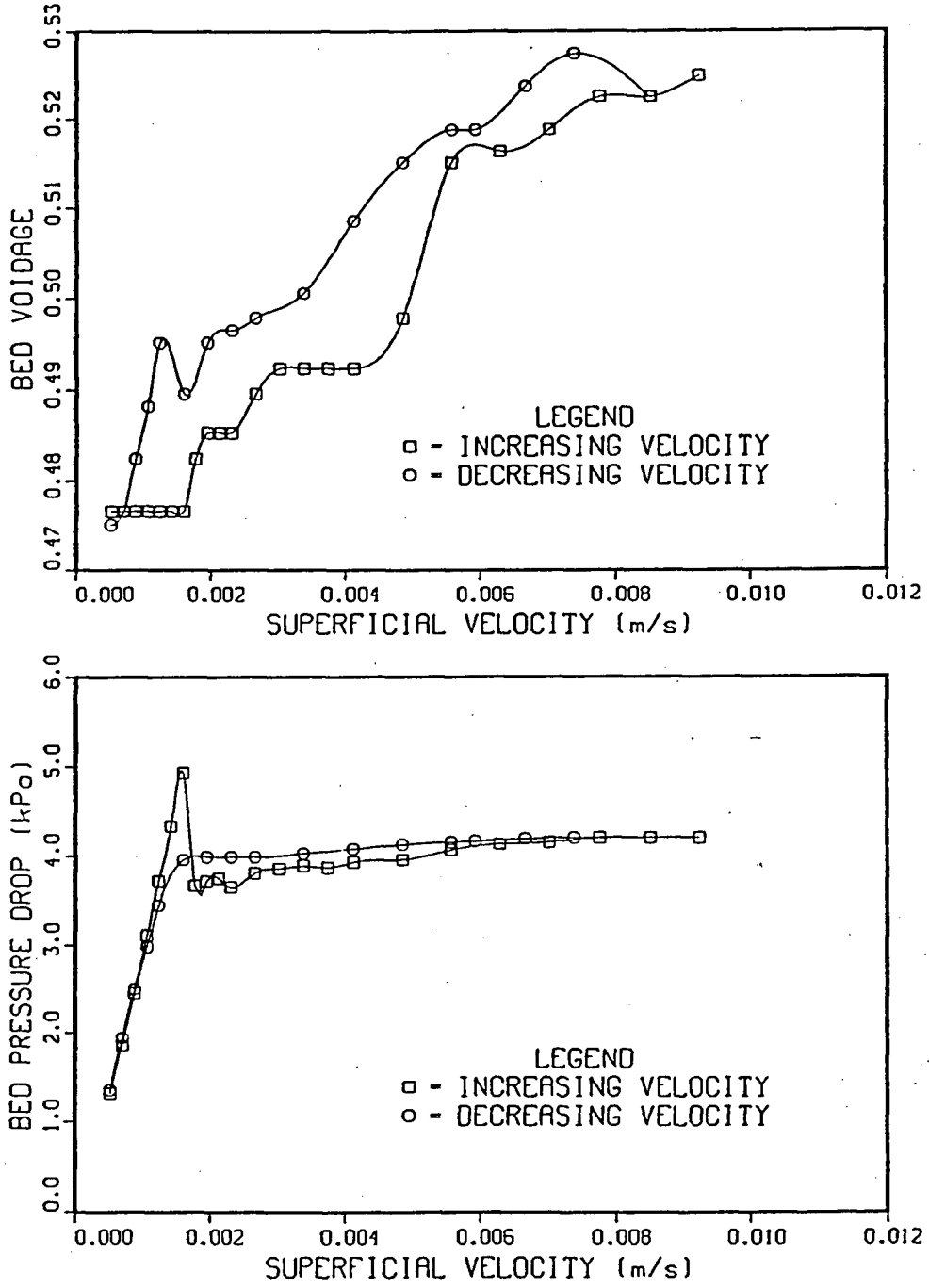

Figure A.15: Minimum Fluidization Plots for Fine Distribution of Glass Beads. Static bed height is 3.2 times bed diameter.

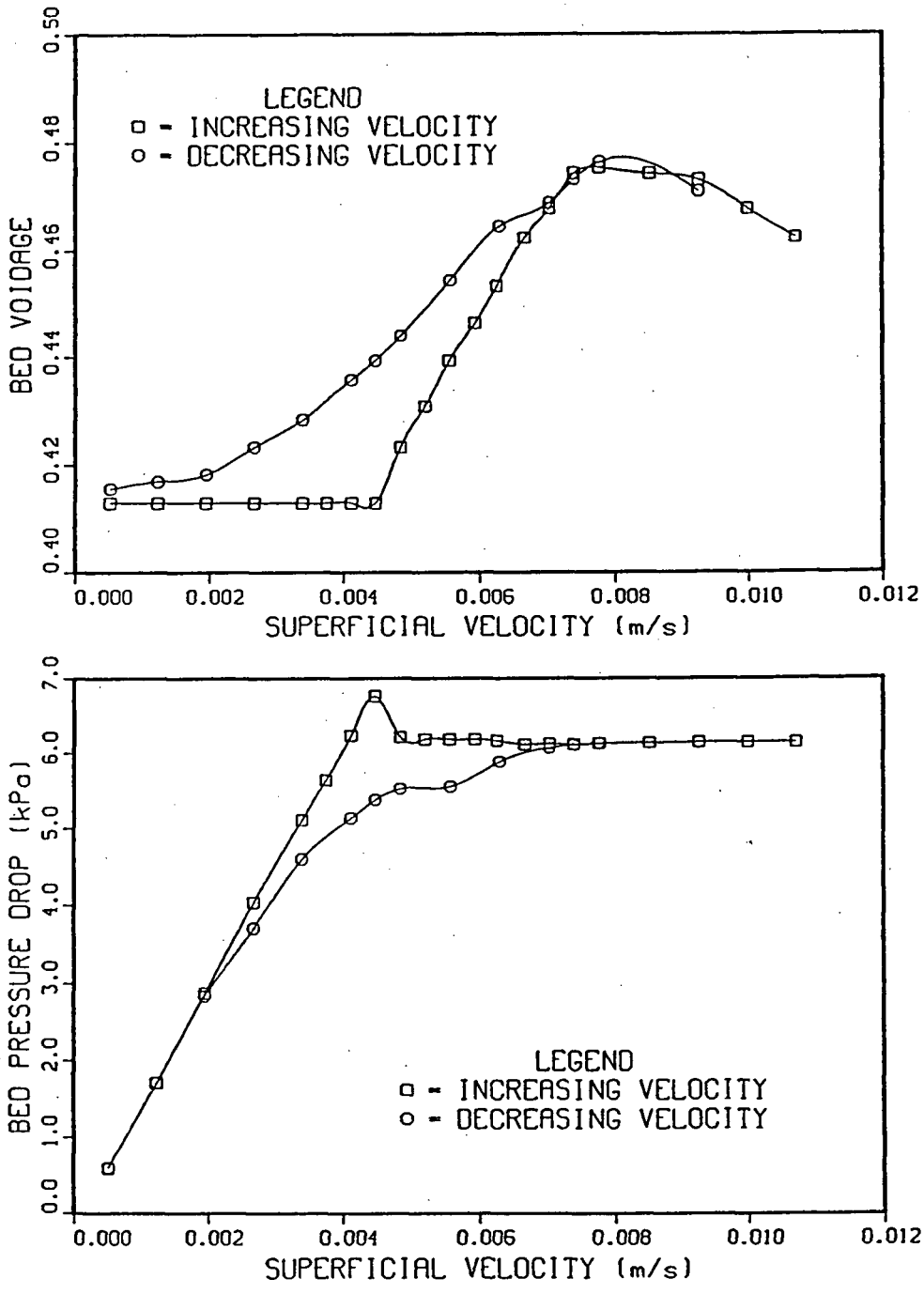

Figure A.16: Minimum Fluidization Plots for Wide Distribution of Glass Beads. Static bed height is 4.4 times bed diameter.

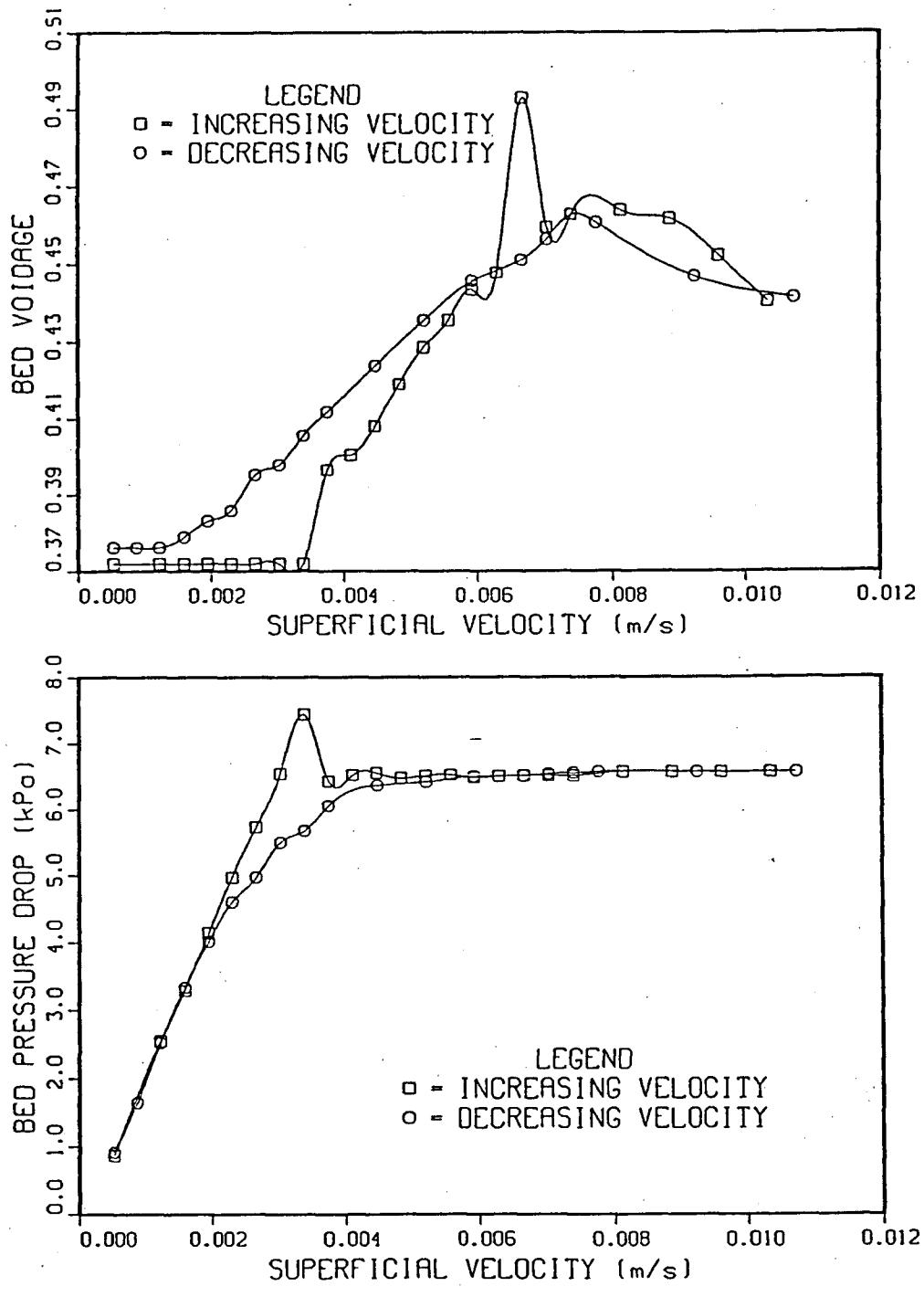

Figure A.17: Minimum Fluidization Plots for Bimodal Distribution of Glass Beads. Static bed height is 4.4 times bed diameter.

Appendix B

Terminal Velocities

Table B.1: Terminal Settling Velocity Correlations for Spheres (Grace, 1986).

d_p^* Range	U_t^* Range	Equation
≤ 3.8	≤ 0.624	$U_t^* = (d_p^*)^2/18 - 3.1234 * 10^{-4}(d_p^*)^5 + 1.6415 * 10^{-6}(d_p^*)^8 - 7.278 * 10^{-10}(d_p^*)^{11}$
3.8 to 7.58	0.624 to 1.63	$\log_{10}U_t^* = -1.5466 + 2.9162\omega - 1.0432\omega^2$
7.58 to 227	1.63 to 28	$\log_{10}U_t^* = -1.64758 + 2.94786\omega - 1.09703\omega^2 + 0.17129\omega^3$
227 to 3350	28 to 91.7	$\log_{10}U_t^* = 5.1837 - 4.51034\omega + 1.687\omega^2 - 0.189135\omega^3$

$d_p^* = d_p * [g * \rho_g * (\rho_p - \rho_g)/\mu^2]^{0.333}$
$U_t^* = U_t * [\rho_g^2/\mu g(\rho_p - \rho_g)]^{0.333}$
$\omega = \log(d_p^*)$

Table B.2: Terminal Velocities, Reynolds Numbers and indices 'n' for Different Distributions of FCC. The indices are predicted using Richardson and Zaki's correlations (See Section 1.3.2)

Size Distributions	d_p^*	U_t (m/s)	Re_t	n
Original	2.20	0.124	0.560	5.19
Coarse	4.02	0.287	2.395	4.09
Intermediate	2.61	0.168	0.898	4.50
Fines	1.71	0.079	0.270	6.45
Wide	2.58	0.164	0.872	4.54
Bimodal	2.64	0.172	0.927	4.46

Table B.3: Terminal Velocities, Reynolds Numbers and indices 'n' for Different Distributions of Glass Beads. The indices are predicted using Richardson and Zaki's correlations (see Section 1.3.2).

Size Distributions	d_p^*	U_t (m/s)	Re_t	n
Coarse	6.59	0.813	9.18	3.58
Intermediate	4.24	0.437	3.18	3.98
Fines	2.18	0.146	0.54	5.24
Wide	4.20	0.430	3.10	3.99
Bimodal	4.26	0.440	3.22	3.97

Appendix C

Raw Data from Collapse Tests

Table C.1: Raw Data from Collapse Tests on Original FCC Distribution. Four runs were performed for each set of data.

Original Distribution of FCC				
H = 3.3D				
Superficial Velocity (mm/s)	Dense Phase Voidage		Superficial Dense Phase Velocity (mm/s)	
	Mean	Standard Deviation	Mean	Standard Deviation
2.77	0.511	0.002	2.37	0.04
4.26	0.548	0.000	4.04	0.02
5.71	0.555	0.003	3.97	0.17
7.20	0.546	0.001	3.49	0.05
8.69	0.540	0.001	3.18	0.02
10.20	0.535	0.002	3.02	0.04
13.46	0.526	0.002	2.70	0.08
17.81	0.518	0.000	2.62	0.04
21.55	0.513	0.002	2.67	0.15
24.97	0.510	0.001	2.89	0.14
28.90	0.508	0.000	2.89	0.15
34.13	0.504	0.002	2.82	0.10
38.91	0.503	0.003	2.81	0.12
H = 4.4D				
2.77	0.510	0.000	2.42	0.01
4.24	0.547	0.001	4.01	0.10
5.73	0.550	0.003	4.06	0.14
7.23	0.537	0.007	3.45	0.27
8.76	0.533	0.002	3.30	0.08
10.24	0.525	0.001	2.90	0.03
13.65	0.516	0.000	2.66	0.01
17.96	0.508	0.001	2.41	0.10
21.83	0.501	0.001	2.37	0.06
25.15	0.498	0.000	2.43	0.06
29.20	0.496	0.001	2.41	0.09
34.43	0.493	0.001	2.39	0.09
39.07	0.494	0.000	2.36	0.10

Table C.2: Raw Data from Collapse Tests on Coarse FCC Distribution. Four runs were performed for each set of data.

Coarse Distribution of FCC				
H = 3.3D				
Superficial Velocity (mm/s)	Dense Phase Voidage		Superficial Dense Phase Velocity (mm/s)	
	Mean	Standard Deviation	Mean	Standard Deviation
7.29	0.487	0.001	5.39	0.01
8.80	0.501	0.000	6.63	0.04
10.33	0.499	0.000	6.21	0.05
13.55	0.500	0.001	5.87	0.27
17.89	0.492	0.001	5.40	0.11
21.33	0.487	0.001	5.70	0.21
25.11	0.486	0.001	5.89	0.01
29.79	0.484	0.000	6.04	0.14
34.37	0.485	0.001	5.85	0.38
39.24	0.485	0.001	5.97	0.14
H = 4.4D				
7.31	0.485	0.000	5.20	0.08
8.82	0.500	0.001	6.60	0.03
10.34	0.497	0.002	6.11	0.25
13.72	0.481	0.001	5.59	0.29
18.12	0.474	0.001	5.54	0.21
21.42	0.469	0.001	5.60	0.05
25.45	0.468	0.000	5.75	0.10
29.80	0.469	0.000	5.86	0.10
34.77	0.468	0.000	5.79	0.00
39.60	0.468	0.000	5.95	0.06

Table C.3: Raw Data from Collapse Tests on Intermediate FCC Distribution. Three runs were performed for each set of data.

Intermediate Distribution of FCC				
H = 3.3D				
Superficial Velocity (mm/s)	Dense Phase Voidage		Superficial Dense Phase Velocity (mm/s)	
	Mean	Standard Deviation	Mean	Standard Deviation
4.27	0.531	0.000	3.60	0.00
5.74	0.545	0.000	4.12	0.07
7.25	0.541	0.000	3.86	0.00
8.70	0.539	0.000	3.76	0.01
10.20	0.532	0.000	3.53	0.03
13.48	0.522	0.001	3.39	0.08
17.77	0.514	0.000	3.16	0.00
21.72	0.512	0.000	3.22	0.03
24.97	0.509	0.002	3.31	0.17
28.92	0.507	0.002	3.24	0.05
H = 4.4D				
3.56	0.509	0.001	2.52	0.04
4.30	0.527	0.000	3.53	0.01
5.79	0.537	0.002	3.87	0.10
7.25	0.537	0.001	3.77	0.08
8.73	0.532	0.002	3.50	0.08
10.46	0.525	0.002	3.21	0.06
13.75	0.512	0.000	2.78	0.02
18.17	0.507	0.001	2.69	0.18
22.13	0.505	0.001	2.64	0.03
25.83	0.504	0.001	2.82	0.03
29.24	0.502	0.000	2.73	0.02
34.57	0.501	0.001	2.79	0.10
38.92	0.501	0.001	2.75	0.13

Table C.4: Raw Data from Collapse Tests on Fine FCC Distribution. Four runs were performed for each set of data.

Fine Distribution of FCC				
H = 3.3D				
Superficial Velocity (mm/s)	Dense Phase Voidage		Superficial Dense Phase Velocity (mm/s)	
	Mean	Standard Deviation	Mean	Standard Deviation
7.29	0.487	0.001	5.39	0.01
8.80	0.501	0.000	6.63	0.04
10.33	0.499	0.000	6.21	0.05
13.55	0.500	0.001	5.87	0.27
17.89	0.492	0.001	5.40	0.11
21.33	0.487	0.001	5.70	0.21
25.11	0.486	0.001	5.89	0.01
29.79	0.484	0.000	6.04	0.14
34.37	0.485	0.001	5.85	0.38
39.24	0.485	0.001	5.97	0.14
H = 4.4D				
7.31	0.485	0.000	5.20	0.08
8.82	0.500	0.001	6.60	0.03
10.34	0.497	0.002	6.11	0.25
13.72	0.481	0.001	5.59	0.29
18.12	0.474	0.001	5.54	0.21
21.42	0.469	0.001	5.60	0.05
25.45	0.468	0.000	5.75	0.10
29.80	0.469	0.000	5.86	0.10
34.77	0.468	0.000	5.79	0.00
39.60	0.468	0.000	5.95	0.06

Table C.5: Raw Data from Collapse Tests on Wide FCC Distribution. Four runs were performed for each set of data.

Wide Distribution of FCC				
H = 3.3D				
Superficial Velocity (mm/s)	Dense Phase Voidage		Superficial Dense Phase Velocity (mm/s)	
	Mean	Standard Deviation	Mean	Standard Deviation
3.51	0.497	0.001	3.06	0.02
4.25	0.509	0.000	3.74	0.04
5.35	0.530	0.000	4.96	0.04
5.70	0.536	0.001	5.00	0.27
7.19	0.531	0.003	4.40	0.15
8.66	0.526	0.001	4.13	0.08
10.20	0.518	0.003	3.68	0.08
13.42	0.508	0.001	3.53	0.03
17.73	0.500	0.001	3.56	0.14
21.67	0.495	0.000	3.59	0.12
24.87	0.491	0.001	3.55	0.19
28.83	0.487	0.001	3.36	0.10
33.92	0.488	0.001	3.40	0.18
38.78	0.488	0.001	3.48	0.10
H = 4.4D				
3.57	0.494	0.001	3.00	0.01
4.31	0.506	0.000	3.68	0.03
5.42	0.527	0.001	4.95	0.04
5.78	0.534	0.001	4.61	0.12
7.25	0.525	0.001	4.10	0.20
8.77	0.515	0.002	3.64	0.06
10.27	0.511	0.002	3.43	0.04
13.59	0.496	0.003	3.02	0.13
17.94	0.488	0.000	3.01	0.04
21.83	0.481	0.001	2.96	0.03
25.20	0.480	0.002	3.03	0.06
29.16	0.482	0.001	3.17	0.08
34.38	0.478	0.002	3.08	0.14
39.19	0.479	0.002	3.12	0.07

Table C.6: Raw Data from Collapse Tests on Bimodal FCC Distribution. Four runs were performed for each set of data.

Bimodal Distribution of FCC				
H = 3.3D				
Superficial Velocity (mm/s)	Dense Phase Voidage		Superficial Dense Phase Velocity (mm/s)	
	Mean	Standard Deviation	Mean	Standard Deviation
3.52	0.495	0.000	2.97	0.02
4.26	0.507	0.001	3.72	0.06
5.36	0.524	0.001	4.87	0.04
5.71	0.530	0.001	5.26	0.10
7.18	0.535	0.001	4.82	0.07
8.67	0.528	0.003	4.36	0.23
10.16	0.524	0.001	4.00	0.11
13.41	0.511	0.001	3.78	0.16
17.74	0.500	0.001	3.66	0.14
21.55	0.494	0.001	3.61	0.08
24.88	0.493	0.001	3.56	0.16
28.79	0.494	0.001	3.49	0.13
34.01	0.492	0.002	3.56	0.13
38.91	0.491	0.001	3.62	0.17
H = 4.4D				
3.50	0.492	0.000	2.84	0.07
4.24	0.503	0.000	3.66	0.02
5.35	0.519	0.001	4.76	0.06
5.10	0.526	0.001	5.20	0.11
7.20	0.529	0.002	4.46	0.23
8.75	0.515	0.001	3.91	0.02
10.23	0.507	0.001	3.56	0.08
13.60	0.502	0.001	3.40	0.14
17.95	0.490	0.000	3.13	0.13
21.80	0.485	0.002	3.11	0.06
25.15	0.485	0.000	3.09	0.08
29.13	0.485	0.002	3.26	0.18
34.40	0.482	0.000	3.20	0.05
39.20	0.482	0.001	3.34	0.20

Table C.7: Raw Data from Collapse Tests on Intermediate Glass Bead Distribution. Four runs were performed for each set of data.

Intermediate Distribution of Glass Beads				
H = 4.4*D				
Superficial Velocity (mm/s)	Dense Phase Voidage		Superficial Dense Phase Velocity (mm/s)	
	Mean	Standard Deviation	Mean	Standard Deviation
6.87	0.473	0.000	4.75	0.03
7.65	0.480	0.000	5.42	0.03
9.19	0.488	0.001	5.84	0.08
10.74	0.481	0.001	4.90	0.12
14.17	0.471	0.001	4.14	0.17
18.57	0.466	0.001	3.95	0.29
22.54	0.466	0.001	4.93	0.07
26.00	0.466	0.001	5.08	0.32
30.12	0.464	0.001	5.16	0.24
35.56	0.465	0.001	5.03	0.33
40.60	0.464	0.001	5.05	0.22

Table C.8: Raw Data from Collapse Tests on Wide Glass Bead Distribution. Four runs were performed for each set of data.

Wide Distribution of Glass Beads				
H = 4.4*D				
Superficial Velocity (mm/s)	Dense Phase Voidage		Superficial Dense Phase Velocity (mm/s)	
	Mean	Standard Deviation	Mean	Standard Deviation
6.11	0.453	0.001	4.75	0.07
7.69	0.470	0.000	5.76	0.00
9.23	0.472	0.001	5.28	0.08
10.78	0.462	0.001	4.47	0.03
14.28	0.455	0.002	3.70	0.06
18.64	0.439	0.000	4.81	0.08
22.50	0.434	0.001	4.98	0.11
26.09	0.432	0.000	4.94	0.15
30.07	0.431	0.001	4.96	0.42
35.63	0.431	0.001	4.96	0.06
40.75	0.431	0.001	5.04	0.02

Table C.9: Raw Data from Collapse Tests on Bimodal Glass Bead Distribution. Four runs were performed for each set of data.

Bimodal Distribution of Glass Beads				
H = 4.4*D				
Superficial Velocity (mm/s)	Dense Phase Voidage		Superficial Dense Phase Velocity (mm/s)	
	Mean	Standard Deviation	Mean	Standard Deviation
4.51	0.418	0.001	3.57	0.02
6.11	0.439	0.001	5.05	0.04
7.65	0.459	0.001	6.30	0.04
9.23	0.457	0.002	5.26	0.25
10.81	0.449	0.001	4.43	0.07
14.29	0.431	0.002	4.30	0.03
18.69	0.408	0.003	3.34	0.08
22.73	0.401	0.000	3.61	0.04
26.18	0.396	0.001	3.56	0.13
30.44	0.398	0.003	3.55	0.05
35.88	0.395	0.001	3.78	0.21
40.88	0.396	0.002	3.67	0.06